POLITECNICO
MILANO 1863

SCUOLA DI INGEGNERIA INDUSTRIALE
E DELL'INFORMAZIONE

Electrification of Gasification Reactors for Biomass-to-Methanol Plants: Techno-Economic Analysis

TESI DI LAUREA MAGISTRALE IN
ENERGY ENGINEERING
INGEGNERIA ENERGETICA

Candidates:
Matteo CARBONI - 964686
Francesco ENNI - 968619

Advisor: Matteo Carmelo Romano
Co-advisor: Andrea Nava
Academic Year: 2021-22

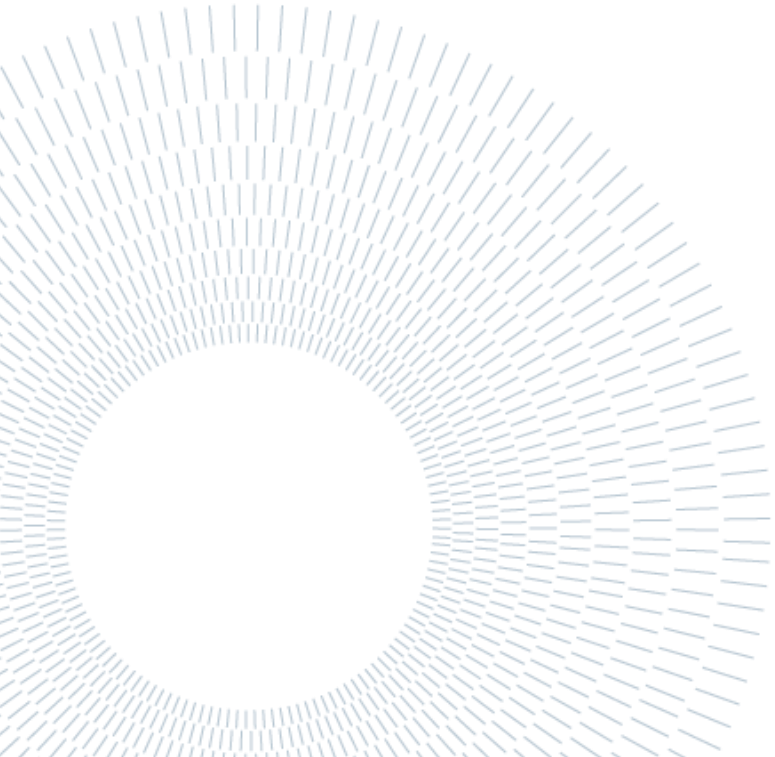

Abstract

This Thesis Work is carried out in the context of Biomass-To-Liquids processes and deals with the design, simulation and technical-economic analysis of systems for the conversion of biomass into methanol through gasification.

Two state-of-the-art alternative paradigms for gasification are considered: reactor heating can be performed directly, with an oxygen stream entering the gasifier and oxidizing part of the biomass, or indirectly, where a combustor fed with part of the available biomass provides thermal load. The resulting biomass consumption permits to avoid the use of a fossil fuel; nevertheless, in this way process carbon efficiency is reduced.

This research study considers gasifier electrification, achieved by inserting resistive elements inside the gasification reactors, as an alternative to satisfy the requested thermal load. Following signal prices of the national electric grid, gasifiers, once equipped with the electric resistors, can operate alternately with the traditional operation, by means of biomass oxidation, or in full electric mode, through Joule effect. Electric resistance mode permits to save biomass, allows to obtain an extra product of biochar and raises Power-to-Methanol and Carbon efficiencies of the process.

Electrified configurations are modelled and simulated with *Aspen Plus*® software; from the obtained results, the influence of the resistances on plant performances is estimated through the comparison of Key Performance Indicators. The creation of hybrid mode maps allows through a differential economic analysis to verify whether this alternative can be competitive and under which conditions. Ultimately the adoption of PV solar field and Li-ion battery to satisfy electricity load is simulated: in this way the plant can reach partial grid independence and hedge against price fluctuations.

Key-words: Gasification, Gasifier, Biomass, Biofuels, Bio-Methanol, Electrification, National Grid, Carbon capture and storage, Solar field, Battery.

Sommario

Il presente lavoro di Tesi è svolto nell'ambito dei processi Biomass-to-Liquids e riguarda la progettazione, la simulazione e l'analisi tecno-economica di sistemi per la conversione di biomassa in metanolo per mezzo della gassificazione.

Due paradigmi alternativi per la gassificazione sono considerati: il riscaldamento del reattore può infatti essere eseguito direttamente, grazie ad una combustione interna al gassificatore mediante l'uso di un ossidante (Aria/Ossigeno), o indirettamente, dove un bruciatore alimentato con parte della biomassa fornisce la potenza termica necessaria. Se da un lato il consumo di biomassa per il riscaldamento dei reattori consente di evitare l'uso di un combustibile fossile, dall'altro la Carbon Efficiency del processo ne risulta penalizzata.

Il seguente studio di ricerca considera l'elettrificazione del gassificatore, ottenuta inserendo elementi resistivi all'interno dei reattori, come alternativa per soddisfare il carico termico richiesto. Seguendo l'andamento di prezzo della rete elettrica nazionale, è possibile soddisfare il carico termico dei gassificatori alternativamente con il sistema tradizionale, ossidando parte della biomassa disponibile, o attraverso le resistenze elettriche per effetto Joule. In questo modo si ottiene un risparmio della biomassa, un extra prodotto, il biochar, e si innalzano le efficienze Power-to-Methanol e di Carbonio.

Le configurazioni elettrificate sono modellate e simulate con il software *Aspen Plus®*; l'influenza delle resistenze sulle prestazioni dell'impianto è stimata attraverso il confronto dei KPIs. La creazione di mappe di funzionamento ibrido permette attraverso un'analisi economica differenziale di verificare se questa alternativa può essere competitiva e a quali condizioni. Inoltre, per rendere l'impianto parzialmente autonomo dalla rete elettrica, viene simulata anche l'adozione di un campo solare con uno stoccaggio di energia variabile per mezzo di batterie a ioni di litio.

Parole chiave: Gassificazione, Gassificatore, Biomassa, Biocarburanti, Bio-metanolo, Elettrificazione, Rete Nazionale, Cattura e stoccaggio della CO_2, Campo solare, Batteria.

Contents

1 Introduction

Energy-related environmental concerns have risen significantly in the last decade: gradually, the common conscience has acknowledged the importance of the reduction of CO_2 emissions and of the deployment of clean energy technologies [1]. At the global level, the effort and commitment shown towards climate change led to the Paris Agreement in 2015, a legally binding international agreement with the explicit purpose of limiting global warming to well below 2°C and pursuing efforts to limit it to 1.5°C by 2050 [2].

In support of the abatement in greenhouse gas (GHG) emissions objective, the European Climate Foundation (ECF) [3] delivered the Roadmap 2050 [4], which provides a practical guide to a low-carbon Europe, highlighting urgent policies needed over the coming years, especially in the transport sector.

During the last decades of rapid technic - economic growth of the European countries the rising necessity and diffusion of means of transport was supported by an ever-increasing exploitation of the oil sector. Fossil fuels were the main protagonists (and only actors) of the last decades World energy mix (TPES [5]) and transportation sector, for their high energy density and lower costs. As a result, great amounts of greenhouse gases and pollutants has been released into the atmosphere causing the so called "Global Warming". The main responsible for long-term changes are carbon dioxide emissions. According to the International Energy Agency (IEA) almost a quarter of the global CO_2 emissions are transports related [6].

If, for stationary applications as electric [7], there are technical solutions to reduce or even avoid CO_2 emissions, such as Carbon Capture and Storage (CCS), for the transports sector a change of approach is envisaged with the target of traditional fuels substitution with alternative ones. The decarbonization of the transports sector is not trivial due to the fuel requirements of the most diffuse machine in this field: the internal combustion engine. As a result, the search for new, clean, and renewable energy sources has increased importance, especially for the purpose of supplying power to vehicles. In this context, electric vehicles (EVs) could be the most significant replacement for conventional motors. Nonetheless, despite their undeniable lack of

direct emissions (Tank-to-Wheel emissions equal to zero), electricity production in many countries is still mainly based on fossil fuels, which can significantly influence the indirect emissions of carbon dioxide (Well-to-Wheel emissions [8]). As a result, indirect emissions from electric vehicles may be equivalent, if not higher, than direct emissions from regular vehicle use [9]. Another strong candidate for internal combustion engine replacement is represented by fuel cell technology, among which stand out Proton Exchange Membrane (PEM) Fuel Cell [10]. Even in this case some crucial constraints appear unsolved, like high cost, low stack durability and hydrogen storage security problem [11].

In this context, biofuels can have a crucial role, since they require fewer technological improvements to operate and are compatible with the current transport infrastructure [12]. It is estimated that biofuels could replace the 27% of the total transportation fuel consumption by 2050 and it is predicted that their production can occupy the 64% of the renewable energy consumption by 2030 to reach the Net Zero Emissions target by 2050 Scenario (between 2010 and 2019, global biofuel consumption expanded 5% on average per year) [13].

However, the achievement of the 14% average annual growth depicted for Net Zero Scenario's between 2021 and 2030 will require considerably stronger policies, as one can note from *Figure 1-1*.

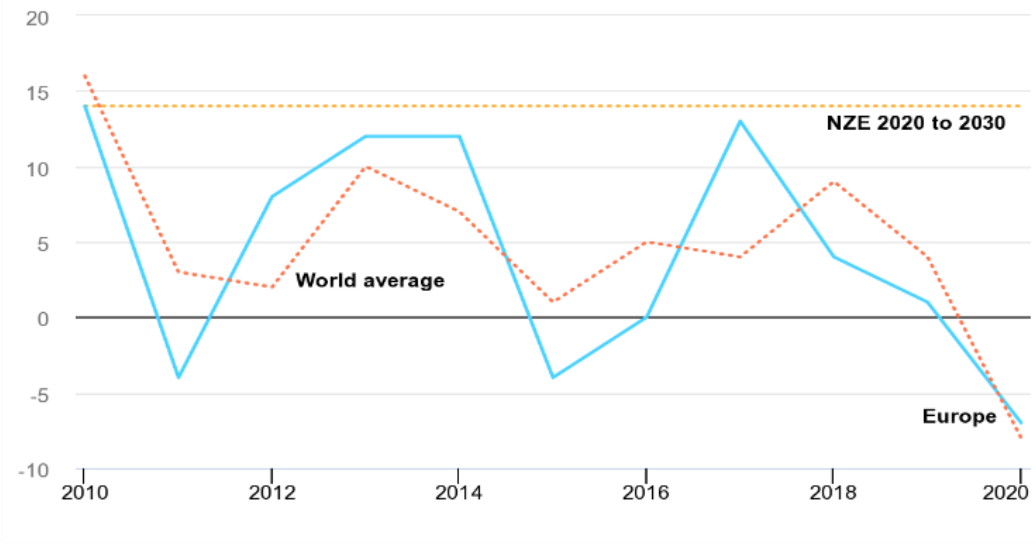

Figure 1-1: biofuel annual consumption growth. In blue EU trend, in red World average one and in yellow the annual target to reach the Net Zero Scenrario in 2030

In this thesis work Biomass to Methanol (BtMeOH) plants are considered. The aim of these plants is to convert hydrocarbon sources into a liquid and zero emissions biofuel through gasification processes. In particular, the work is focused on the feasibility of the electrification of reactors for biomass gasification when the electricity price signal from the grid is low (or with a dedicated solar field). In the latter case the fuel produced will be totally carbon free due to the zero-carbon emission of biomass considering its entire life cycle; nonetheless, exploiting carbon capture technologies, biomass to methanol plant would be recognizable even as carbon negative [14].

Nowadays, the number of pilot synthesis plants in the field of biofuels is steeply increasing. Assessed, already built and active operational plants are reported in *Figure 1-2* [15].

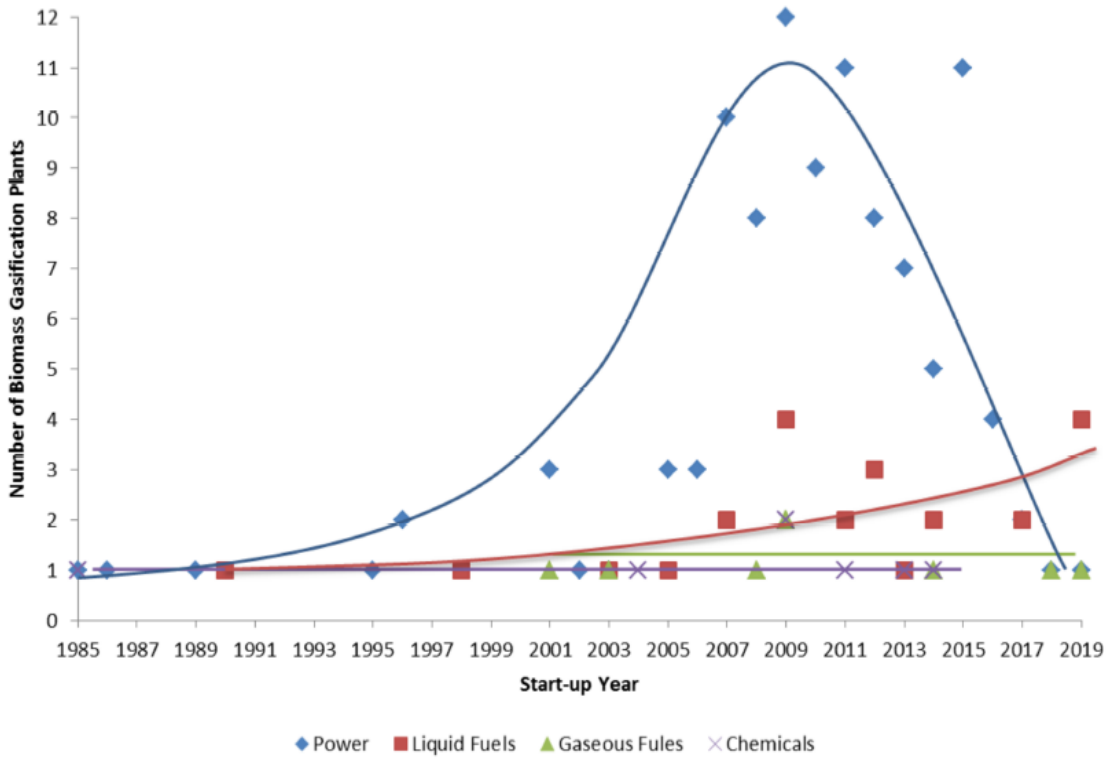

Figure 1-2: trend of number of biomass gasification plants (operational/idle/on hold/under construction/planned) as a function of start-up time.

1.1. Syngas

Synthesis gas, mainly known as syngas, is a chemical commodity mainly composed by hydrogen and carbon monoxide. It's obtainable from natural gas, through steam reforming process, from refinery flue gases, from biogas through dry or steam reforming, or from the gasification of coal and biomass [16]. Literature refers to syngas with the word "commodity" for the wide-ranging use in power to x scenarios and for the large pool of different chemicals that can be synthetize starting from it. In *Figure 1-3*, the main applications that can arise from the use of the syngas are highlighted. It is chosen to list them starting from three macro areas: power generation, direct use of syngas for the synthesis of chemicals, and product derived by methanol [17], which is the main topic of *chapter 1.2*.

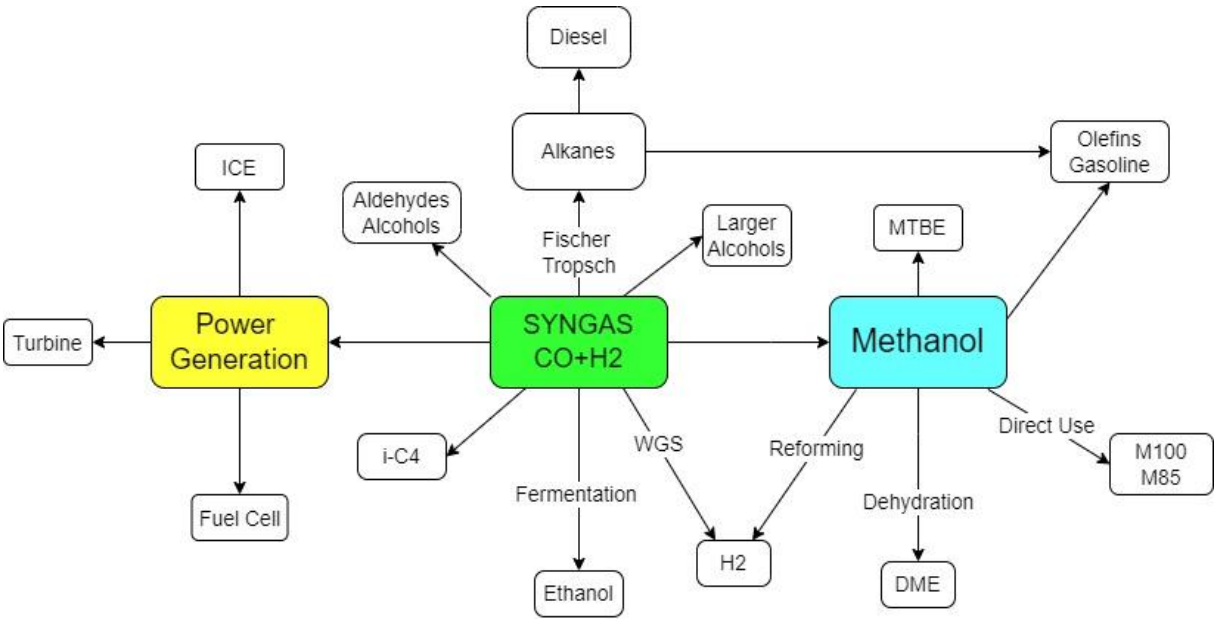

Figure 1-3: syngas applications block scheme

Syngas is used to produce gasoline and diesel through Fischer-Tropsch process; the method, developed in Germany in 1925 by Franz Fischer and Hans Tropsch to hedge against gasoline shortage periods (e.g., it was largely used in WWII in the transport sector) [18], it is increasingly gaining popularity as a method for the production of carbon-neutral liquid hydrocarbon fuels and could partially substitute the actual crude oil distillation [19].

Syngas can be used also for hydrogen production with a Water Gas Shift (WGS) reactor (or through separation with selective membranes) to satisfy the large hydrogen demand of refinery and chemical industry [20]. In addition, it could represent a completely green fuel, according to the recent boost of hydrogen technologies and patents by Europe (as depicted by IEA, some key new applications for hydrogen are showing promising signs of progress)[21].

The fields of application of this energy vector are in constant expansion; below are some of the most promising. One year after the first demonstration project for using pure hydrogen in direct reduction of iron began, the number of announcements for new steel mill projects is rapidly increasing [22]. The first fleet of hydrogen fuel cell trains started operating in Germany [23]; in Italy FNM Group has recently designed a full operative hydrogen train for Brescia-Edolo line [24]. Over 100 pilot and demonstration projects for using hydrogen and its derivatives in shipping are being developed [25]; large corporations are already forming strategic alliances to ensure the availability of these fuels [26]. In the power sector, the use of hydrogen and ammonia is attracting more attention; announced projects stack up to almost 3.5 GW of potential capacity by 2030 [6].

Finally, hydrogen may help to improve energy diversification by reducing reliance on fossil fuels, either by substituting fossil fuels in end-use applications or by transitioning from fossil-based hydrogen generation to renewable hydrogen production. In addition, the creation of an international hydrogen market will increase the range of possible energy sources, hence improving energy security for energy-importing countries [27].

1.2. Methanol

Methanol is a chemical soluble liquid which scientific name is methyl alcohol (formula CH_3OH). It is exploited as a precursor to other common chemicals such as formaldehyde, acetic acid, methyl tert-butyl ether (MTBE), methyl benzoate, dimethyl ether (DME), with over 20 million tons produced annually [28].

Almost 50% of its production is related to olefins and formaldehyde synthesis; 15% of the actual market is deployed for MTBE production, a chemical compound largely used for the refining of gasoline to increase the RON (Research Octane Number). A residual 18% is instead used directly for transport application as biodiesel and gasoline blending as shown in *Figure 1-4* [28].

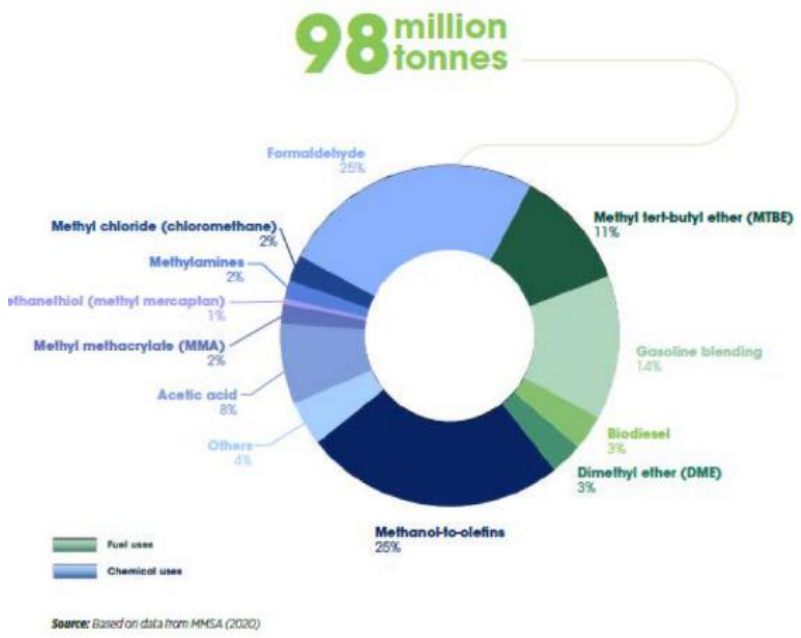

Figure 1-4: annual tons of produced methanol divided in derivatives percentage

Analysis of recent trends shows that methanol demand is constantly increasing with a rate of 5% per year; in the last years this trend has peculiarly been stressed to help the decarbonization of energy-intensive sectors with limited green options, like marine transportation or feedstock in chemical industries.

In this thesis work the production of green methanol is achieved by using biomass as source and exploiting a CCS unit that is able to capture 95% of CO_2 produced by gasification of biomass. It is important to highlight that 95% is a precautionary value which doesn't represent full theoretical potential of the technology (potentially CCS plant is able to capture up to 99% of CO_2). In this way, if the entire life cycle of biomass is considered, the emissions of CO_2 appear negative (emission from biogenic source)[29]. Nowadays, methanol market is very solid and pushed mainly in Asia with a price oscillating between 400 €/ton to 600 €/ton [30].

1.3. Biochar

Biochar is a carbonaceous substance produced in an oxygen-restricted environment through thermochemical processes like pyrolysis, gasification, torrefaction, and hydrothermal and flash carbonization [31].

Thanks to its intrinsic characteristics, char have become increasingly important over the last few years. Its peculiarities include a highly porous structure, the presence of oxygen - containing surface functional groups (OCFGs), outstanding Cation Exchange Capacity (CEC), wide surface area, strong adsorption capacity, high structural stability, and enrichment with minerals and trace metals [32].

Biochar has a wide range of applications, including soil improvement, pollutants removal, carbon sequestration, reduction of greenhouse gas emissions from the soil environment, use as conductive materials and additives in anaerobic digestion, composting, and microbial fuel cells [33]. Because of their plentiful availability, renewability, and cost-effectiveness, lignocellulosic materials are being explored as a viable feedstock to produce biochar [34].

From the production of chemicals and biochar with lignocellulosic waste, two advantages arise: the reduction of open field biomass burning and the simultaneous utilization of waste biomass as a feedstock for the manufacture of biochar and bio-oil. In gasification processes, gaseous product is the predominant chemical; hence, the yield of biochar from the gasification is often low when compared to slow or fast pyrolysis [35].

Biochar is now being used in environmental management for waste to energy generation, agronomic benefits and soil quality improvement, GHG reduction, and energy storage and conversion devices [36]. It can be made solely from waste materials such as crop residues, forestry, animal manure, food processing, paper mill, municipal solid waste, algal waste, and sewage sludge.

The addition of biochar to soil provides long-term stability, which is a critical aspect in lowering CO_2 emissions from the atmosphere [37]. According to Lehmann et al. 2021 [37], the typical residence time of carbon in soil varies between 90 and 1600 years, depending on the labile and intermediate stable carbon molecules. Several additional researchers have discussed the potential of biochar as a soil amendment for GHG mitigation.

1.4. Electrification

Electricity emerges as a critical energy vector and crucial opportunity to fuel a clean energy transition and energy decarbonization. European Union pledges to be more ambitious in terms of climate change, reducing greenhouse gas emissions by at least 55% by 2030 compared to 1990 levels, with the goal of achieving climate neutrality by 2050. In this scenario, the penetration of electricity in the final demand for energy will

rise from the current 23% to 30-31% by 2030, and between 47% and 60% by 2050, while the current penetration of electricity in the major sectors is around 2% in transportation, 33% in education, and 32% in industry [38].

This result is possible supporting "direct" electrification, which involves transitioning from fossil fuels to carbon - free electricity in final energy uses. In "hard to abate" sector this process can be integrated with the use of green/blue hydrogen and e-fuel, in cases where direct replacement of fossil fuels is not economically feasible (e.g., in heavy industry, navigation, and aviation) [39].

Nevertheless, it is important to emphasize the source of origin of this electricity: each country, according to its history, geography and local resource, has developed its own energy mix to satisfy the energy demand. During the last decades in Europe all the countries have tried to reduce the exploitation of oil for power generation, gradually replacing their market portion with less carbon intensive resources. In Italy the progressive abandonment of coal and oil was historically hedged with natural gas; recently an important boost was given to solar PV and wind power plants installation (e.g., "Conto Energia", 2013 [40]) as shown in *Figure 1-5*:

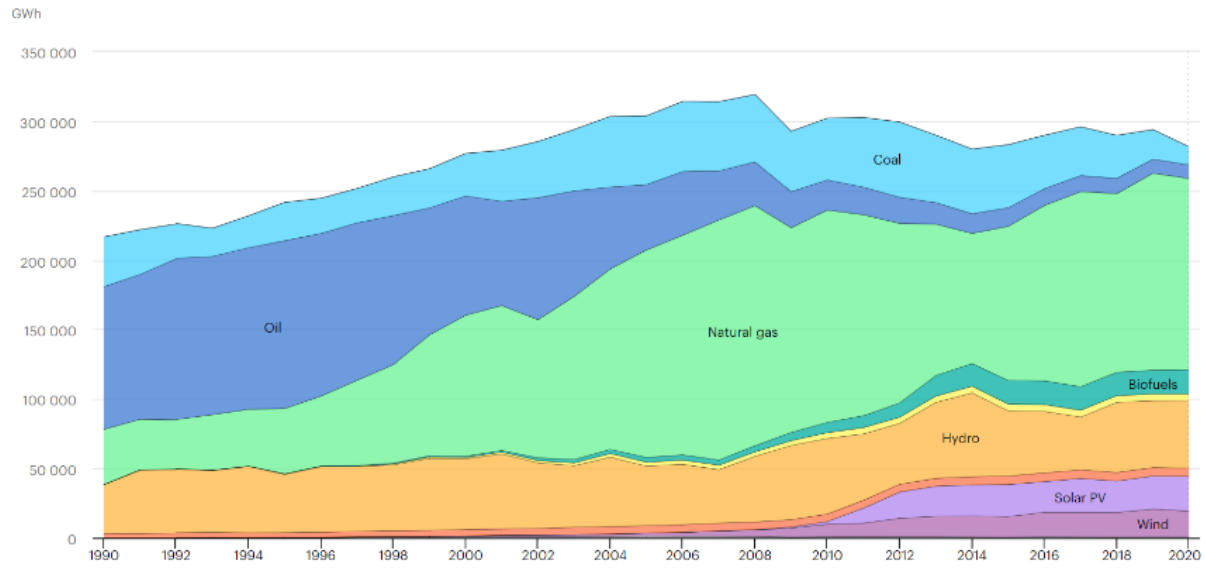

Figure 1-5: Italy energy mix by exploited sources

The increasing penetration of renewable resources in national grid is affecting electrical prices, reducing the absolute electricity price (while increasing distribution and dispatchment cost) [41].

In the current research study, the declared goal is to assess the techno economic feasibility of electrified gasifiers for BtMeOH plants. The idea is to discover a profitable alternative for reactor heating by utilizing electrical resistances within gasification reactors. Following national electric grid signal prices, reactor thermal load is satisfied using either the traditional system or the Joule effect.

Future grids with high expected renewable penetration will have significant variation in electricity prices during the day and season; as a result, it will be possible to shape specific times when electric mode is economically profitable [42].

1.5. Scope of the work

This Thesis Work explores the techno-economic feasibility of the electrification of gasifiers for Biomass-to-Methanol plants. Two state-of-the-art alternative paradigms for gasification are considered: a directly heated gasifier and an indirectly heated one. Electrification is achieved by inserting resistive elements inside the gasification reactors to satisfy the requested thermal load through the Joule effect. Gasifiers, once equipped with the electric resistors, can operate alternately with the traditional operation, therefore based on the oxidation of part of the inlet biomass, in full electric mode or in hybrid configuration.

The scope of this research study is to perform a differential economic analysis of the aforementioned electrified plants with respect to conventional ones to establish the set of conditions for a cost-effective investment. Operating the plant with partial or complete aid of electrical resistances permits to save biomass, allows to obtain an extra product of biochar and raises Power-to-Methanol and Carbon efficiencies of the process. The drawback is inherent to the significant increase in plant dependence on the electricity grid. To hedge against price fluctuation, the adoption of a PV solar field and Li-ion battery is proposed.

2 Biomass to liquid fuels: an overview

The thermochemical processes that support Biomass to liquid fuels conversion can be split into some principal steps: biomass pre-treatment, gasification, syngas cooling and cleaning, syngas conditioning or gas shift (to adjust the syngas composition before entering the synthesis reactor) and fuel synthesis.

One of the industrial methods for large-scale conversion of a wide range of biomass streams into liquid transportation fuels has been identified as gasification. Indeed, produced syngas can be conditioned to support hydrogen, methanol, dimethyl-ether (DME), or diesel and gasoline production (through Fischer-Tropsch processes). In addition to the large pool of synthesizable products, advantages of gasification are the large-scale capabilities (industrial coal industry rely on gasification [43]), the pressurization, and the improved gas quality (high temperature and low tar formation maximize CO and H_2 generation [44]).

Existing methods are limited in term of carbon efficiency since carbon and hydrogen are partially lost (i.e., oxidized) in the gasification reactor to produce energy for the endothermic gasification processes. From this limitation arises the idea of this research study: provide thermal heat exploiting electrical resistances working inside gasification reactors. It is hence possible to raise carbon efficiency of the process, save biomass or obtain an extra product (i.e., biochar).

A general operative block scheme of biomass to liquid fuel plants is reported in *Figure 2-1*. In green the fundamental biomass to liquid plant components are shown, while in light green alternative technical arrangements are reported.

The general plant layout is composed by a multitude of subsystems whose tasks are briefly explained in dedicated paragraphs.

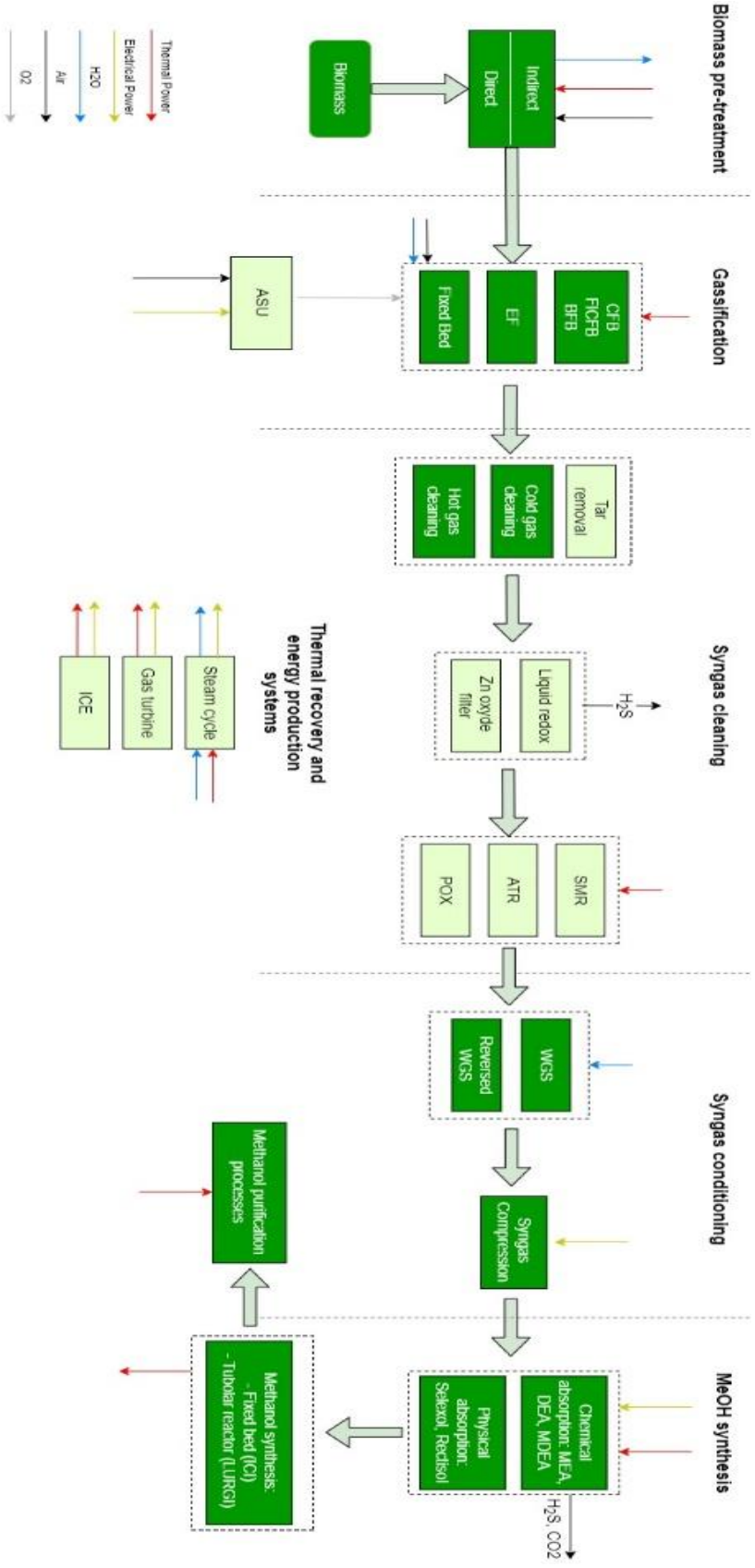

Figure 2-1: Biomass to liquids fuel general block scheme plant

2.1. Biomass pre-treatments

The first step in this kind of plants is biomass drying since "as received" wood biomass generally shows a moisture level around 40%.

Drying process is carried out to achieve a better Cold Gas Efficiency (CGE) and to avoid wasting thermal power in water evaporation that can lead to a reduced syngas production.

For this kind of applications biomass is dried at the moisture value of 15% [45]. To achieve this target the biomass feedstock is heated up in a direct or indirect drying process. Literature refers to direct drying whenever the thermal vector has a direct contact with the biomass (e.g., hot air or steam that dry the biomass). Conversely, indirect drying implies that the biomass is heated up with a fluid which is not in direct contact with the biomass itself. There are a multitude of different components that can perform the drying process; here are reported the most common ones: belt, tube bundle, fluidized bed steam driers.

According to the Horizon 2020 programme the drier used in the studied plant is a belt one with hot air as thermal vector [46].

A classical pre-treatment section also includes feeding flow reduction into particles to match gasifier size target. Among the processes exploited in state-of-the-art plants for biomass applications, the most common ones are torrefaction, pyrolysis and pelletization, that achieve the right size of the feed flow particles (order of magnitude of millimetres) and have a beneficial effect on the CGE [47].

The size of the incoming biomass into the plant is already considered suitable for gasification, hence, there is not a grinder unit [46].

2.2. Gasification section

Fixed bed gasifiers, fluidized bed gasifiers, and entrained flow gasifiers are three different categories that aggregate biomass gasification methods.

From a technical and financial perspective, fixed bed technology is preferred for small plants with reduced thermal input ranging from 1 to 10 MW_{th} [12].

Fixed bed gasifiers are divided in two categories [48]:

- Updraft configuration: in this kind of application the biomass is introduced into the gasifier from the top while the gasifying agent is blown from the bottom in a counter current configuration. The biomass undergoes the following

processes: in order drying, pyrolysis, reduction and, at the end, combustion. The syngas is drawn out from the top of the gasifier. For this reason, the gaseous pyrolysis products can be found in the outlet syngas.

- Downdraft configuration: in this kind of application the biomass and the gasifying agent are introduced into the gasifier in a co-current configuration. The biomass undergoes drying, pyrolysis, combustion and reduction. The outlet syngas is extracted from the bottom of the gasifier after the reduction zone.

In both cases the operative temperature range go from a minimum of 650 °C to a maximum of 1150 °C. Updraft configuration has a higher thermal efficiency due to the better contact between the biomass and the oxidant because of the counter-current configuration. On the other hand, updraft configuration has a higher tar presence in the outlet product respect to the downdraft configuration where the syngas is extracted from the bottom [12].

Fluidized bed gasifiers are preferred, due to their more easily scalability, for large-scale power plants. They are categorized as:

- Bubbling fluidized dual-bed gasifiers: this technology exploits two different gasification bed. One is a bubbling fluidized bed in which gasification occurs with high gasifying agent velocity around 5 – 10 m/s; the other provides the needed thermal supply with a combustor. The thermal power is obtained by burning part of the biomass. The heat is distributed through a solid recirculation from the "combustor bed" to the gasification one. The gas outlet is cleaned with a cyclone [12].

- Bubbling fluidized bed gasifier: in this set-up feeding biomass is fluidized, according to the fluidization of solid bed fundamentals, with a gasifying agent velocity of 2 - 3 m/s. The gasifying agent corresponds also to the fluidization agent in this case. The syngas is cleaned, after the gasification processes, by a cyclone that removes the solids particles that are still present in the outlet product [12].

Typical range of temperatures goes from 700 °C to 900 °C. High mass and heat transfer rates in fluidized bed gasifiers ensure consistent temperatures throughout the device and high toleration of various biomass feedstock types.

Entrained flow gasifiers find their best applications in large-scale plants. Indeed, because of the use of oxygen as gasifying agent and the high operating temperatures (1300 – 1500 °C), the tar production is lower with respect to fixed or bubbling bed gasifiers. As drawback, entrained flow reactors, necessitate a fine size of biomass inlet particles (i.e., 0.1 – 1 mm). Since biomass torrefaction process requires a lot of energy this results in a disadvantage for this kind of reactors. Generally, entrained flow reactors, used pressurized (20 – 70 bar) oxygen as gasifying agent in a top feeding co-current with biomass configuration. The outlet product is drawn from the side-bottom of the gasifier while ashes are taken out from the bottom [12].

2.3. Syngas cleaning & conditioning

Raw syngas produced at the outlet of the gasifier presents, as part of its composition, tar and dust particles that can clog the catalyst and cause the fouling of syngas coolers exchangers; for these reasons a cleaning process is needed.

Moreover, its composition may not be suitable for the next synthesis section; a conditioning process is therefore necessary.

Consequently, a syngas processing and cleaning has to be placed between the gasifier and the synthesis hierarchy, as depicted in *Figure 2-1*.

2.3.1. Tar removal

Tars are highly viscous and high-boiling organic compounds that condense at temperatures below 300–400 °C; their peculiarities make them compete for active sites in subsequent catalytic conversion processes. They are removable components, but the presence of tars filters and cleaning lines hardly penalize gasification efficiency [49].

A variety of methods it's available at the state-of-the-art for tar treatments; they are classified as primary, that occurs into the gasifier, and secondary which removal occurs out of the gasifier [50].

Primary procedures entail a treatment occurring inside the gasifier itself. They find a common application in entrained flow situation in which almost all tars have already reacted due to the high temperatures of the reaction zone. For primary catalytic treatments, there are two types of materials that can be added to the gasifier bed: one is based on nickel and lime, and the other is based on dolomite and lime [51].

For secondary procedures there are two main strategies that can be used: thermal and catalytic treatments, or physical methods. The existence of a steam reformer is a

solution that is frequently used for fluidized bed gasifiers, but it is not required for an entrained flow reactor; it allows tar elimination as well as remotion of unconverted hydrocarbons [52]. Conversely, the adoption of a separate thermal cracking unit that operates at extremely high temperatures results in significant efficiency losses for the entire plant. In terms of physical methods, tar droplets are removed utilizing wet scrubbers or dry systems as electrostatic precipitators, which are technologies used for particulate treatments.

One of these physical technologies is an oil-based cleaning method called OLGA that ECN has patented [53]. It was tested successfully in 2003 and has the potential to lower the dew point of tar to well below zero degrees Celsius.

2.3.2. Dust removal

Dust removal unit is part of cleaning and processing equipment; it is divided into hot, cold, and warm gas cleaning regimes, based on the temperature of the gas that exits the clean-up device [54].

One of the most significant advancements in commercial syngas applications in the past thirty years has been focused on high temperature particulate clean-up. Numerous techniques have been used for hot gas particulate clean-up: the majority is based on the physical principles of inertial separation, barrier filtration, or electrostatic separation.

In the plant, cyclones separators are adopted; their principle of operation is based on centripetal acceleration, exploited to shorten times needed for small particles to settle by gravity.

2.4. Reforming section

In biomass to fuel plants, reforming major function is to increase the CO and H_2 concentration in the syngas with respect to methane that does not participate in the methanol reactions. This application of the steam reforming aims to an increase in the methanol production. Moreover, the steam reforming reactor convert any remaining tar and higher hydrocarbons presents in the syngas.

In a classical steam reformer, the following reactions, depicted in (2-1), (2-2), (2-3), (2-4), (2-5) and (2-6) can occur.

$$CH_4 + H_2O \rightarrow CO + 3H_2 \quad \text{methane steam reforming} \quad (2\text{-}1)$$

$$2H_2 + O_2 \rightarrow 2H_2O \quad \text{hydrogen oxidation} \quad (2\text{-}2)$$

$$CH_4 + 2O_2 \rightarrow CO_2 + 2H_2O \quad \text{methane oxidation} \quad (2\text{-}3)$$

$$CH_4 + CO_2 \rightarrow 2CO + 2H_2 \quad \text{dry methane reforming} \quad (2\text{-}4)$$

$$CO + H_2O \rightarrow CO_2 + H_2 \quad \text{water gas shift} \quad (2\text{-}5)$$

$$C_xH_y + xH_2O \rightarrow xCO + (x + \frac{y}{2})H_2 \quad \text{general reforming} \quad (2\text{-}6)$$

The reactions are carried out in multi-tubular packed bed reactors. These reactors are realised comprising a series of long and narrow tubes that are placed into the combustion chamber of an industrial furnace, supplying the energy required to keep the reactor at the set temperatures during operation. The length of the tubes is typically 12 m, while the external diameter varies from 70 to 160 mm; for small size reformers it is preferred to use shorter tubes (7m) to limit pressure drop [55]. Furnace designs differ according to combustor arrangement, which is commonly classified as top-fired, bottom-fired, or side-fired [56].

To fasten the reactions, the combination of steam and methane inside the tubes is kept in touch with a nickel catalyst with high surface-to-volume ratios to handle diffusion constraints caused by high working temperatures.

Two main options can be settled in relation to the reformer configuration:

a) Fired tubular reformer (FTR) consists in a bunch of metallic tubes filled with catalyst that are heated up externally by flame combustors into a combustion chamber. The latter configuration can generate syngas with a very high H2/CO ratio. However, this option is energy intensive: as mentioned in the work of Ali et al. [57], the reformer is operated at a high temperature, often close to 950°C, to assist the conversion of CH4 and other tars. From an environment with the following characteristics results a very high H_2/CO ratio (e.g., approximately 3), which is unsuitable for direct methanol synthesis.

b) The auto-thermal reformer (ATR) is another option; it shows less size-related problems, allowing for lower investment costs, and at same time it results to be

less energy-intensive because it is only marginally endothermic. It consists in a three-section reactor: combustor, combustion, and catalytic section. In the first section the inlet feeds are mixed together and originate a turbulent diffusion flame. In combustion zone the partial oxidation reactions occurs and in catalytic zone the outlet gas reaches the chemical equilibrium. In comparison to a traditional steam reformer (SR), it produces syngas with minor H2/CO ratios and requires lower steam to carbon (S/C) ratios (an ATR can achieve S/C ratios of approximately 1-2). However, this lower ratio may result in incomplete methane conversion.

2.5. Water gas shift section

Water Gas Shift Reactors are industrially exploited in the synthesis of chemical commodities such as ammonia, hydrocarbons, methanol, and hydrogen, and are typically placed downstream steam reformer reactors for carbon monoxide conversion [58]. In biomass to methanol plant, water gas shift units are instrumental to adjust produced syngas composition and make it complaint with methanol reactors feed composition constraints.

In the WGS reactor the reaction depicted (2-7) in occurs.

$$CO + H_2O \rightarrow CO_2 + H_2 \qquad (2\text{-}7)$$

To meet high CO conversions, a water gas shift reactor is divided into two separate units, a high temperature (HTS, 400 °C) and a low temperature one (LTS, 200 °C). The first one adopts a Fe/Cr catalyst while the second one used a Cu based catalyst. Using this method, the high temperature of the first reactor favours kinetics, while the low temperature of the second favours thermodynamics, resulting in a high H_2 yield.

In the current overview depicted in *Figure 2-1*, WGS unit is placed before the acid gas removal section.

2.6. Acid gas removal section

Sulphur compounds, which primarily consist of hydrogen sulphide and carbonyl sulphide, pose a significant issue for synthesis reactors. Depending on the used feedstock, they can easily reach dangerous concentrations in syngas, causing catalysts poisoning and metal surfaces corrosion. In addition, syngas can contain significant

amounts of CS_3 when gasification occurs at low temperatures and with low steam concentration [59].

Numerous methods for removing acid gas have been patented over the years.

For what concerns high temperature technologies adsorption techniques are the most prevalent. Metal oxides are frequently used as in large-scale plants upstream the synthesis reactor [60]; zinc oxide's exothermic reaction with H_2S represents the dominant trend.

For biomass to liquid fuel plants, it was discovered that a low temperature process is frequently preferred. These treatments, typically based on chemical or physical processes, produce sulfuric acid or elemental sulphur as a useful by-product; from its recovery it is then possible to generate an extra income. Taking chemical adsorption as reference, the most common options at the state-of-the-art for absorption solvents are potassium carbonate, monoethanolamine, methyl-diethanolamine, and diethanolamine [47]. Conversely, physical solvent procedures outweigh amine absorption whenever feed gas is available at pressure greater than 20 bar or if the acid gas partial pressure exceeds 10 bar. The heats of adsorption of physical process, and hence regeneration energy losses, are lower if compared to chemical one; for this reason, when application ranges of chemical and physical process overlap, physical treatments are preferable [62].

2.7. Methanol synthesis

The methanol synthesis is a catalytic and overall exothermic process. The associated reactions are listed in the Equations (2-8) (2-10).

Reaction (2-8) is the catalyst-required methanol synthesis reaction; it is followed by reverse water gas shift reaction (RWGS) (2-9).

$$CO + 2H_2 \leftrightarrow CH_3OH \quad \Delta H° = -22\frac{kcal}{mol} \tag{2-8}$$

$$CO_2 + H_2 \leftrightarrow CO + H_2O \quad \Delta H° = +10\ kcal\ /mol \tag{2-9}$$

$$CO_2 + 3H_2 \leftrightarrow CH_3OH + H_2O \quad \Delta H° = -12\ kcal\ /mol \tag{2-10}$$

As shown in Equation (2-10)(2-10), the overall reaction exhibits a decreasing number of moles, making the reaction favoured at high pressures. The conversion of hydrogen and carbon oxides during the catalytic synthesis of methanol results in an overall exothermal reaction; hence, as expressed by Van't Hoff equation, it is favoured at low temperatures, typically between 220 and 300 °C.

Historically, methanol production was sustained with the use of $ZnO\text{-}Cr_2O_3$ based catalysts (BASF process, 1923) [63]. Nonetheless, the method, operated at very high pressures (300-400 bar), presenting various limitations:

- $ZnO\text{-}Cr_2O_3$ is active at 400°C, far higher the range of temperatures that favour methanol kinetics.
- $ZnO\text{-}Cr_2O_3$ base catalyst are susceptible to Fe, Ni, and S poisoning.
- At temperatures and operating pressures, Methanation parasitic reaction (2-11)(2-11) is favoured; the latter, not only penalises methanol synthesis yields, but also generates heat (due to the high exothermicity) which further penalizes methanol synthesis kinetics.

$$CO + 3H_2 \rightarrow CH_4 + H_2O \quad \Delta H° = -50\ kcal\ /mol \tag{2-11}$$

To overcome the following critical issues, between 1966 and 1972 ICI process was developed. Exploiting $Cu/ZnO/Al_2O_3$ or $Cu/ZnO/Cr_2O_3$ based catalysts, it is able to perform the reaction at lower pressions (between 50 and 100 bar), meeting kinetics favoured temperature range [63].

Nevertheless, parasitic reactions risk is unavoidable and must be carefully controlled to avoid high decreases of process yields. In addition, the formation of by-products makes the purification of methanol more complex and expensive: the high exothermicity of the formation of CH_4 and higher alcohols complicates thermal control. For these reasons parasitic control is managed through kinetic inhibition with appropriate catalyst with high selectivity.

The composition of the syngas that enters the reactor is another crucial factor to take into account. The syngas module (M), defined in Equation (2-12), is a key process parameter that must be maintained near 2 to ensure optimal conversions [50]. In the formula $\dot{n}_{H2}$, $\dot{n}_{CO_2}$, $\dot{n}_{CO}$ respectively represent molar flow of hydrogen, carbon dioxide and carbon monoxide.

$$M = \frac{\dot{n}_{H2} - \dot{n}_{CO_2}}{\dot{n}_{CO} + \dot{n}_{CO_2}} \tag{2-12}$$

It is also preferred a high CO/CO_2 ratio to reduce water formation and increase the per-pass methanol yield, hence lowering the reactor size.

There are primarily two types of reactors for methanol synthesis: ICI and Lurgi ones. According to Hamelinck et al. [65], the former, which has a fixed bed design with a cold injection of unreacted gas between the various catalyst layers (quench reactor), is inefficient. In the latter, which has a shell and tube design and a semi-isothermal reactor, gases react in tubes that exchange heat with boiling water [66].

Between the two configurations just shown, the Lurgi configuration appears to be the most popular for heat recovery possibility.

3 Biomass to methanol: plant modelling

In this section the main assumptions and modelling methods of the current BtMeOH plant are reported; every thermo-chemical process and unit operations is modelled with the software *Aspen Plus®*.

In *Figure 3-1* the block diagram of the studied BtMeOH plants is reported.

Two configurations are studied: direct and indirect biomass gasification. As consequence, it is chosen to report in green the unit operations that are shared between the two configuration, whereas in light green are the peculiar blocks of a configuration.

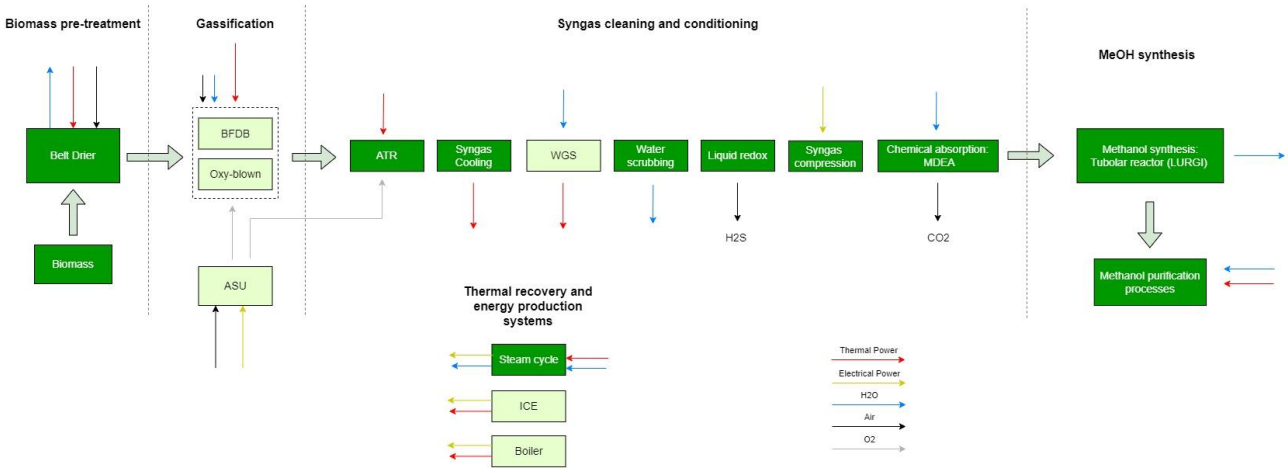

Figure 3-1: biomass to methanol block scheme layout

The plant, characterized by a 100 MWth (LHV based) biomass input, is composed of five sections: biomass pre-treatment, gasification, syngas cleaning and conditioning, methanol synthesis and heat recovery.

In the pre-treatment section the biomass is dried through a belt air drier: moisture content passes from 45% to 15%. Dried biomass is then sent to gasification section where it is converted in syngas through a gasifier.

Two types of gasification reactors are analysed: a directly heated oxygen-blown gasifier and an indirectly heated dual fluidized bed gasifier. In the direct

configuration, which operates at 870°C and 4 bar, reactor thermal load is satisfied through the heat generated by an oxygen combustion inside the reactor itself. An air separation unit (ASU) is employed to obtain an entering flow composed by 95% of oxygen; a stream of low-pressure steam is also inserted in the gasifier to adjust the steam to carbon ratio. The indirectly heated gasifier relies on a dual fluidized bed composed of a bubbling fluidized bed gasifier and a circulating fluidized bed combustor. An inert heat carrier composed by olivine is heated up in the air combustor and then recirculated in the fluidized bed, which operates at 815°C and 1.43 bar; a stream of low-pressure steam at 400°C is directed to the gasifier to adjust the steam to carbon ratio.

To make the syngas compliant with methanol synthesis requirements, several unit operations are adopted in the syngas cleaning and conditioning sections. An autothermal reformer (ATR), which operates respectively at 915°C and 800°C in direct and indirect configuration, cracks unconverted hydrocarbons and contributes to tar remotion, exploiting a pure oxygen flow from the ASU. Then syngas is cooled down to 250°C through syngas coolers. In the direct configuration a Water Gas Shift (WGS) reactor is exploited to adjust syngas composition. Proceeding downstream, water is removed in the water scrubber section and syngas is cooled down to 40°C. H2S conversion to elemental sulphur is performed thorough LIQUID REDOX component (LO-CAT process) which separates and removes the converted sulphur. A multistage intercooled compressor then pressurizes the syngas from 4 to 30 bar to meet Carbon Capture and Storage (CCS) component requirements. MDEA amine-based chemical solvent is used in aqueous solution to separate 95% of the incoming CO_2. In the indirect plant, the rate of CO_2 removal is controlled and varied to adjust the syngas composition for the synthesis section. After the acid gas removal section, the pressure is furtherly increased up to 92 bar to boost methanol production yields.

Once conditioned, syngas is sent to the fuel synthesis section where it is converted to methanol with a 99.85% of mass purity [67]. The by-product of methanol purification, a purge stream mainly composed by hydrogen and unconverted hydrocarbons, is partially recirculated to maximize fuel output and partially burnt in an internal combustion engine (ICE) to avoid the buildup of inert components in the system and recover chemical energy.

Gasifiers, reboilers and CCS components require a continuous flow of low-pressure steam to operate. Hence, a one pressure level heat recovery steam cycle (HRSC) is integrated in the plants: it recovers the excess thermal power generated along the plant from several units, generating electricity and satisfying the steam demands.

All the blocks rely on the RKS-BM thermodynamic model (Redlich-Kwong-Soave-Boston-Mathias). This Equation of State (EoS) model is ideal for hydrocarbon and light-gases processing applications including gas processing, refinery, and petrochemical operations; its outcomes are comparable to the Peng-Robinson-Boston-Mathias equation-of-state [68]. Water scrubber unit of operations represents the unique exception, since it is modelled with ELECNRTL; the choice is motivated by the peculiar accuracy for electrochemical reactions modelling, which can handle mixed solvent systems at large pool of concentrations [68].

3.1. Biomass definition & pre-treatment

3.1.1. Biomass definition

In this study the biomass characteristics are reported in *Table 3-1* according to FLEDGED specifications [46].

The biomass is modelled in *Aspen Plus*® as non-conventional component; this approach enables the definition of its thermochemical properties with the only use of proximate analysis information, i.e., without knowing the substance's chemical structure.

Table 3-1: "as received" biomass characteristics

Description	Biomass
LHV [kj/kg$_{AR}$]	9.747
HVV [kj/kg$_{AR}$]	11.574
Moisture [%$_{w}$]	45
Proximate Analysis [%$_{w,dry}$]	
Fixed Carbon	18.84
Volatile matter	80
Ash	1.16
Ultimate Analysis [%$_{w,dry}$]	
Carbon	51.19
Hydrogen	6.08
Nitrogen	0.2
Chlorine	0.05
Sulphur	0.02
Oxygen	41.3
Ash	1.16

The above model is in accordance with the one implied for coal modelling; in these cases fuel composition is generally unknown whereas ultimate analysis is commonly available.

3.1.2. Biomass pre – treatment

As reported in *Table 3-1* the moisture of "as received" biomass is around 45%, hence a pre – treatment section is needed to achieve 15% moisture.

Dryer effect can be measured comparing the lower heating values of "as received biomass" and "after drying biomass" as reported in *Table 3-2*.

The implemented air belt drier allows to achieve the 15% moisture goal with a specification on the outlet air humidity fixed at 80%. Ultimately, the dry biomass enters in the gasifier at 80 °C and with a moisture level of 15%.

To satisfy air belt drier thermal power request, heat from water scrubbing cooling section is recovered.

Table 3-2: biomass LHV in "as received" and dry conditions

	LHV [MJ/kg]	Moisture Content [%]
AR biomass	9.747	45
AD biomass	16.369	15

3.2. Biomass gasification

Following the necessary pre-treatments, biomass is transferred to the gasifier section.

As mentioned in the introduction of *section 3*, it is crucial to highlight the fundamental distinction between the two plants can be seen: one conversion plant uses an indirect air-blown gasifier, the other relies on a direct oxygen-blown gasifier; both configurations are investigated.

3.2.1. Direct gasification

Direct gasifier adopted relies on a direct oxygen – blown configuration, *Figure 3-2*, and it is modelled as an RYield reactor in *Aspen Plus®*.

Oxygen as oxidizer agent is chosen to limit the presence of N_2 that would lower the gasifier efficiency and increase its size. The oxidizer flow composed by 95% of oxygen is obtained by an Air Separation Unit (ASU).

The operative conditions of the gasifier are reported in *Table 3-3*.

A fundamental parameter to allow the correct functioning of the gasifier is the steam to carbon ratio (S/C) that has to approach 1 inside the reactor (this value is required by

ATR, as mentioned in *section 2.4*). In *Aspen Plus®* environment, the achievement of the right S/C ratio is attained through a design specification that regulates the slightly superheated steam inlet coming from the backpressure heat recovery steam cycle.

The gasification section is controlled by a calculator that provides, after mass balances, the outlet syngas composition. The calculator model is based on experimental data taken from an existing oxygen – blown reactor situated in Varkaus, Finland.

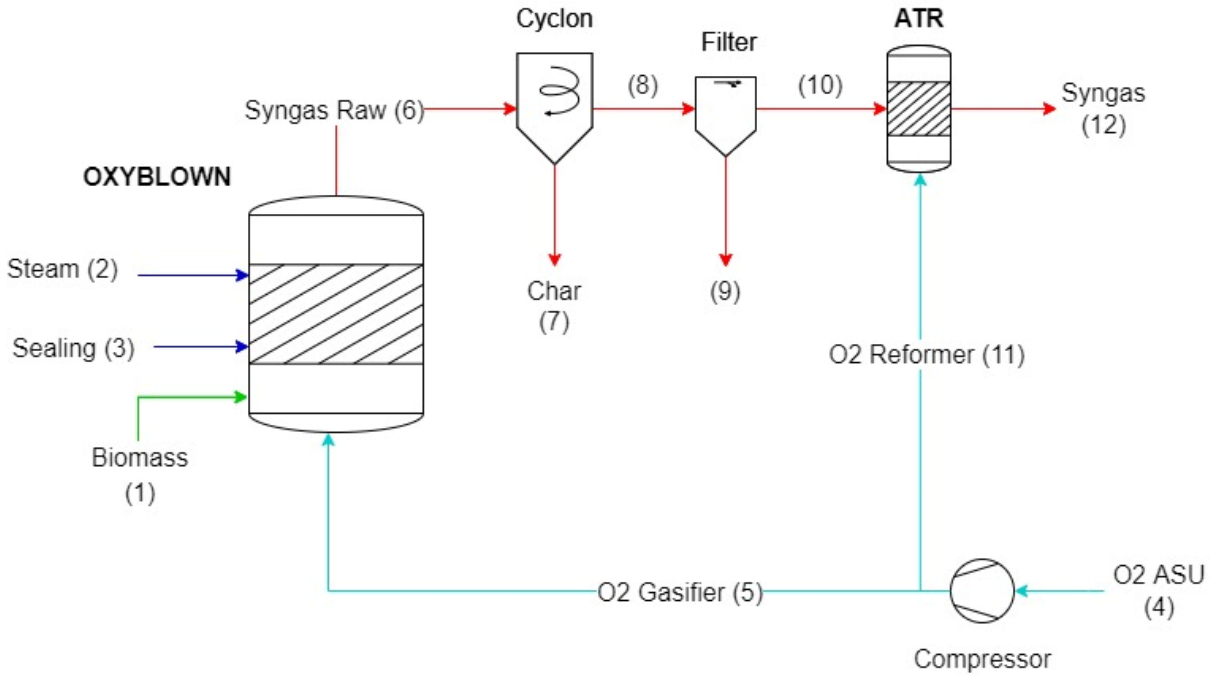

Figure 3-2: oxygen blown gasifier layout

Recoverable residual char is fixed as 4.5% of the total carbon inlet [54]; the amount of carbon that remains solid (fixed carbon) is nested in the char recovery term.

The gasification model exploits the partial chemical equilibrium of a WGS reaction to compute the syngas output composition, as depicted in Equations (3-1), (3-2), (3-3). The so called $pdelta$ parameter, listed in Equations (3-1), regulate the final syngas composition with respect to equilibrium constant K_{eq}.

$$pdelta = \log_{10}\frac{K_{eq}}{K(T)} = -0.16 \tag{3-1}$$

$$Log_{10}K(T) = -2.4198 + 0.0003855 * T_{gas} + 2180.6/T_{gass} \tag{3-2}$$

$$Keq = \frac{\prod \dot{n}_{wgs,products}}{\prod \dot{n}_{wgs,reactants}} \tag{3-3}$$

Pdelta allows to keep the distances from the reaction chemical equilibrium; in this way it is possible to control the progress of the reaction. This parameter depends on the reactor temperature.

Following the scheme *Figure 3-1*, a cleaning section is needed to model ashes and solid carbon (char) removal from the bottom of the gasifier; a filter and a cyclone are implied.

After these treatments the syngas enters an Auto Thermal Reformer (ATR) reactor, where any remaining tar presents in the syngas are converted and the presence of CO and H_2 is increased with respect to CO_2. In this reactor the chemical equilibrium is assumed, and the inlet oxygen flow rate is regulated to obtain the set point temperature of 915 °C of the outlet syngas following the steam methane reforming reaction. The reactor is designed to convert 90% of methane and reach the complete conversion of all the others hydrocarbons. The gasifier main operative points are reported in *Table 3-3*.

Table 3-3: gasifier operative conditions.

In the table there are three mass flow rates related to mixed (Gm), conventional (Gc), and non-conventional (Gnc) Aspen Plus © compounds. Molar flow rate Qm is related to mixed compounds. The composition section is divided in molar composition (x) for mixed compounds, mass composition (y) for non-conventional compounds, and mass composition (z) for conventional compounds.

Streams								
Variable	Biomass	Steam	Sealing	O2 gasifier	Syngas raw	Syngas raw	Syngas	Char
	(1)	(2)	(3)	(5)	(6)	(10)	(12)	(7)
T [°C]	80.00	200.00	200.00	108.42	870.00	870.00	915.00	
P [bar]	1.01	5.90	5.90	4.50	4.00	3.80	3.60	
Gm [kg/s]	-	2.66	0.80	1.93	12.04	12.04	12.68	
Gc [kg/s]	-	-	-	-	0.13	-	-	0.129
Gnc [kg/s]	6.64	-	-	-	0.07	-	-	
Qm [kmol/s]		0.15	0.04	0.06	0.57	0.57	0.65	
Composition								
xCH4	-	-	-	-	4.43%	4.43%	0.39%	-
xC2H4	-	-	-	-	2.00%	2.00%	0.00%	-
xCO	-	-	-	-	14.56%	14.56%	19.02%	-
xCO2	-	-	-	-	17.23%	17.23%	15.82%	-
xH2	-	-	-	-	19.95%	19.95%	29.93%	-
xH2O	-	100.00%	100.00%	-	40.21%	40.21%	33.27%	-
xO2	-	-	-	95.00%	-	-	0.00%	-
xN2	-	-	-	2.00%	1.28%	1.28%	1.18%	-
xAr	-	-	-	3.00%	0.32%	0.32%	0.37%	-
zCaO	-	-	-	-	-	-	-	-
zCaCO3	-	-	-	-	-	-	-	-
zCchar	-	-	-	-	100%	-	-	100%
yBio	100%	-	-	-	-	-	-	-
yash	-	-	-	-	100%	-	-	-

3.2.1.1. Syngas cleaning & conditioning

Syngas conditioning and cleaning section is necessary to modify the syngas composition after the reforming, in order to make it compliant with the requirements of the methanol synthesis section. The WGS reactor and the acid gas removal unit operations work in sequence to achieve a syngas module of 2.05, required at the inlet of the methanol reactor. M is imposed equal to 2.05 with a low H_2 excess with respect to M=2, to avoid damages to the catalyst [28].

A heat exchanger is necessary to lower the temperature of the syngas before it enters the shift reactor because the latter operates at 250 °C (further cooling is stopped to avoid tar deposition). The heat generated during this process is recovered in a heat recovery steam cycle. Temperature is chosen according to the low temperature catalysts available on the market, typically Cu – Zn and Cu – Mn [70]. WGS reactor is modelled as an adiabatic RGibbs block where only the water gas shift reaction is allowed to take place and inerts are specified. Only a fraction of the total syngas flow rate enters the water gas shift reactor; the flow fraction is regulated by a design specification in order for the synthesis gas entering the methanol hierarchy to reach the correct module M equal to 2.05.

After the WGS, syngas flow has to be cleaned removing the remained impurities; among those, NH_3 and HCL traces must be managed carefully since contribute to downstream catalysts poisoning. To perform this cleaning steps, syngas flow enters in the water scrubber, modelled as a RadFrac block. Cleaned syngas leaves the column at the temperature of 40 °C, whereas water is heated up reaching 100 °C, making water-cooling heat suitable for the air biomass drier as mentioned before.

Proceeding downstream, H_2S conversion to elemental sulphur is performed thorough LIQUID REDOX component (LO-CAT process) [71]. The process, which is able to perform H2S conversion down to 1 ppm, it is a commercial technology; it is modelled in *Aspen Plus*® as a "black-box", following data from Kazemi, et al. [72]. It returns the syngas purified and cooled, taking as input a limited energy consumption. The specific energy consumption of the unit operation is calculated with the Equation (3-4).

$$LIQ - RED_{consumption} = 2.968 \left[\frac{kWh}{lb}\right] * S_{removed} \left[\frac{lb}{h}\right] \quad (3\text{-}4)$$

A multistage intercooled compressor then pressurizes the syngas from 4 to 30 bar to meet the Carbon Capture component requirement, since working at higher pressure supports the absorption of the CO_2. The latter is modelled as a SEP block in the *Aspen Plus*® environment that separates 95% of CO_2 mass flow in the syngas. The low partial pressure of CO_2 requires the adoption of chemical absorption processes; in this case, Methyl-diethanolamine (MDEA), a tertiary amine, is used in aqueous solution. Compared to physical absorption processes, a thermal power for solvent regeneration (i.e., for the reboiler of the stripping columns) is required. Removed CO_2 is compressed and stocked; this procedure allows to reduce the CO_2 emissions and adjust the syngas module M before entering the methanol reactor. The energy consumption for MDEA regeneration is assumed as 1 MJ/kg_{CO2} [69].

After the acid gas removal section, the pressure is increased up to 92 bar to guarantee the 90-bar gas pressure inside the methanol reactor.

3.2.2. Indirect gasification

The indirect gasifier is composed by a dual-fluidized bed: the first bed is the gasifier, where dried biomass is converted to syngas, the second one is the combustor, which provides the thermal load requested by the gasifier.

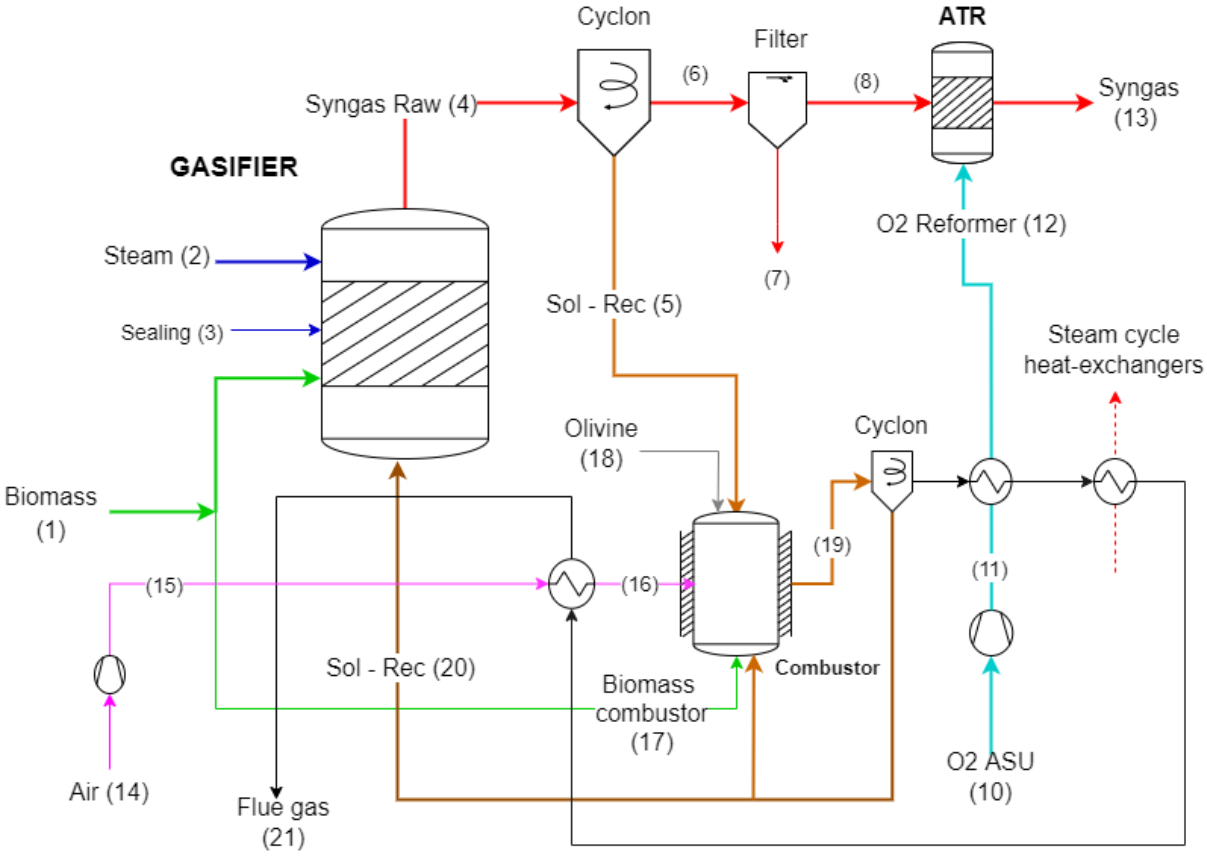

Figure 3-3: indirect gasifier layout

Indeed, the heat request of the gasifier is satisfied with an external system with respect to the oxy-blown system depicted in *3.2.1*. For this reason, in this study it is referred to the configuration as "indirect gasifier".

The external heating system is composed in the following way: part of the dried biomass is diverted to the combustor; the heavy solids separated by the cyclone converged in the latter and the combustion process is performed (in this configuration it is possible to use air as oxidizer in the combustor). An olivine flow represents the thermal vector: they are heated up in the combustor and moving in the gasifier bring the thermal energy necessary to support the gasification reactions.

The gasifier is modelled as an RYield block, while the combustor is an adiabatic RGibbs reactor where temperature and pressure are fixed respectively to 910 °C and 1.43 bar.

A fundamental parameter to allow the correct functioning of the gasifier is the steam to carbon ratio (S/C) that it must be 1 inside the reactor (this value is required by ATR, as mentioned in *section 2.4*).The achievement of the right S/C ratio is attained through a design specification that regulates the slightly superheated steam inlet coming from the backpressure heat recovery steam cycle. Indirect gasifier necessitates a superheated steam flow at the higher temperature of 400 °C (as depicted in Poluzzi et al. [69]), achieved through the exploitation of combustor flue gases, as depicted in the heat recovery steam cycle section.

The gasification section is controlled by a calculator that provides, after mass balances, the outlet syngas composition. The calculator model is based on experimental data taken are calibrated to reproduce the syngas composition from the GoBiGas demonstration plant, Gothenburg [73]; recoverable residual char is fixed as: 17% of the total carbon inlet . The amount of carbon that remains solid (fixed carbon) is nested in the char recovery term.

The gasification model exploits the partial chemical equilibrium of a WGS reaction to compute the syngas output composition, following the Equation (3-6) and (3-7). The so called $pdelta$ parameter, listed in Equation (3-5), regulate the final composition with respect to equilibrium constant K_{eq}.

$$pdelta = \log_{10} \frac{K_{eq}}{K(T)} = -0.18 \tag{3-5}$$

$$Log_{10}K(T) = -2.4198 + 0.0003855 * T_{gas} + 2180.6/T_{gass} \tag{3-6}$$

$$Keq = \frac{\prod \dot{n}_{wgs,products}}{\prod \dot{n}_{wgs,reactants}} \tag{3-7}$$

$Pdelta$ allows to keep the distances from the reaction chemical equilibrium; in this way it is possible to control the progress of the reaction. This parameter depends on the reactor temperature.

Following the scheme reported in *Figure 3-3*, the indirect gasifier employees a boil-bed separator and a cyclone used for separating the solid components from the syngas as olivine, char and ashes that will be recirculated in the combustor.

After these treatments the syngas enters an Auto Thermal Reformer (ATR) reactor, where any remaining tar presents in the syngas are converted and the presence of CO

and H_2 is increased with respect to CO_2. In this rector the chemical equilibrium is assumed, and the inlet oxygen flow rate is regulated to obtain a set point temperature of 800 °C of the outlet syngas following the steam methane reforming reaction, equation.

The reactor is designed to convert the 90% of methane and reach the complete conversion of all the others higher hydrocarbons. The main gasifier operative points are reported in *Table 3-4*.

Table 3-4: indirect gasifier operative points.

Gasifier operative conditions. In the table there are three mass flow rates related to mixed (Gm), conventional (Gc), and non-conventional (Gnc) Aspen Plus © compounds. Molar flow rate Qm is related to mixed compounds. The composition section is divided in molar composition (x) for mixed compounds, mass composition (y) for non-conventional compounds, and mass composition (z) for conventional compounds.

	Streams													
Variable	Biomass feed	Steam - in	Steam sealing	Burner air	Syngas raw	Syngas raw	Syngas raw	Combustor biomass	Solid recycle	Olivine make up	Combustor recycle	Combustor out	Solid recycle	Flue gases
	(1)	(2)	(3)	(16)	(4)	(8)	(13)	(17)	(5)	(18)	(20)	(19)	(20)	(21)
T [°C]	80.00	400.00	400.00	270.00	815.00	815.00	800.00	80.00	814.78	25.00	909.55	909.55	909.55	910.00
P [bar]	1.01	3.90	3.90	1.60	1.43	1.23	1.10	1.01	1.43	1.01	1.43	1.43	1.43	1.43
Gm [kg/s]	-	2.62	0.69	11.65	8.72	8.72	9.21	-	-	-	-	12.99	-	12.99
Gc [kg/s]	-	-	-	-	165.66	-	-	-	165.66	0.28	60.88	226.40	226.17	0.23
Gnc [kg/s]	5.71	-	-	-	4.11	-	-	3.70	4.11	-	1.50	5.62	5.56	0.06
Qm [kmol/s]		0.15	0.04	0.40	0.47	0.47	0.55		1.03	0.00		0.43		0.43
	Composition													
xCH4	-	-	-	-	6.07%	6.07%	0.52%	-	-	-	-	-	-	-
xC2H4	-	-	-	-	1.61%	1.61%	0.00%	-	-	-	-	-	-	-
xCO	-	-	-	-	14.47%	14.47%	17.90%	-	-	-	-	-	-	-
xCO2	-	-	-	-	12.48%	12.48%	12.84%	-	-	-	-	15.90%	-	15.90%
xH2	-	-	-	-	27.99%	27.99%	40.57%	-	-	-	-	-	-	-
xH2O	-	100%	100%	-	36.25%	36.25%	27.05%	-	-	-	-	8.20%	-	8.20%
xO2	-	-	-	20.70%	-	-	0.00%	-	-	-	-	3.00%	-	3.00%
xN2	-	-	-	77.30%	1.11%	1.11%	1.01%	-	-	-	-	71.98%	-	71.98%
xAr	-	-	-	0.97%	0.00%	0.00%	0.08%	-	-	-	-	0.90%	-	0.90%
zCaO	-	-	-	-	-	-	-	-	-	-	-	-	-	-
zCaCO3	-	-	-	-	-	-	-	-	-	-	-	-	-	-
zCchar	-	-	-	-	100%	-	-	-	3.42%	-	-	-	-	-
zOlivFE	-	-	-	-	-	-	-	-	39.44%	40.84%	40.84%	40.84%	40.84%	40.84%
zOliveMG	-	-	-	-	-	-	-	-	57.13%	59.16%	59.16%	59.16%	59.16%	59.16%
yBio	100%	-	-	-	-	-	-	100%	-	-	-	-	-	-
yash	-	-	-	-	100%	-	-	-	100%	-	100%	100%	100.00%	100%

3.2.2.1. Syngas cleaning & conditioning

Cleaning and conditioning sections are modelled in the same way for the two types of gasifiers. However, since the composition of the syngas leaving the gasification section is different, consequently the regulation of its composition differs between the two cases. Syngas exiting ATR respectively exhibits a syngas module of 0.43 and 0.9 for direct and indirect configurations. In the former case, M is adjusted through WGS reaction. Conversely, given the higher starting value, in this second case regulation of CO_2 rate of removal is enough to obtain the desired module composition for methanol

synthesis. The WGS reactor is not required and hence, after the reformer, the flow is cooled down to 220 °C to comply with the requirements set by the syngas cleaning components, which include a water scrubber, a bulk sulphur removal, an acid gas removal section, and two compressors.

3.3. Key performance indicators

To track plant performances and compare the different type of gasifier adopted the following key performance indicators are used.

Fuel efficiency, η_{fuel} , is calculated as the ratio between the chemical power content of the plant output (in this research study, methanol) and the chemical power content of the inlet of the plant (dry biomass). Both chemical power contents are calculated on LHV basis with the Equation (3-8).

$$\eta_{fuel} = \frac{\dot{m}_{methanol} * LVH_{methanol}}{\dot{m}_{biomass,dry} * LHV_{biomass,dry}} \tag{3-8}$$

Methanol carbon efficiency, $\eta_{MeOH,C}$, reported in Equation (3-9), is calculated as the ratio between the carbon atoms in the product of the plant and the carbon atoms entering in the plant through biomass feedstock.

$$\eta_{MeOH,C} = \frac{\dot{n}_{MeOH} * x_{c,MeOH}}{\dot{m}_{biomass} * \frac{y_{c,biomass}}{MM_C}} \tag{3-9}$$

Biochar carbon efficiency, $\eta_{biochar,C}$, is calculated in Equation (3-10) as the ratio between the carbon atoms in the produced biochar and the carbon atoms entering in the plant through biomass feedstock:

$$\eta_{biochar,C} = \frac{\dot{n}_{biochar}}{\dot{m}_{biomass} * \frac{y_{c,biomass}}{MM_C}} \tag{3-10}$$

Captured carbon efficiency, $\eta_{CO_2,C}$, is obtained in Equation (3-11) as the ratio between the carbon atoms in the captured CO_2 and the carbon atoms entering in the plant through biomass feedstock.

$$\eta_{CO_2,C} = \frac{\dot{n}_{CO_2,captured}}{\dot{m}_{biomass} * \frac{y_{c,biomass}}{MM_C}} \quad (3\text{-}11)$$

Global carbon efficiency, η_C, that consider the carbon in the produced methanol, the captured CO_2 and the biochar respect to the biomass plant feed carbon is depicted in Equation (3-12).

$$\eta_C = \frac{\dot{n}_{MeOH} * x_{c,MeOH} + \dot{n}_{CO_2\ eq,biochar} + \dot{n}_{CO_2} * x_{C,CO_2\ captured}}{\dot{m}_{biomass} * \frac{y_{c,biomass}}{MM_C}} \quad (3\text{-}12)$$

Global methanol yield, Y_{global}, is calculated in Equation (3-13).

$$Y_{global} = \frac{\dot{n}_{MeOH,reactor}}{(\dot{n}_{CO} + \dot{n}_{CO_2})_{MeOH\ synthesis\ section\ inlet\ syngas}} \quad (3\text{-}13)$$

In formula, $\dot{n}_{MeOH,reactor}$ is the molar production of methanol in the reactor. $\dot{n}_{CO,syngas}$ and $\dot{n}_{CO2,syngas}$ are the molar flows of carbon monoxide and carbon dioxide in the syngas pre recycle. These types of plants boost methanol production through the partial recirculation of light gases, which are by-products of methanol distillation process. The trade-off for recirculation adoption is between boost of methanol yields and reactor size.

At this level of study, is interesting to considered also the single pass methanol yield, $Y_{single\ pass}$, reported in Equation (3-14).

$$Y_{single\ pass} = \frac{\dot{n}_{MeOH,reactor}}{(\dot{n}_{CO} + \dot{n}_{CO_2})_{MeOH\ reactor\ inlet\ syngas}} \quad (3\text{-}14)$$

With this parameter it is possible to track how much carbon goes from syngas into methanol during the synthesis process.

E_{CO_2} parameter shows CO_2 emissions in grams per kilograms of useful output produced as depicted in Equation (3-15).

$$E_{CO_2}\left[\frac{g\mathrm{CO}_2}{kg_{MeOH}}\right] = \frac{\dot{m}_{CO_2,emitted}}{\dot{m}_{MeOH}} \tag{3-15}$$

$\dot{m}_{CO_2,emitted}$ includes carbon dioxide in the vented flue gases. In this parameter, the CO_2 captured through CCS with MDEA is not accounted as emission.

Cold Gas Efficiency (CGE) is calculated as reported in Equation (3-16).

$$CGE_{unit\ operation} = \frac{\dot{m}_{product} LHV_{product}}{\dot{m}_{feeding} LHV_{feeding}} \tag{3-16}$$

CGE represent the chemical efficiency of the processes and it is calculated as the ratio between the product chemical power content and reactant the chemical power content (LHV based) of a component. For this parameter the unit operations considered are:

- Gasifier, with raw syngas as product and biomass as feed
- WGS reactor, with shifted syngas as product and raw syngas from gasifier as feeding
- Methanol reactor, with raw methanol as product and conditioned syngas as reactor feeding

Net Gasifier Efficiency (NGE) defined and reported in Equation (3-17) takes in account the thermal power of the implemented resistances as energy input.

$$NGE = \frac{\dot{m}_{syngas} LHV_{syngas}}{\dot{m}_{biomass,dry} LHV_{biomass,dry} + P_{th,resistances}} \tag{3-17}$$

NGE can be assimilated to a cold gas efficiency since it does not take into account the temperature of the products but only their LHV. It differs from the latter because it

weighs the performance of an electrified reactor over the total power input (i.e., reactant LHV plus electrical power).

The CO conversion of the WGS reactor, that represents the amount of CO converted into CO_2 through the water gas shift reactor, is computed in Equation (3-18).

$$\eta_{CO,WGS} = \frac{\dot{n}_{CO_2,out} - \dot{n}_{CO_2,in}}{\dot{n}_{CO,in} - \dot{n}_{CO,out}} \quad (3\text{-}18)$$

3.4. Methanol synthesis

After cleaning and conditioning sections, syngas is sent to the methanol synthesis hierarchy, *Figure 3-4*, which presents the same layout for both direct and indirect gasifier plants.

Syngas enters this section with the fixed module 2.05 and it is mixed with a recycle stream to increase the overall methanol conversion. The recycle stream is composed by light-gases (mainly H_2) coming from methanol distillation column; mixing process raises the module entering the reactor up to 10. The trade-off for recirculation adoption is between boost of methanol yields (which raises as recirculation flow rate raises) and reactor size. An *Aspen Plus*® design specification fixes recirculation ratio (RR, ratio between molar flow rate of the recycle stream and entering syngas) at the value of 5 [54].

Subsequently, mixed syngas enters a heat exchanger that recover the heat from the reactor outlet and heat up the inlet flow to match the catalyst temperature range; than syngas enters the synthesis reactor.

Methanol reactor is a Lurgi multi-tubular reactor, which works at the fixed pressure of 90 bar. Temperature control is managed through the evaporation water at 32.2 bar: in this way possible overheating due to exothermic methanol reactions is avoided and a stream of saturated steam is generated.

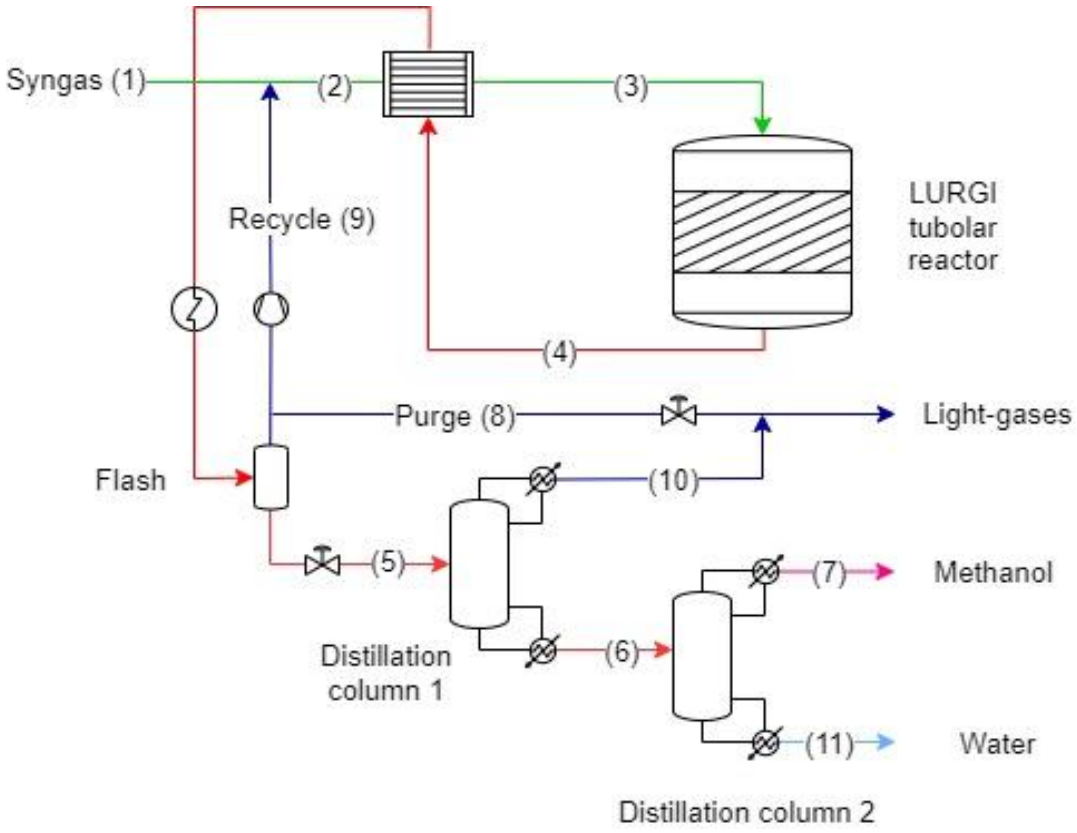

Figure 3-4: methanol synthesis layout scheme

The methanol reactor taken in consideration in this thesis is an *Aspen Plus*® model realized in the work of Poluzzi, at al [69]. The reactor is modelled as an RPlug block and it operates with a Vanden Bussche (VB) kinetics [74], with a gas hourly space velocity equal to 5000 $Nm^3/h/m^3_{cat}$ [69]. Reactor design specifications are reported in *Table 3-5*. Other parameters such as bed voidage, pressure drop across the reactor, diameter and sphericity of the particles are computed by a dedicated calculator; pressure drops are derived with Ergun correlation. The catalyst employed is the low temperature commercial $Cu/ZnO/Al_2O_3$ [69].

Table 3-5: methanol reactor design specification

Heat transfer coefficient (U), [kW/m^2-K]	0.6
Number of tubes	4336
Tube length, [m]	6
Tube diameter, [m]	0.04
GHSV (gas hourly space velocity), [$Nm^3/h/m^3_{cat}$]	5000

3.4.1. Methanol distillation

Raw methanol stream need cleaning to be compliant with commercial specific.

The stream firstly enters two recuperative heat exchanger; the first one preheats the syngas entering the methanol reactor, whereas the second one further cool down the products down to 40°C; this temperature is set to enable flash separation of the light gases inside the stream from the liquid phase, which is rich in methanol.

The methanol remaining in the bottom product is recovered in the distillation section to obtain commercial methanol with 99.85% mass purity.

The first column separates remaining light gases traces, which include unconverted hydrocarbons (i.e., synthesis by-products due to metallic catalysts), inerts (Ar, N_2) and de-hydration compounds (i.e., H_3COCH_3, $HCOOCH_3$). The second one removes heavier compounds, such as alcohols and water. The heat duty of the two reboilers coupled to the columns is provided by a feed of superheated steam from the heat recovery section.

Light gases exiting the first column are mixed with the ones coming from the flash; this purge system is fundamental to avoid the build-up of inert components inside the methanol reactor.

Distillation columns are modelled in in *Aspen Plus®* as RadFrac blocks; design specifications for the two columns are reported in *Table 3-6.*

Table 3-6: methanol distillation columns design specification

	First Column	Second Column
Number plates	20	40
Reflux ratio	0.114	0.368
Distillate to feed ratio	0.022	0.950
Condenser pressure, [bar]	1.35	1.013
Column pressure drop, [bar]	0.35	0
Heat duty, [kW_{th}]	~800	~5500

Light-gases energy potential is then recovered in an internal combustion engine (ICE) generating electrical power. The composition of the light gases from the methanol synthesis is reported *Table* 3-7 and *Table 3-8.*

The internal combustion engine generates around 2 MW of electrical power and the exhaust gases are thermically recovered to produce steam. The *Aspen Plus*® model of ICE was implemented in the thesis work of Catania, et al [75].

3.4.2. Methanol synthesis operative points

In this paragraph methanol synthesis operative points are reported in *Table 3-7* and *Table 3-8* respectively for direct and indirect configurations. Their differences are related to the different gasification methods exploited.

Table 3-7: oxygen blown gasifier methanol synthesis section operative points

	Streams										
Variable	**Syngas feed**	**Syngas recycle**	**Syngas - in**	**MeOH reactor out**	**Light - gases flash**	**Recycle**	**MeOH flash bottom**	**light - gases 1st column**	**MeOH bottom 1st column**	**MeOH**	**Waste Water**
	(1)	**(2)**	**(3)**	**(4)**	**(8)**	**(9)**	**(5)**	**(10)**	**(6)**	**(7)**	**(11)**
T [°C]	115.21	58.01	187.42	238.10	40.00	47.12	41.47	32.28	79.00	64.51	94.68
P [bar]	92.00	92.00	90.16	90.16	86.36	92.00	2.00	1.35	1.70	1.01	1.01
Gm [kg/s]	3.83	32.90	32.90	32.90	29.43	29.07	3.46	0.09	3.38	3.28	0.09
Gc [kg/s]	-	-	-	-	-	-	-	-	-	-	-
Gnc [kg/s]	-	-	-	-	-	-	-	-	-	-	-
Qm [kmol/s]	0.34	2.03	2.03	1.82	1.71	1.69	0.11	0.00	0.11	0.10	0.01
	Composition										
xCH4	0.75%	8.04%	8.04%	8.95%	9.50%	9.50%	0.44%	16.86%	0.00%	-	-
xC2H4	-	-	-	-	-	-	-	-	-	-	-
xCH3OH	-	0.51%	0.51%	6.22%	0.61%	0.61%	93.07%	17.86%	95.09%	99.78%	1.99%
xCO	29.07%	6.42%	6.42%	1.78%	1.89%	1.89%	0.02%	0.82%	0.00%	-	-
xCO2	1.88%	1.56%	1.56%	1.45%	1.49%	1.49%	0.74%	28.39%	0.00%	-	-
xH2	65.31%	46.49%	46.49%	40.16%	42.73%	42.73%	0.26%	9.95%	0.00%	-	-
xH2O	0.00%	0.02%	0.02%	0.31%	0.02%	0.02%	4.76%	0.04%	4.88%	0.18%	97.99%
xO2	-	-	-	-	-	-	-	-	-	-	-
xN2	2.28%	28.79%	28.79%	32.05%	34.09%	34.09%	0.35%	13.54%	0.00%	-	-
xAr	0.72%	8.16%	8.16%	9.08%	9.65%	9.65%	0.32%	12.37%	0.00%	-	-

Table 3-8: indirect gasifier methanol synthesis section operative points

Streams											
Variable	**Syngas feed**	**Syngas recycle**	**Syngas - in**	**MeOH reactor out**	**Light - gases flash**	**Recycle**	**MeOH flash bottom**	**light - gases 1st column**	**MeOH bottom 1st column**	**MeOH**	**Waste Water**
	(1)	**(2)**	**(3)**	**(4)**	**(8)**	**(9)**	**(5)**	**(10)**	**(6)**	**(7)**	**(11)**
T [°C]	115.01	57.63	186.34	238.14	40.00	46.88	41.66	34.10	79.12	64.52	89.25
P [bar]	92.00	92.00	90.16	90.16	86.41	92.00	2.00	1.35	1.70	1.01	1.01
Gm [kg/s]	3.73	27.51	27.51	27.51	24.01	23.78	3.50	0.07	3.43	3.31	0.12
Gc [kg/s]	-	-	-	-	-	-	-	-	-	-	-
Gnc [kg/s]	-	-	-	-	-	-	-	-	-	-	-
Qm [kmol/s]	0.34	2.02	2.02	1.82	1.70	1.69	0.11	0.00	0.11	0.10	0.01
Composition											
xCH4	0.85%	11.38%	11.38%	12.68%	13.48%	13.48%	0.61%	25.89%	0.00%	-	-
xC2H4	-	-	-	-	-	-	-	-	-	-	-
xCH3OH	-	0.49%	0.49%	6.29%	0.59%	0.59%	92.54%	19.49%	94.32%	99.77%	7.95%
xCO	29.16%	6.08%	6.08%	1.38%	1.47%	1.47%	0.02%	0.68%	0.00%	-	-
xCO2	2.08%	1.33%	1.33%	1.15%	1.18%	1.18%	0.58%	24.62%	0.00%	-	-
xH2	66.12%	52.00%	52.00%	46.15%	49.17%	49.17%	0.29%	12.30%	0.00%	-	-
xH2O	0.00%	0.02%	0.02%	0.36%	0.02%	0.02%	5.52%	0.06%	5.65%	0.21%	91.85%
xO2	-	-	-	-	-	-	-	-	-	-	-
xN2	1.65%	26.75%	26.75%	29.82%	31.77%	31.77%	0.32%	13.56%	0.00%	-	-
xAr	0.14%	1.95%	1.95%	2.17%	2.31%	2.31%	0.08%	3.20%	0.00%	-	-

4 Gasifier electrification

The aim of this work is to assess the techno – economic feasibility of electrified biomass gasifiers. To satisfy the gasifier thermal power request in a traditional plant biomass is oxidated; as depicted in *paragraph 3.2.1,* in the direct gasifier oxidation is performed directly in the main reactor (using O2 with purity of 95% as an oxidant), whereas for indirect gasification a dedicated combustor performs an air combustion. Biomass consumption for reactor heating permits to avoid the use of a fossil fuel; nevertheless, in this way process carbon efficiency is reduced. Because renewable biomass is a limited resource, replacing a significant portion of fossil fuels with biofuels entails transferring as much renewable carbon into biofuels as possible.

An alternative way to supply the required thermal power, without reduction of carbon efficiency, is to use electrical resistances through Joule effect.

The electrification of the two gasifiers leads to several advantages depending on the realized models. In addition to the increase in carbon efficiency it is possible to obtain:

- biomass saving
- lower CO2 emissions
- increased methanol production
- production of an extra product (biochar).

Nevertheless, it is important to emphasize the source of origin of this electricity: each country, according to its history, geography and local resource, has developed its own energy mix to satisfy the energy demand, and hence its own greenhouse gas impact (gCO_2/kWh). There's a trade-off between the intrinsic benefit related to the increase in carbon efficiency and the significant share of indirect emissions carried by the used electricity.

Hence, the condition a priori of the current study is to consider as source of electricity a future grid with high penetration of renewable and near-zero specific emission.

As an alternative the feasibility of the application of a solar field coupled with plant is studied; in this way a renewable source for electricity is ensured.

In *paragraphs 4.1, 4.2* and *4.3 Aspen Plus®* models of the electrified gasifiers are illustrated.

Modelling of electrified gasifiers poses a major challenge: the lack of literature and applied case of study. To overcome this scarcity, the models implemented are based on hypotheses and assumptions, critically discussed.

4.1. Direct electrified gasifier: model 1

An oxygen blown gasifier, deprived of the necessary incoming oxygen stream, loses its intrinsic peculiarity: oxy-combustion that provided the thermal demand no longer exists as depicted in *Figure 4-1*.

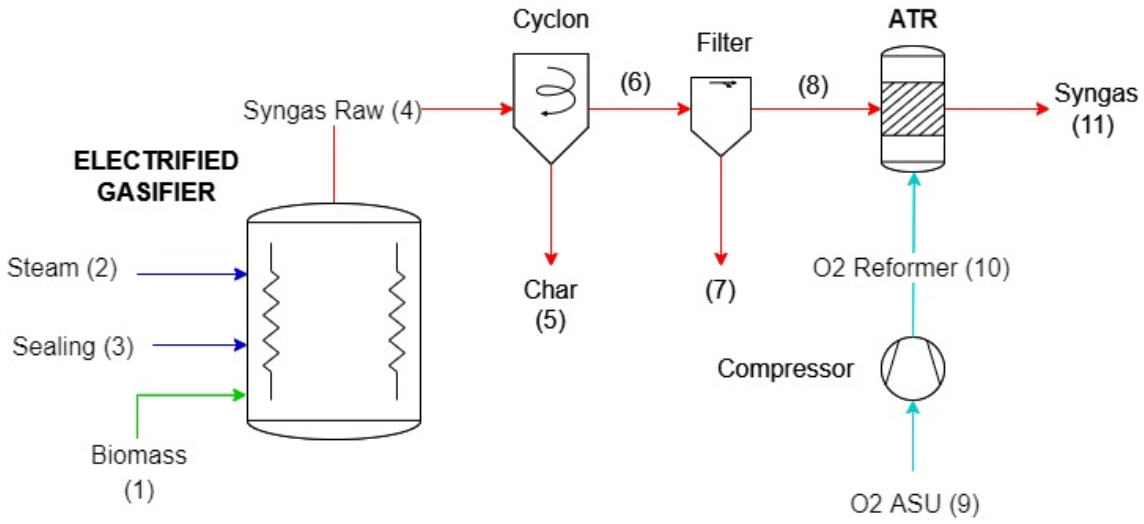

Figure 4-1: electrified direct gasifier plant layout model 1

The implemented electrical resistances cover this heat duty, through Joule effect; the following heating is comparable to an indirect heating since it does not occur by modifying the internal composition of the biomass and produced gas (oxidation no longer affects biomass). For this reason, gasifier performances are aligned with the indirect ones (in that case the heating was equally indirect but was implemented by the recirculation of hot solids). Therefore, modelling hypotheses must take in considerations indirect gasifier assumptions.

As depicted in *section 3.2.1*, gasification is controlled by a calculator that provides, after mass balances, the outlet syngas composition. The fundamental parameters on which the modelling of the reactor is supported are three:

- Recoverable residual char
- Gasifier temperature

- $pdelta = \log_{10} \frac{K_{eq}}{K(T)}$; which regulates the final composition with respect to equilibrium constant K_{eq}

For what concern recoverable residual char, the parameter increases from 4.5% of the inlet carbon (direct gasifier reference value) to 17% (indirect gasifier reference value). Indeed, a gasifier in which no oxy-combustion occurs shows a greater share of residual char with respect to an analogous oxy-blown one where a not negligible part of the carbon is oxidized.

To ensure plant reliability, it is crucial that the switch between baseline case and electric mode does not generate slow transients and maintain the functioning of the gasifier. Hence, gasifier temperature is kept at the constant value of 870°C. For this reason, it is chosen to maintain constant also $pdelta$ value since this parameter varies in function of the reactor temperature.

The kinetics that determines the output from the reactor is therefore the same as in the baseline case, as shown from Equations (3-1), (3-2), and (3-3).

From a technical point of view, to avoid thermal inertia damages during the mode switching phases, the electrical resistances are implemented directly inside the reactor.

Nonetheless it is important to clarify that the stated hypotheses are strong assumptions.

Given the uncertainty of the assumptions, an alternative model is presented in *paragraph 4.2.*

4.1.1. Model results

In this section, the results of the new adopted model are reported in *Table 4-1* and compared with the ones obtain in the baseline case, *section 3.2.1*.

Table 4-1: main operative points of model 1 electrified gasifier

Streams									
Variable	Biomass (1)	Steam-in (2)	Inert-in (3)	Syngas raw (4)	Syngas raw (6)	Syngas raw (11)	ATR oxygen (9)	ATR oxygen (10)	Char (5)
T [°C]	80.00	200.00	200.00	870.00	870.00	915.00	15.00	108.42	870.00
P [bar]	1.01	5.90	5.90	4.00	3.80	3.60	2.00	4.50	4.00
Gm [kg/s]	-	2.97	0.80	10.06	10.06	10.69	0.62	0.62	-
Gc [kg/s]	-	-	-	0.49	-	-	-		0.49
Gnc [kg/s]	6.64	-	-	0.07	-	-	-		-
Qm [kmol/s]		0.16	0.04	0.56	0.56	0.64	0.02	0.02	-
Composition									
xCH4	-	-	-	4.56%	4.56%	0.40%	-	-	-
xC2H4	-	-	-	2.05%	2.05%	0.00%	-	-	-
xCO	-	-	-	16.11%	16.11%	19.94%	-	-	-
xCO2	-	-	-	11.16%	11.16%	11.03%	-	-	-
xH2	-	-	-	29.07%	29.07%	38.81%	-	-	-
xH2O	-	100.00%	100.00%	35.93%	35.93%	28.69%	-	-	-
xO2	-	-	-	-	-	0.00%	95.00%	95.00%	-
xN2	-	-	-	1.10%	1.10%	1.02%	2.00%	2.00%	-
xAr	-	-	-	0.00%	0.00%	0.09%	3.00%	3.00%	-
zCaO	-	-	-	-	-	-	-	-	-
zCaCO3	-	-	-	-	-	-	-	-	-
zCchar	-	-	-	100.00%	-	-	-	-	100%
yBio	100.00%	-	-	-	-	-	-	-	-
yash	-	-	-	100.00%	-	-	-	-	-

Syngas composition that comes out from the gasifier changes. As reported in *Figure 4-3*, the absence of oxygen lead to a lower CO_2 production inside the reactor. Since the model is based on the WGS chemical equilibrium a lack in CO_2 leads to an increase of H_2, CO presence and a decrease H_2O presence. Tar and higher hydrocarbons production remains almost the constant, hence a steam reforming is required. The compositions obtained after the ATR reactor are reported in *Figure 4-2*. Not only compositions are changed but also syngas mass flow rate. Indeed, the absence of oxygen leads to a decrease in the syngas flow rate from 12 kg/s to 10 kg/s.

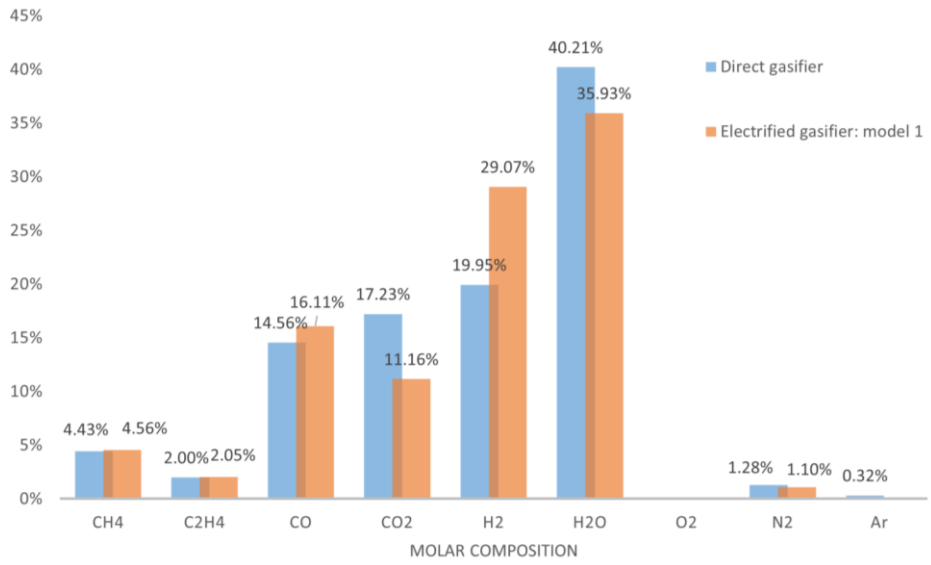

Figure 4-3: molar composition comparison between direct gasifier and model 1 electrified gasifier at gasifier output

Another interesting consequence of the gasifier electrification is the increased production of biochar, generated by the increasing recoverable residual char value.

Biochar is produced as gasifier solid bottom reject and it is recovered as commercial product as explained in *section 1.3*; its production increases from 0.1288 kg/s to 0.4866 kg/s.

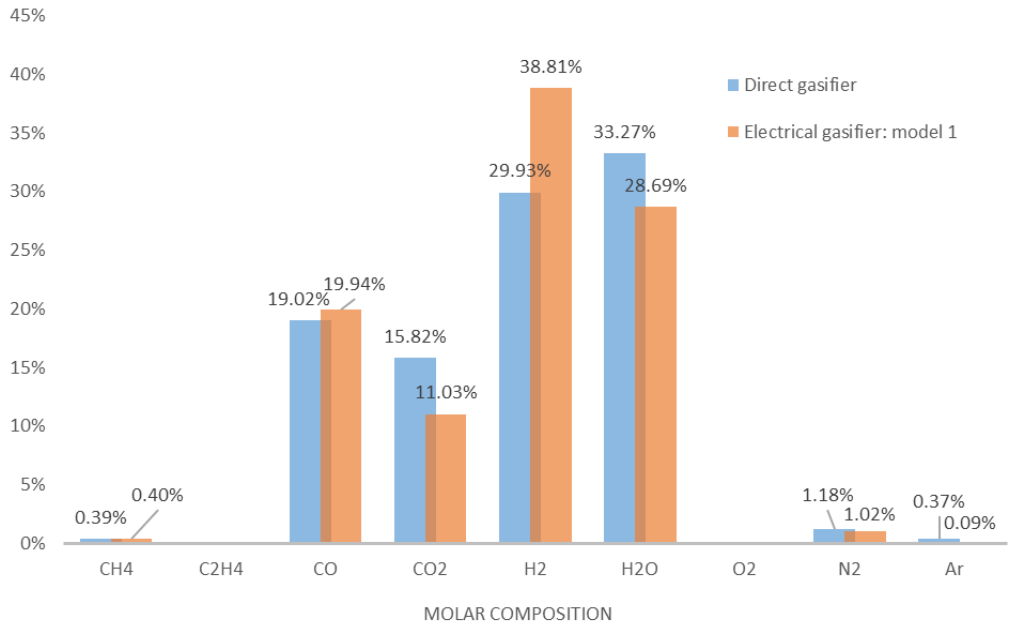

Figure 4-2: molar composition comparison between direct gasifier and model 1 electrified gasifier at reformer output

Moreover, comparing the syngas composition at the reformer output, reported in *Figure 4-2*, it is possible to notice a higher content of H2 and CO and lower content of H2O and CO2..

The module of the syngas entering the methanol reactor increases from 5.63 to 6.88 due to the lower CO2 presence. $Y_{single\ pass}$, reported in Equation (3-14), increases too, from 64% to 72%.

The result is the boost of reactor yields, which generates an increase in methanol production; the latter is achieved also with the support of the higher syngas mass flow rate at the inlet of the methanol reactor

This higher mass flow rate is due to the lower CO_2 captured in the CO_2 separation process. In electrical mode the CO_2 captured is lower simply because it is not produced with oxidation, as mentioned before. Furthermore, for the same reason the scrubber absorbs less water from the syngas.

These effects lead to an increase methanol production from 3.283 kg/s to 3.877 kg/s.

Required electrical power is increased; resistances absorb at full load 23.45 MW of electric power, raising the total require power of the plant up to 29.8 MW. This electric duty can be satisfied by the grid or by the coupled solar field, as explained in *chapter 8*.

4.2. Direct electrified gasifier: model 2

As depicted in *4.1*, the lack of literature and applied case of study complicates the modelling procedures of electrified gasifiers. In direct gasifier model 1, some strong hypotheses are formulated (data from both direct and indirect gasifier models are taken). The results obtained from that model are purely theoretical and could not respect a real behaviour of a direct electric gasifier. In *Figure 4-4* the scheme of the general direct electrical gasifier hierarchy model 2 is reported.

Given the uncertainty of those assumptions, this alternative model is presented.

To gain consistency, this electrified mode needs to consider the original values of recoverable residual char and *pdelta*, obtained from the analysis of experimental from Varkaus plant. The Equations (3-1), (3-2), and (3-3) report the characteristic assumptions of the model. The recoverable residual char of 4,5% of the total carbon inlet and a gasifier temperature of 870 °C complete the model assumptions.

These parameters are valid for a direct gasification (oxy-blown gasifier).

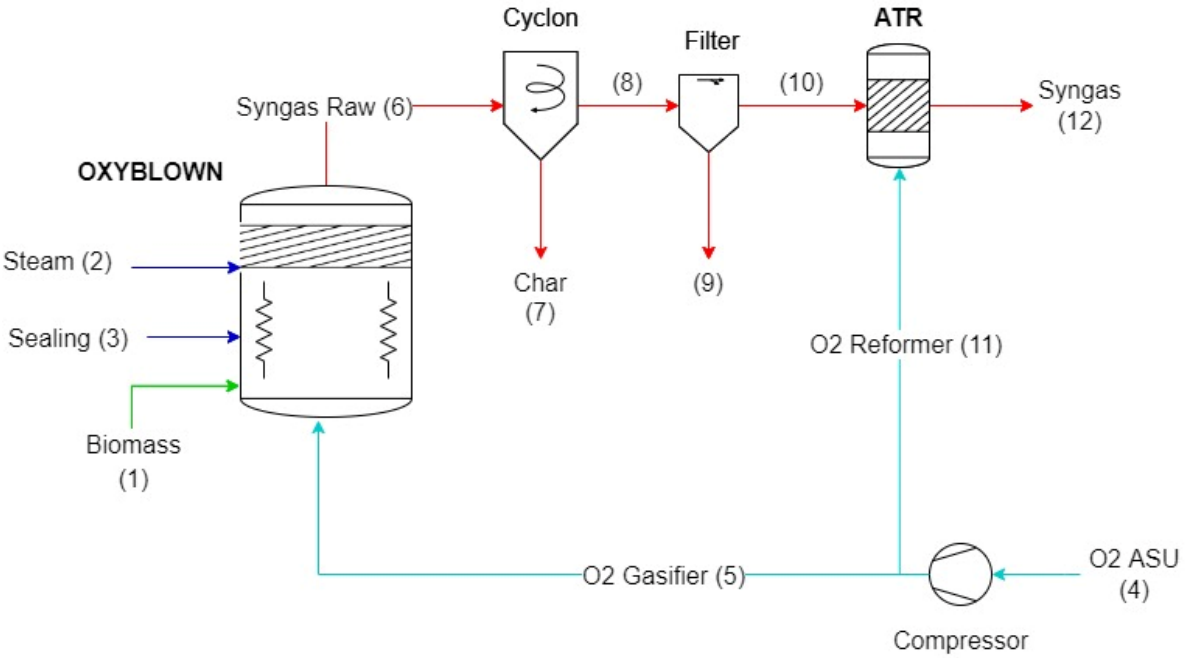

Figure 4-4: direct electric gasifier plant layout model 2

To continue rely on this set of assumptions even with an electrified configuration, it is necessary to keep a minor oxygen feed to the reactor, while the major part of the thermal power is provided with resistances inserted in the reactor. With the same logic, the hybrid operating models reported in the *section 4.2.2.* are realized.

To be compliant with model 1, it is chosen to provide the same 23.45 MW of electric power to the resistors. Keeping the same original kinetics, some extra power is needed and, hence, supplied with a stream of oxygen that passes from 1.93 kg/s (baseline case) to 0.42 kg/s.

4.2.1. Model results

In this section, the results of the new adopted model are reported in *Table 4-2* and compared with the biomass oxidation.

Table 4-2: model 2 gasifier operative points.

Gasifier operative conditions. In the table there are three mass flow rates related to mixed (Gm), conventional (Gc), and non-conventional (Gnc) Aspen Plus © compounds. Molar flow rate Qm is related to mixed compounds. The composition section is divided in molar composition (x) for mixed compounds, mass composition (y) for non-conventional compounds, and mass composition (z) for conventional compounds.

	Streams							
Variable	Biomass (1)	Steam-in (2)	Inert-in (3)	Oxy-gass (5)	Syngas raw (6)	Syngas raw (10)	Syngas raw (12)	Char (7)
T [°C]	80.00	200.00	200.00	108.42	870.00	870.00	915.00	870.00
P [bar]	1.01	5.90	5.90	4.50	4.00	3.80	3.60	4.00
Gm [kg/s]	-	4.27	0.80	0.42	12.14	12.14	12.82	-
Gc [kg/s]	-	-	-	-	0.13	-	-	0.13
Gnc [kg/s]	6.64	-	-	-	0.07	-	-	-
Qm [kmol/s]		0.24	0.04	0.01	0.66	0.66	2662.34	-
	Composition							
xCH4	-	-	-	-	3.85%	3.85%	0.34%	-
xC2H4	-	-	-	-	1.73%	1.73%	0.00%	-
xCO	-	-	-	-	12.63%	12.63%	18.63%	-
xCO2	-	-	-	-	14.95%	14.95%	12.10%	-
xH2	-	-	-	-	30.90%	30.90%	36.32%	-
xH2O	-	100%	100%	-	34.89%	34.89%	31.53%	-
xO2	-	-	-	95.00%	-	-	0.00%	-
xN2	-	-	-	2.00%	0.97%	0.97%	0.92%	-
xAr	-	-	-	3.00%	0.06%	0.06%	0.14%	-
zCaO	-	-	-	-	-	-	-	-
zCaCO3	-	-	-	-	-	-	-	-
zCchar	-	-	-	-	100%	-	-	100%
yBio	100%	-	-	-	-	-	-	-
yash	-	-	-	-	100%	-	-	-

The same considerations made for model 1 with respect to baseline case (no resistances) are applicable to model 2; the only difference is that in this case a residual oxidation of biomass is still present. Hence, with respect to Model 1, syngas stream exiting gasifier hierarchy presents a higher mass flow rate (result of the oxygen injection), a higher CO_2 molar flow (result of the partial oxidation), and a lower char recovery (recoverable residual char pass from 17% to 4,5% of the total carbon inlet).

As a consequence, in Model 2, biochar stream decreases from 0.4886 kg/s (Model 1) to 0.1288 kg/s. However, in this way carbon availability for methanol synthesis production increases; methanol production passes from 3.283 kg/s of the baseline case to 3.877 kg/s of the Model 1 to 4.21 kg/s for Model 2.

A comparison between the electrification models for direct gasifier is reported in *Table 4-3*.

Table 4-3: comparison between electrification models for direct gasifier

	Streams		
Variable	**Direct**	**Model 1**	**Model 2**
MEOH [kg/s]	3.283	3.877	4.212
Biochar [kg/s]	0.129	0.487	0.129
Bio svd [kg/s]	-	-	-
Power consumption [MW]	6.640	28.108	28.981
CO2 captured [kg/s]	5.321653	3.239	4.079
CO2 emissions [kg/s]	0.210193	0.181	0.191
	Syngas out gasfier		
xCH4	0.39%	0.40%	0.34%
xC2H4	0.00%	0.00%	0.00%
xCO	19.02%	19.94%	18.63%
xCO2	15.82%	11.03%	12.10%
xH2	29.93%	38.81%	36.32%
xH2O	33.27%	28.69%	31.53%
xO2	0.00%	0.00%	0.00%
xN2	1.18%	1.02%	0.92%
xAr	0.37%	0.09%	0.14%
	Syngas inlet methanol sysnthesis		
xCH4	0.75%	0.65%	0.60%
xCH3OH	-	-	-
xC2H4	-	-	-
xCO	29.07%	30.65%	30.46%
xCO2	1.88%	1.00%	1.16%
xH2	65.31%	65.88%	65.93%
xH2O	-	-	-
xO2	-	-	-
xN2	2.28%	1.68%	1.61%
xAr	0.72%	0.15%	0.25%

4.2.2. Direct configuration hybrid modes

The modelling of partial electric hybrid plants makes again evident the lack of literature and, as a consequence, the weakness of models developed on the basis of strong hypotheses. To hedge against uncertainty of assumptions, direct hybrid modes are designed taking direct gasifier Model 2, depicted in *section 4.2*, as a case reference.

Starting from baseline mode, hybrid cases are designed progressively decreasing the mass flow rate of oxygen into the gasifier.

According to Klein et al [76], state-of-the-art air separation units can be operated in load-flexible mode with a reduction of the overall process efficiency. To design a load-flexible ASU with optimal efficiency in each operating point, it is necessary to adapt ASU operation to the variable load, implementing dynamic process regulations and control strategies.

Reducing oxygen flow rate, biomass oxidation, that is responsible of the required thermal power supply, is decreased and as consequence the gasifier needs extra thermal power to allow the biomass gasification. The latter is given by the electrical resistances functioning at partial load. The starting model is the direct configuration with the oxygen blown reactor: gasification model remains the same used into the oxygen blown direct configuration explained in *section 3.2.1.*

With the progressive starting of the resistors, a considerable part of raw material is not completely oxidized: the result obtained at the exit of the reactor is a syngas stream of lower mass flow and different composition. The lower mass flow is justified with the reduction of oxygen; nevertheless, the lack of oxidation of part of the biomass causes the syngas leaving the gasifier to be richer in CO and poorer in CO_2. As consequence, after CO_2 removal, the new stream entering the methanol synthesis section presents a higher mass flow rate and, hence, a higher methanol production.

Following this modelling logic, three hybrid configurations are realised: DIR_EL_25%, DIR_EL_50% and DIR_EL_75%. The percentage is referred to the thermal power required by the gasifier in the full electric direct configuration (i.e. 23.45 MW_{th}).

Being built on the basis of the logic implemented in the direct electrified gasifier Model 2, the results of the hybrid modes are perfectly connected with the two utmost operating points of the system (i.e., baseline case and electrified gasifier Model 2).

Conversely, since the adopted assumptions model differs, hybrid mode results are not compatible with electrified gasifier model 1.

Model 2 is then chosen as the definitive model for complete electrification; due to the fact that the model share design methodology with the hybrid modes, in the later part of the current study it is referred to it as DIR_EL_100%.

Nonetheless, moving forward in the analysis, the results and considerations associated with the Model 1 are reported to provide a critical comparison; in this way it is intended to highlight the differences that can arise from two different sets of assumptions.

The results of the investigated operative points are reported in *Appendix A*.

4.2.2.1. Direct hybrid maps

In this section, hybrid mode results are reported and critically discussed; the purpose is to realize the so-called "hybrid maps" that illustrate the trends of peculiar quantities of interest as an increasing share of resistances is switched on.

In the following diagrams the main plant parameters are reported:

- Methanol production
- Biochar production
- CO_2 emissions
- Captured CO_2
- Power consumption
- Gasifier O_2 consumptions

Starting from the main product of the plant, reported in *Figure 4-5*, methanol, electrification results in a constant positive increase of production switching from oxygen blown (0% electrification) to the full electric configuration.

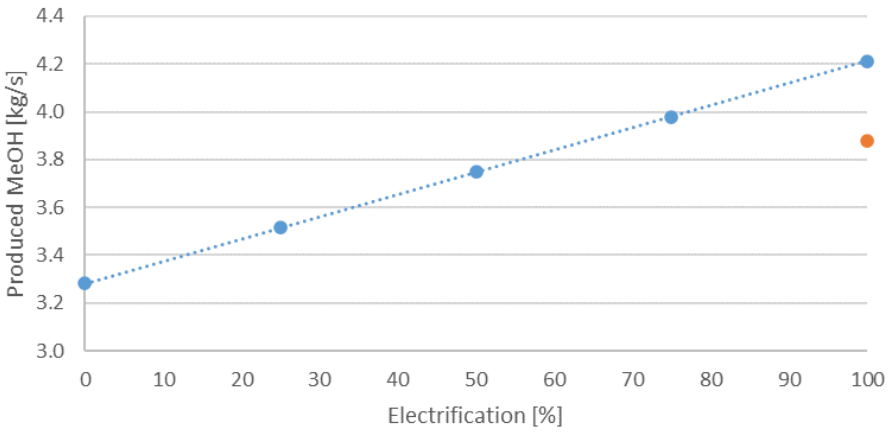

Figure 4-5:methanol production with respect to the electrification of the gasifier

The lack of oxygen during the operation of the resistances leads to a lower CO_2 production in favour of CO generation. With the progressive starting of the resistors, a considerable part of raw material is not completely oxidized: the result obtained at the exit of the reactor is a syngas stream of lower mass flow and different composition. As depicted in *paragraph 4.1*, the lower mass flow is justified with the reduction of oxygen; nevertheless, the lack of oxidation of part of the biomass causes the syngas leaving the gasifier to be richer in CO and poorer in CO_2. As consequence, after CO_2 removal, the new stream entering the methanol synthesis section presents a higher mass flow rate, hence a higher methanol production with respect to the oxygen blown configuration.

In *Figure 4-5*, it is possible to notice the discrepancy of the models adopted. Indeed, electrified gasifier designed with Model 1 is realised with the specifics of an indirect gasifier as aforementioned in *section 4.1*. The presence of a larger recoverable residual char in the gasifier model and the absence of oxygen leads to a lower syngas mass flow rate and lower CO_2 production with respect to DIR_EL_100% (i.e., Model 2). This decrease affects the methanol synthesis reactor that produces a lower mass flow rate of methanol since, after the CO_2 removal, mass flow rate entering synthesis section is considerably lower with respect to the one in DIR_EL_100% (4.26 vs 4.64 kg/s).

As reported in *Figure 4-6*, biochar production remains constant during oxygen blown and hybrid modes functioning, whereas it faces a step increase for Model 1.

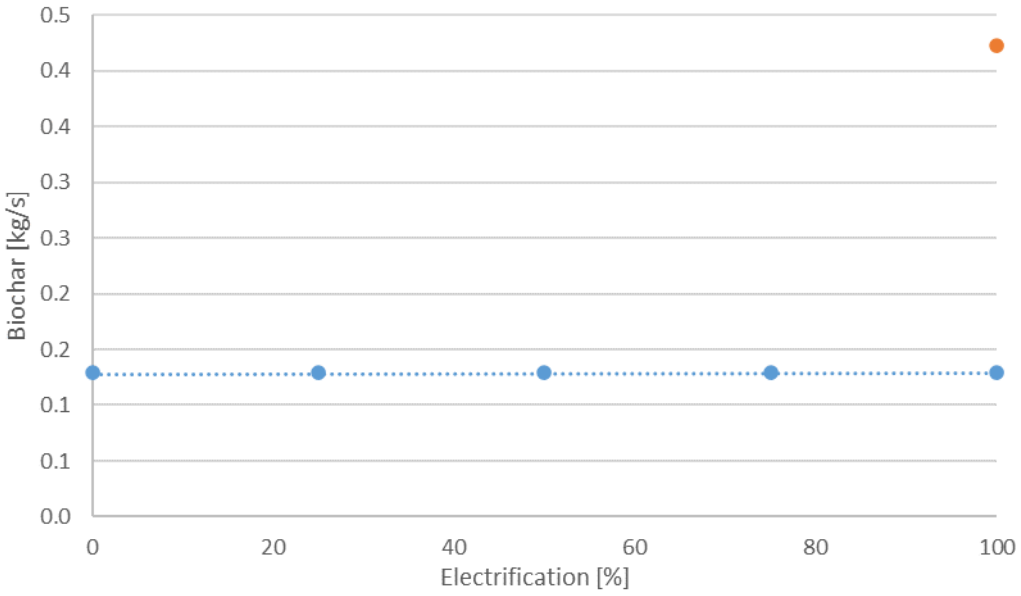

Figure 4-6: biochar production with respect to the electrification of the gasifier

This trend is related to the different recoverable residual char hypotheses adopted for the gasifiers. Hybrid modes gasifiers adopt the same gasification model of the oxygen blown reactor, while Model 1 adopts the indirect gasification value, hence, a higher recoverable residual char (4,5% vs 17% of inlet carbon).

For what concern CO_2 emissions and captured ones the trends are reported in *Figure 4-7*.

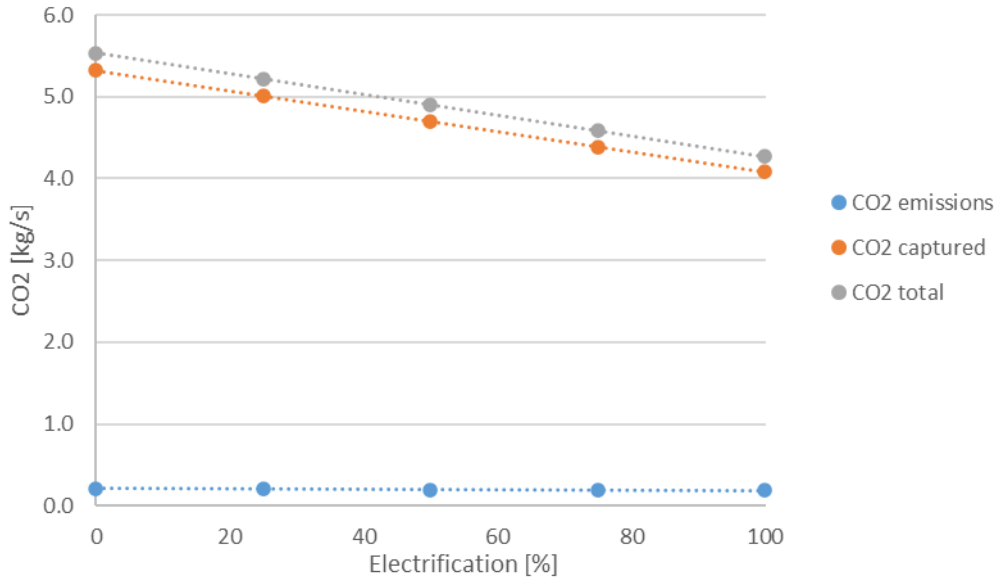

Figure 4-7: CO_2 produced with respect to the electrification of the gasifier

It is possible to notice a decrease in the CO_2 captured by switching on the electric resistances. The phenomenon stems from the CO_2 capture system implemented; the capture percentage is fixed at 95% of the mass flow rate of CO_2 presents in syngas for all the plants. Low oxygen presence in the gasifier results in a lower CO_2 concentration in the syngas; hence, capture system separates less CO_2 where a greater oxidation has occurred.

From *Figure 4-7*, it is not possible to appreciate the slightly decreasing trend of the CO_2 emissions into atmosphere (from 0.21 kg/s to 0.18 kg/s). The direct emissions of direct/hybrid direct plants are only related to carbon dioxide presents in ICE flue gases which is ultimately vented in atmosphere. This emission term decreases switching to electric mode because the presence of carbon species in the light–gases is reduced.

Power consumption trends are reported in *Figure 4-8*.

Requested resistances power increases linearly since the hybrid models are realized linearly rising electric power load. Proceeding with the switch on of the resistances,

variations in the electrical production of the Heat Recovery Steam Cycle (HRSC) occur; furthermore, as the oxygen request from the gasifier decreases, as reported in *Figure 4-9*, the electrical consumption of Air Separation Unit (ASU) has a minor weight on the total required power. Those variations are highlighted in the diagram in the plant base operations load trendline.

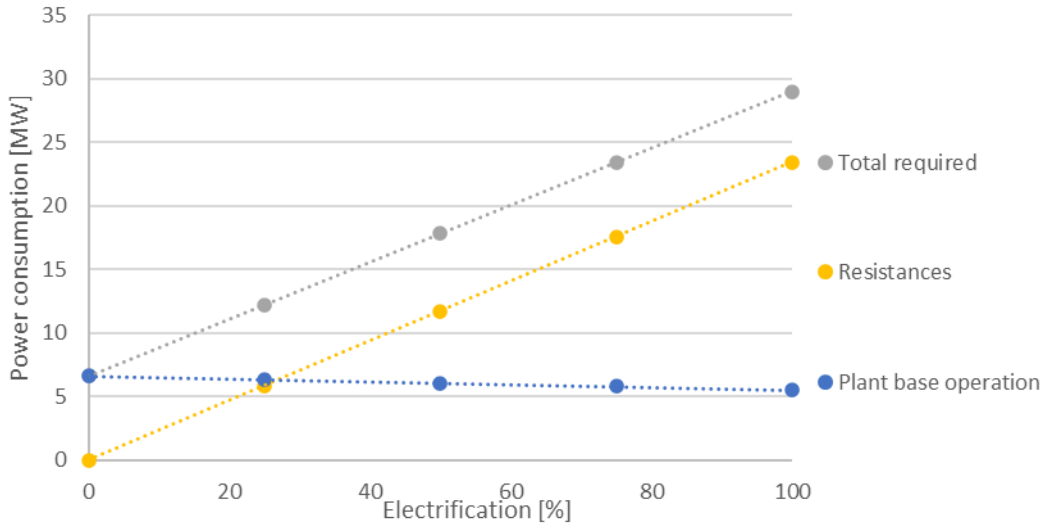

Figure 4-8: power consumption of resistances, plant base operation and total required with respect to the electrification of the gasifier

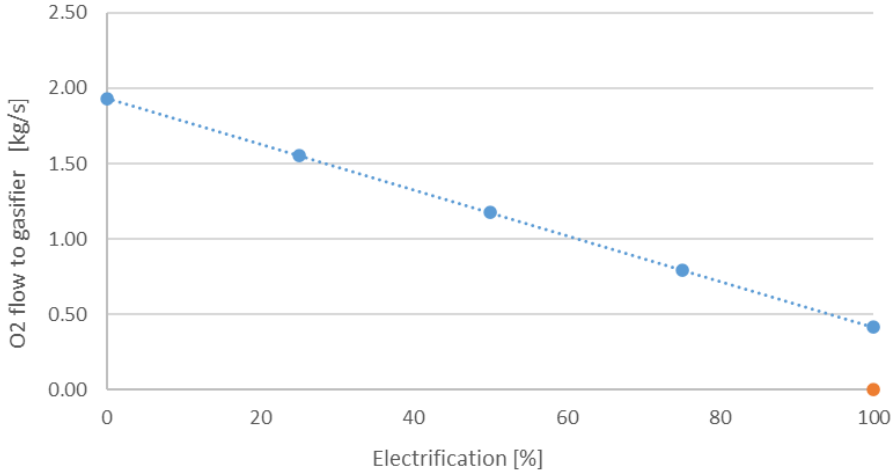

Figure 4-9: O_2 consumption with respect to the electrification of the gasifier

4.3. Indirect electrified gasifier

In order to model the electrified indirect plant, it is possible to maintain the indirect configuration and model. The gasifier model and assumptions are the same described in section 3.2.2.

The electrical resistances are implemented in the gasifier to supply the required thermal power. When electric mode is on, the olivine solid flow is maintained to keep the combustor warm and decrease the thermal inertia problems of the combustor itself.

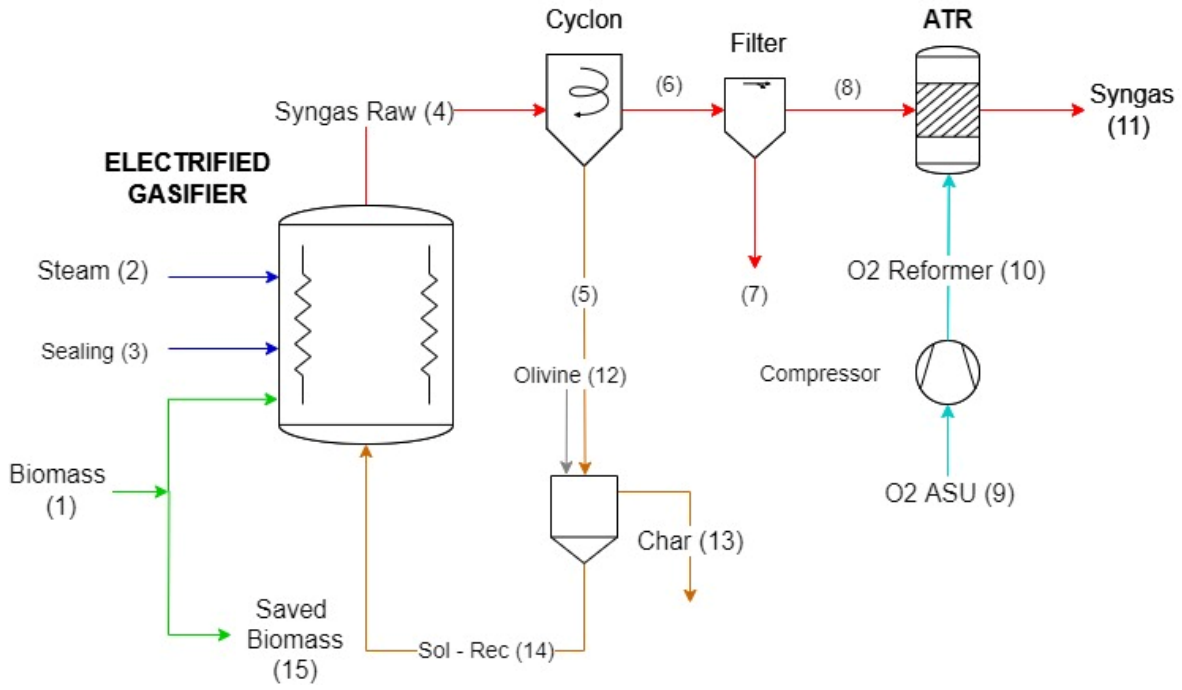

Figure 4-10: indirect electric gasifier plant layout

Comparing the two operative modes it is possible to notice that in electric mode the combustor does not work, hence there's no possibility to recover flue gases that have a key role into the heat recovery steam cycle. This lack of thermal power leads to changes in the steam cycle configuration as described in *section 5.2*.

The gasifier plant scheme remains almost unaltered as shown in *Figure 4-10*. There is no combustor and as consequence no air streams and flue gases.

4.3.1. Model results

In *Table 4-4* the results are reported. This model is set to maintain the same amount of biomass feed into the gasifier, hence there is no off-design of the plant (methanol production remains constant).

The main advantage of the electric mode is biomass saving and biochar production. Biochar is not produced in the normal functioning of the gasifier because it is recirculated into the combustor to contribute to the thermal request. In electric mode biochar is separated as commercial product since there is no needing to burn it.

Another difference between the two modes are CO_2 emissions, that pass from 979.8 to 63.43 gCO_2 per kg of produced methanol, thanks to lack of combustor flue gases (previously vented in atmosphere).

Resistances absorb at full load 17.89 MW of electric power, raising the total require power of the plant up to 23.77 MW. This electric duty can be satisfied by the grid or by the coupled solar field, as explained in chapter *8*.

The electrical power required by the resistances of the indirect gasifier is lower than the one required by the direct gasifier. The reason is the type of modelling: in the indirect case it is chosen to save the biomass previously fed to the external combustor. Conversely, in the direct case, since the oxidation took place inside the oxy-blown reactor itself, the flow rate to the reactor remains unchanged. Consequently, in the direct model a flow rate of 6.64 kg/s of biomass enters the reactor, whereas in the indirect only 5.71 kg/s. From this difference in flow rates descends the higher electrical power required by the direct electrified gasifier and, as a consequence, the higher methanol production.

Table 4-4: Indirect electric gasifier operative points.

In the table there are three mass flow rates related to mixed (Gm), conventional (Gc), and non-conventional (Gnc) Aspen Plus © compounds. Molar flow rate Qm is related to mixed compounds. The composition section is divided in molar composition (x) for mixed compounds, mass composition (y) for non-conventional compounds, and mass composition (z) for conventional compounds.

	Streams											
Variable	**Biomass feed (1)**	**Steam - in (2)**	**Steam sealing (3)**	**ATR oxygen (10)**	**Syngas raw (4)**	**Syngas raw (8)**	**Syngas raw (11)**	**Solid recycle (14)**	**Solid recycle (5)**	**Olivine make up (12)**	**Biochar (13)**	**biosaved (15)**
T [°C]	80.00	400.00	400.00	270.00	815.00	815.00	800.00	910.00	814.50	25.00	814.28	80.00
P [bar]	1.01	3.90	3.90	1.60	1.43	1.23	1.10	1.01	1.01	1.01	1.01	1.01
Gm [kg/s]	-	2.76	0.69	11.65	8.87	8.87	9.38	-	-	-	-	-
Gc [kg/s]	-	-	-	-	164.50	-	-	164.14	164.63	0.07	0.42	-
Gnc [kg/s]	6.64	-	-	-	3.24	-	-	3.18	3.18	-	-	0.93
Qm [kmol/s]		0.15	0.04	0.40	0.48	0.48	0.56	0.99	1.02	0.00	0.04	-
	Composition											
xCH4	-	-	-	-	5.96%	5.96%	0.52%	-	-	-	-	-
xC2H4	-	-	-	-	1.58%	1.58%	0.00%	-	-	-	-	-
xCO	-	-	-	-	12.50%	12.50%	17.29%	-	-	-	-	-
xCO2	-	-	-	-	14.00%	14.00%	12.99%	-	-	-	-	-
xH2	-	-	-	-	29.24%	29.24%	40.10%	-	-	-	-	-
xH2O	-	100.00%	100.00%	-	35.61%	35.61%	28.00%	-	-	-	-	-
xO2	-	-	-	20.70%	-	-	0.00%	-	-	-	-	-
xN2	-	-	-	77.30%	1.09%	1.09%	1.00%	-	-	-	-	-
xAr	-	-	-	0.97%	0.00%	0.00%	0.09%	-	-	-	-	-
zCaO	-	-	-	-	-	-	-	-	-	-	-	-
zCaCO3	-	-	-	-	-	-	-	-	-	-	-	-
zCchar	-	-	-	-	100.00%	-	-	-	3.45%	-	100.00%	-
zOlivFE	-	-	-	-	-	-	-	40.84%	39.44%	40.84%	-	-
zOliveMG	-	-	-	-	-	-	-	59.16%	57.12%	59.16%	-	-
yBio	100.00%	-	-	-	-	-	-	-	-	-	-	100.00%
yash	-	-	-	-	100.00%	-	-	100.00%	100.00%	-	-	-

4.3.2. Indirect configuration hybrid modes

In the indirect baseline configuration, part of the biomass is diverted to the combustor; from heat released by combustion the thermal load of gasifier is satisfied. Modelling of hybrid modes is then realised by simply regulating the mass flow rate of biomass into the gasifier combustor.

In this way the biomass combustion is reduced and as consequence the gasifier needs an extra power to satisfy the thermal request of the indirect gasifier. The thermal power gap is covered by the implemented electrical resistances functioning at partial load.

The starting model is the indirect configuration with the dual-fluidized bed configuration. Gasification model remains the same used for indirect gasification because the inlets streams to the gasifier remains the same; the only change is in the thermal power supply method. In *Figure 4-11* the modified *Aspen Plus*® layout scheme used for indirect hybrid modes is reported.

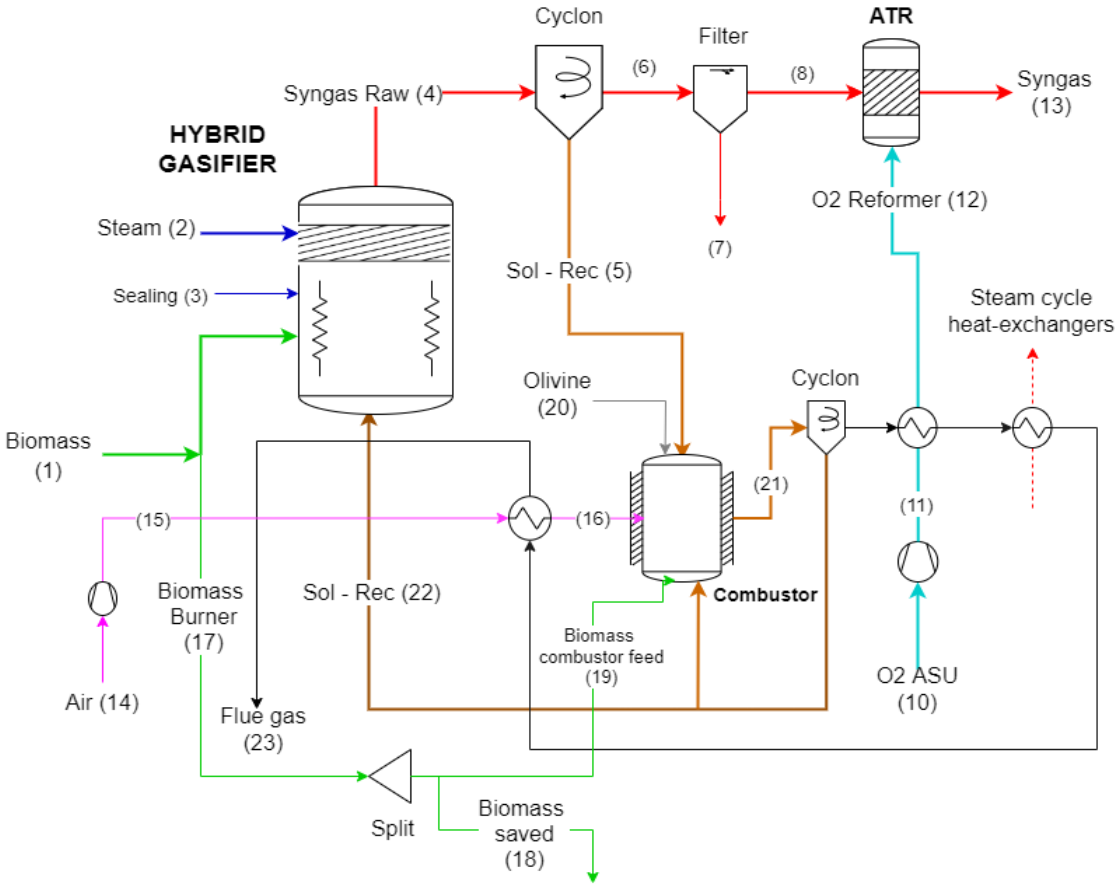

Figure 4-11: indirect hybrid modes plant configuration

As shown in *Figure 4-11*, an increasing part of the dry biomass (stream 17) is removed and saved (stream 18). In this way the thermal power derived from biomass oxidation is reduced and hybrid modes are generated.

The hybridization percentage, in this case, is not related to the electrical power of the resistances since the regulation system is based on biomass flow rate reduction. From the analysis, it is possible to state that there isn't a linear proportion between the reduction of biomass combustor feeding and the electrical power needed by the resistances to fulfil the gasifier thermal request. Following this model, mode 25%/50%/75%/100% biomass saving are realized; in particular, 100% biomass saving mode burns only biochar to partially sustained thermal load.

It is considered of interest to realize also an operating point that, in addition to saving 100% of the biomass, oxidizes in the combustor only a part of the residual char extractable from the reactor. As in the previous configurations, this extra saving leads to an increasing in the electrical power supplied by the resistances to cover the gasifier request.

From an electric power point of view, every hybrid modes corresponds to an achieved grade of electrification. The hybrid modes just explained (i.e., 25%/50%/75%/100% biomass saving + biochar saving mode) respectively correspond to 12%, 26%, 39%, 53%, and 77% of electrification (these percentages are calculated as ratio between the resistances electric power request and the nominal power of installed resistances).

The following thesis sections, it is referred to a specific hybrid mode with the nomenclature: INDIR_EL_[X]%.

The results of the investigated operative points are reported in *Appendix B*

4.3.2.1. Indirect hybrid maps

In this section, hybrid mode results are reported and critically discussed; the purpose is to realize the so-called "hybrid maps" that illustrate the trends of peculiar quantities of interest as an increasing share of resistances is switched on.

In the following diagrams the main plant parameters are reported:

- Methanol production
- Biochar production
- Biomass saving
- CO2 emissions
- Captured CO2
- Power consumptions

Methanol production remains constant during the hybrid modes operations, as one can see from *Figure 4-12*. Indeed, the inlet streams into the gasifier do not change in their quantity or composition and there's no off-design of the gasifier downstream components of the plant. Therefore, the methanol reactor always receives the same amount of syngas with the same composition and, hence, produces the same amount of methanol.

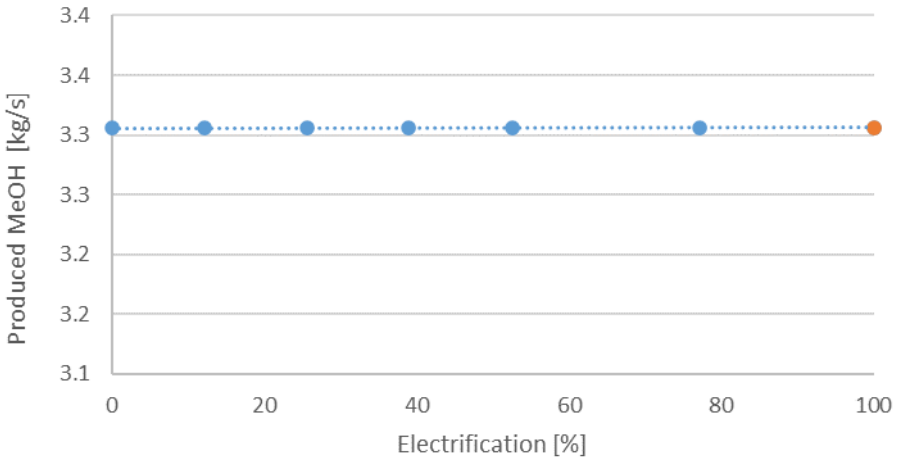

Figure 4-12: produced methanol with respect to the electrification

In *Figure 4-13* the trend of saved biomass is reported within biochar production one.

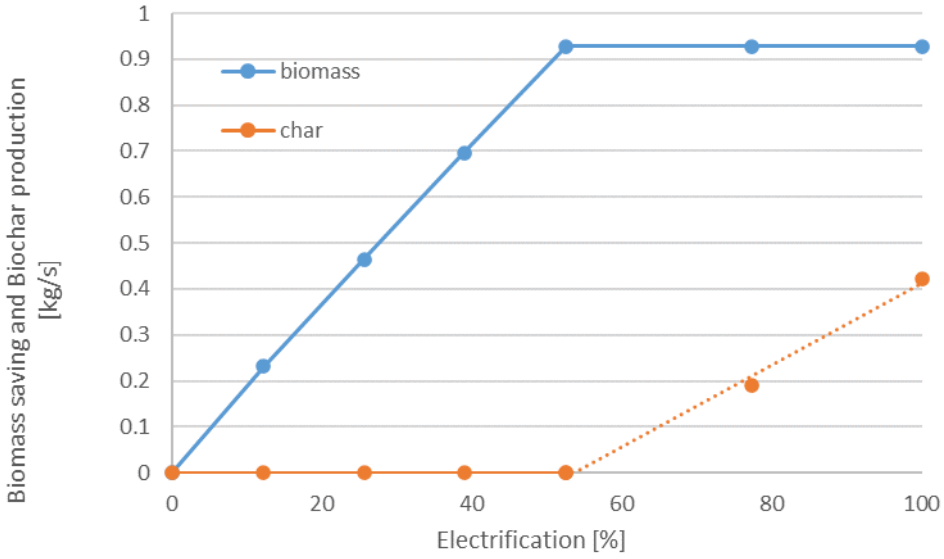

Figure 4-13: biomass saving and biochar production with respect to gasifier electrification

Non-electrified indirect gasifier sustains thermal load burning part of the biomass and the recirculated biochar, as depicted in *section 3.2.2*. Powering the electrical resistances, an increasing part of the biomass previously used for thermal supply is saved; instead, the combustor continues to oxidize the recirculated biochar. However, biochar is burned until 53% level of electrification where no biomass is sent to the combustor; furtherly increasing the electrification percentage, also part of the biochar is saved and

stocked as commercial product, until full electric configuration where the production is 0.42 kg/s.

As one can note in *Figure 4-14*, CO_2 emissions and CO_2 captured trends are reported. The decreasing emissions trend is related to the progressive reduction biomass flow rate sent to the combustor, which leads to a lower CO_2 vented into atmosphere through flue gases.

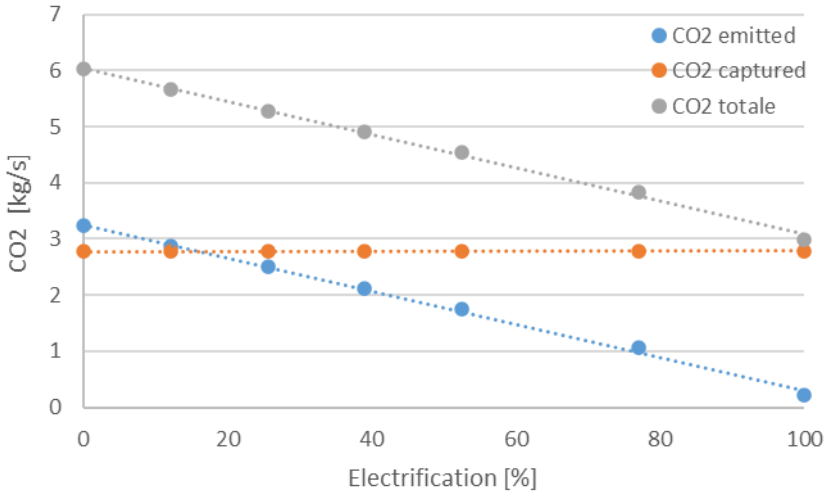

Figure 4-14: CO_2 emissions and captured with respect to the electrification of the gasifier

As reported in *Figure 4-14*, the quantity captured remains constant in all the configurations. Indeed, as mentioned in *section 5.2.2.1* for methanol production, in the indirect cases there's no off-design of the gasifier downstream components of the plant.

In *Figure 4-15* plants power consumptions are reported. In yellow the electric power absorbed by the resistances, in blue the plant baseload, and in grey the sum of the previous terms are reported.

It is highlighted a discrepancy in the linear trend of the plant baseload electric power request (blue line). This trend is related to a lower availability of recovery thermal power; decreasing the biomass burned, flue gases flow rate has a minor impact in the steam cycle recovery section. This reduction leads to several adjustments; among these, the peculiar one is the shutdown of the internal combustion engine, substitute by a light-gases boiler. This stop can be appreciated after INDIR_EL_53% mode, with an offset in plant baseload trendline.

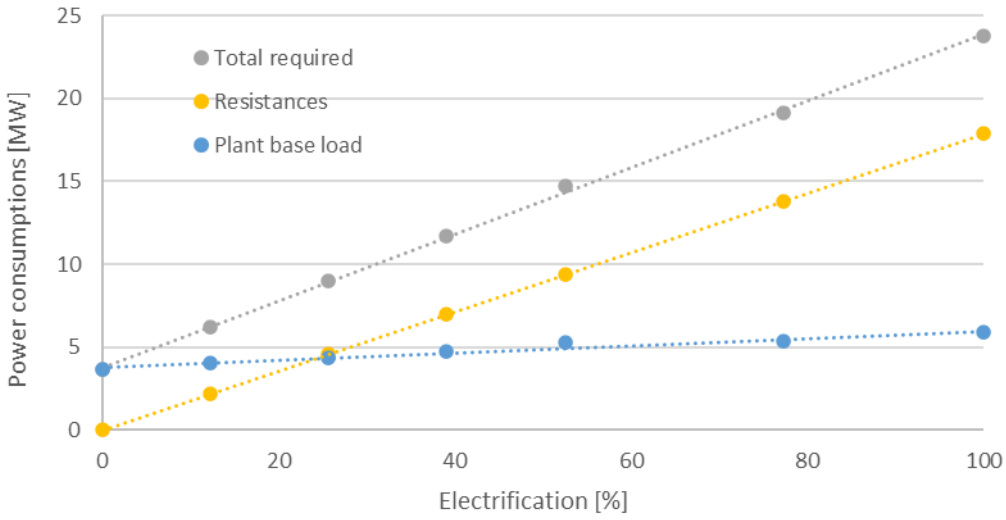

Figure 4-15: power consumption respect with the electrification of the gasifier

5 Heat recovery

Gasifiers, reboilers and CCS components require a continuous flow of low-pressure steam to operate. Hence, a one pressure level heat recovery steam cycle (HRSC) is integrated in the plants: it recovers the excess thermal power generated along the plant from several units, generating electricity and satisfying the steam demands.

Depending on the main configuration of each plant, hot streams coming from water gas shift reactor, combustor or internal combustion flue gases or syngas coolers can be exploited, recovering energy and decreasing second law losses. These hot streams are exploited, in each case, for superheating, evaporation and economizers respecting two constraints:

- Evaporation pressure and temperatures fixed at: 32.2 Bar & 237.8°C
- Maximum achievable temperature limited to 380 degrees.

The first limit is related to the methanol reactor operative temperature. Since the overall methanol synthesis reaction, Equation (5-3), is an exothermic process, it is necessary to cool down the reactor to keep constant the design temperature. The methanol synthesis reaction, Equation (5-1), and the reverse water gas shift reaction, Equation (5-2), that take place in the modelled reactor are shown in the following equations:

$$CO + 2H_2 \leftrightarrow CH_3OH \quad \Delta H° = -22\,\frac{kcal}{mol} \tag{5-1}$$

$$CO_2 + H_2 \leftrightarrow CO + H_2O \quad \Delta H° = +10\ kcal\ /mol \tag{5-2}$$

$$CO_2 + 3H_2 \leftrightarrow CH_3OH + H_2O \quad \Delta H° = -12\ kcal\ /mol \tag{5-3}$$

To keep the operative temperature, the reactor, is cooled with slightly subcooled water at 32.2 bar and 229°C generating steam. Therefore, the reactor temperature imposes the evaporation temperature and pressure for the HRSC.

Second limit is imposed by metal dusting risk: heat exchangers tubes operate in an environment with high carbon activity; syngas, which is rich in CO, shows high corrosivity potential for tube skin temperature ranging from 400° to 800°C [77].

5.1. Direct gasifier steam cycle

5.1.1. Heat Sources

In this plant configuration, *Figure 5-1*, the hot streams available are listed and explained below:

- Syngas cooling pre WGS: reformed syngas exits gasification hierarchy at 915°C. Two syngas coolers are placed in sequence to cool down syngas temperature till 250°C (cooling is then stopped to avoid tar deposition). Cooling process is split due to metal dusting phenomenon: the first cooling is performed through a water evaporator ensuring that syngas temperature entering the second cooler is in the range of 400-430°C. Water at boiling point is chosen because with this technical expedient the tube skin temperature remain under the metal dusting limit. The second cooling process is made through HRSC saturated steam that is heated up from 237.8 °C to 380 °C in the superheater exchanger, cooling down the syngas to the final temperature of 250 °C.

- Syngas cooling after WGS: controlling the inlet syngas module in the methanol synthesis section is important to boost methanol reactor yield. To promote methanol synthesis reactions, syngas module, Equation (5-4), is imposed equal to 2.05 through the adoption of a Water Gas Shift reactor, resulting in H_2 excess, to avoid damages to the catalyst [23].

$$M = \frac{H_2 - CO_2}{CO - CO_2} \tag{5-4}$$

  Target module is reached in the following way: a part of the syngas bypasses WGS reactor in order to have control over the input composition to the synthesis section.

  Since the downstream processes are at low temperature the obtained shifted syngas stream necessitates a further cooling after the exothermic reactions that occurs in the WGS reactor. This cooling is achieved with saturated liquid water

at 32.2 bar, cooling down the syngas till 250 °C when it is suitable for water scrubbing process.

- Methanol reactor cooling: due to the intrinsic exothermic nature of the process, the reactor, a conventional multi-tubular fixed bed, necessitates a dedicated cooling system to ensure the correct temperature of reaction. The reactor is, hence, externally cooled by boiling water at 32.2 bar generating saturated steam used in the HRSC.

- ICE flue gases cooling: light gases, coming from methanol distillation column, are burned in an internal combustion engine. The latter is modelled in *Aspen Plus*® with a combustor with a dedicated calculator which is designed to return the net available useful work, according to the engine size, and a stream of flue gases at a temperature of 400°C. The flue gases stream can be cooled down to 250°C recovering thermal power and increase the efficiency of the plant. To perform this flue gas cooling an HRSC evaporator is used where flue gases heat up saturated liquid water at 32.2 bar to saturated vapor at the same pressure.

- Multistage compressor cooling: methanol synthesis reactions lead to a reduction in the number of moles and are therefore favoured at high pressure (300-400 bar, with ZnO-Cr_2O_3 based catalysts [28]). It is possible to operate the reaction at lower pressures (50-100 bar) with Cu/ZnO/Al_2O_3 or Cu/ZnO/Cr_2O_3 active catalysts. In the plant, a pressure of 90 bar is chosen as the nominal one in agreement with the Laboratory of Catalyst and Catalytic Processes (LCCP); the choice it's the result of a technoeconomic analysis, which underlined how the expenses for the pressure increase up to 100 atmosphere exceeded the additional methanol gain. Compression is performed in two stages, from 3 to 30 bar (before CO2 removal unit) and, from 30 to 92 bar, before methanol reactor. The compressor is a multi-stage inter-refrigerated compressor which exploits water for refrigerate the compressed fluid between stages. This heated up water (~100 °C) is suitable as make up water for the steam cycle.

5.1.2. Steam cycle

In direct configuration, water at 5.9 bar is collected from the utilities and conveyed to the feedwater pump; pressure is increased to 34.3 bar to handle pressure losses occurring in economizer and evaporators heat-exchangers. Pressure losses were considered constant at the value -1.4 bar for the economizers and -0.7 bar for the superheaters. From a purely exergetic point of view the resource could have been exploited wisely: a 580°C superheater could have been realized, given the typical techno-economic limits of a classic Rankine cycle. Given the syngas cooling system, it is however necessary to consider the corrosive effect carried out in a carbon-rich environment: above 400°C metal dusting phenomenon occurs. The achievable maximum overheating is thus fixed to 390°C with 10 degrees of subcooling.

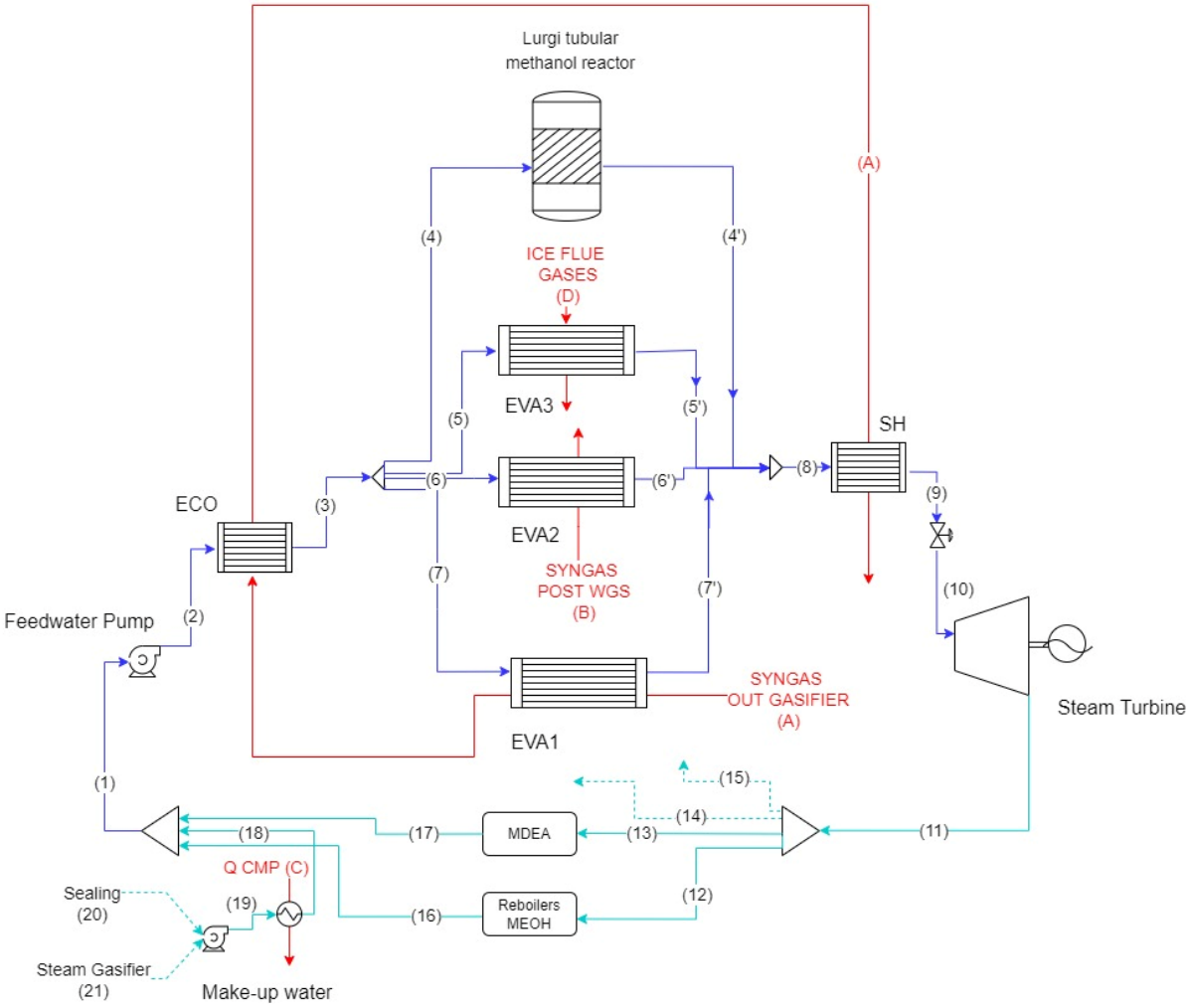

Figure 5-1: direct gasification steam cycle plant layout

The management of thermal resources is realized in the following way:

- Economization is achieved through syngas cooling: part of the high temperature syngas flow is cooled down in the evaporator to reach the 400°C target temperature; before entering the superheater the syngas is further cooled down by liquid water in the economizer. It is considered a subcooling temperature delta of 10°C to prevent the formation of a vapor phase within the economizer.

- The evaporation section consists in four evaporators. The first one is fed by cooling down the syngas leaving the WGS reactor. The second one operates thanks to the engine's flue gases cooling, which are cooled down to a temperature of 250 °C, ensuring a pinch point around 13 °C. In parallel, a fixed flow rate of 3.82 kg/s of subcooled liquid (229 °C) is directed towards the methanol reactor to ensure its cooling. The last evaporator exploits the heat from syngas coolers.

- The superheater, made with the further syngas cooling after the economizer (from 400 °C to 250 °C), overheats the steam generated by the 4 evaporators to reach the temperature of 380 °C.

Steam, prior entering steam turbine, is partially laminated to the pression of 29.65 bar to maintain the same reduced flow rate ($\dot{m}_{rid}$) at the inlet of the turbine. The latter process is realized, however resulting in an exergy loss, to allow the operation of the turbine at partial load. Indeed, the lamination valve is used at partial load to keep the nominal reduced mass flow rate constant, reducing the pressure at the inlet of the turbine according to Equation (5-5).

$$\dot{m}_{rid} = \dot{m}_{steam} \frac{\sqrt{RT}}{P} \tag{5-5}$$

The steam turbine is able to produce 2.92 MW of net electric power in counter-pressure configuration. Counter pressure configuration is employed to satisfy the steam request from some users of the plant. Indeed, low-pressure steam flow rate exiting the turbine at the pressure of 6 bar is divided between 4 different users:

- MDEA: The low partial pressure of CO2 requires the adoption of chemical absorption processes. In this case, Methyl-diethanolamine (MDEA) is used in

aqueous solution. Thermal power for solvent regeneration (i.e., for the reboiler of the stripping columns) is required in the form of low-pressure steam. Indeed, a flow of 3.03 kg/s superheated steam heat up the solution in the column reboiler, condensing from 207 °C to 153.2 °C with 10 degree of subcooling.

- MeOH distillation section: a consistent portion of steam flow is employed in the distillation columns of methanol synthesis section. Methanol stream exiting the reactor necessitate purification: first column extracts light gases in the top section; second one, separate methanol from water achieving the required purity. The thermal loads of the respective reboilers are satisfied by a flow of 2.94 kg/s of steam coming out of the turbine in counter pressure and condensing from 207 °C to 153.2 °C.

- Gasifier: it is important to ensure the optimal steam to carbon ratio (S/C) for the correct gasification of biomass; hence, 2.66 kg/s of steam at 200 °C are supplied by the HRSC.
- Sealing: to satisfy gasifier sealing operations, 0.8 kg/s of steam are requested.

HRSC steam deployed for gasification activities need a reintegration: two stream of makeup water are then arranged; a pump and a heat exchanger (powered by second stage of syngas compressor heat rejection) are used to pressurize and preheat the streams as show in *Figure 5-1*.

Water loop is then closed with the mixing of the 4 pressurized water flows, exiting the utilities.

In the *Figure 5-2* it is shown the T-q diagram of the direct plant. In *Table 5-1* the main HSRC operative points are reported.

Table 5-1: direct steam cycle operative points

Description	**T**	**P**	**Gm**	**Xvapor**
Material flows	°C	bar	kg/s	%
Water (1)	135.48	5.90	9.42	-
Water (2)	135.99	34.30	9.42	-
Water (3,4,5,6,7)	229.00	32.90	9.42	-
Steam (4',5',6',7')	237.82	32.20	9.42	1
Steam (9)	380.00	31.50	9.42	1
Steam(10)	379.25	29.65	9.42	1
Steam(11)	206.97	6.00	9.42	1
Steam(12)	206.97	6.00	2.82	1
Steam(13)	206.97	6.00	3.03	1
Steam(14)	206.97	6.00	0.80	1
Steam(15)	206.97	6.00	2.66	1
Water (16)	153.2	5.9	2.82	-
Water (17)	153.2	5.9	3.03	-
Water (18)	104.6	5.9	3.46	-
Water (19)	25	5.9	3.46	-
Water (20)	25	1.01	0.8	-
Water (21)	25	1.01	2.66	-

Heat streams	**Qth**
	kW
SYNGAS - EVAPORATOR(A)	8663
SYNGAS - ECONOMIZER(A)	3879
SYNGAS - SUPERHEATER(A)	3758
WGS COOLING (B)	1015
WATER-CMP (C)	1152
MEOH REACTOR COOLING	6951
FLUE GASES ICE (D)	489
TOT	25907

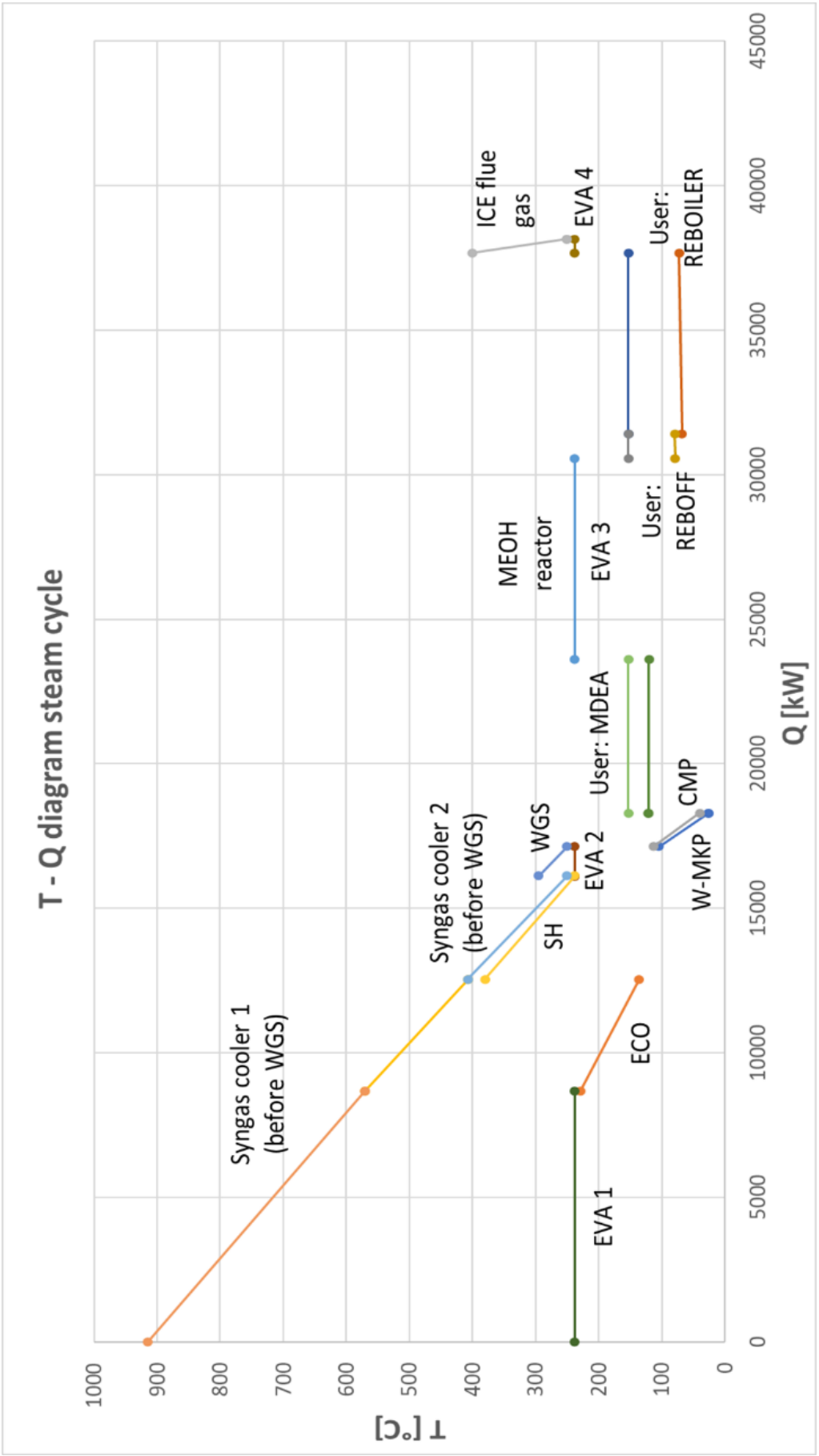

Figure 5-2: direct gasifier steam cycle T-q diagram

5.1.3. Off-design: electric mode

In this chapter, electrification effects on the steam cycle are investigated.

Since the resistors are designed to obtain a useful flow of syngas from the gasification section with the same temperature and pressure, the available heat recoverable remains almost unchanged. Consequently, the operating logic of the recovery plant remains the same.

The plant layout remains the one depicted in *Figure 5-1*, unchanged from the direct case without resistances. TQ diagram of the electrified plant is reported in *Figure 5-3*. In *Table 5-2* the operative points of the HRSC are reported.

Table 5-2: full electric configuration steam cycle operative points

Description	T	P	Gm	Xvapor
Material flows	°C	bar	kg/s	%
Water (1)	130.8	5.9	9.2	-
Water (2)	131.3	34.3	9.2	-
Water (3,4,5,6,7)	229	32.9	9.2	-
Steam (4',5,'6',7')	237.82	32.2	9.2	1
Steam (9)	380	31.5	9.2	1
Steam(10)	379.4	30.78	9.2	1
Steam(11)	208.6	6	9.2	1
Steam(12)	208.6	6	3.89	1
Steam(13)	208.6	6	1.54	1
Steam(14)	208.6	6	0.8	1
Steam(15)	208.6	6	2.97	1
Water (16)	153.2	5.9	3.89	-
Water (17)	153.2	5.9	1.54	-
Water (18)	98.3	5.9	3.77	-
Water (19)	25	5.9	3.77	-
Water (20)	25	1.01	0.8	-
Water (21)	25	1.01	2.97	-

Heat streams	Qth electrified gasifier	Qth direct gasifier
	kW	kW
SYNGAS – EVAPORATOR(A)	7645	8663
SYNGAS – ECONOMIZER(A)	3972	3879
SYNGAS – SUPERHEATER(A)	3497	3758
WGS COOLING (B)	322	1015
WATER-CMP (C)	1156	1152
MEOH REACTOR COOLING	8310	6951
FLUE GASES ICE (D)	448	489
TOT	25350	25907

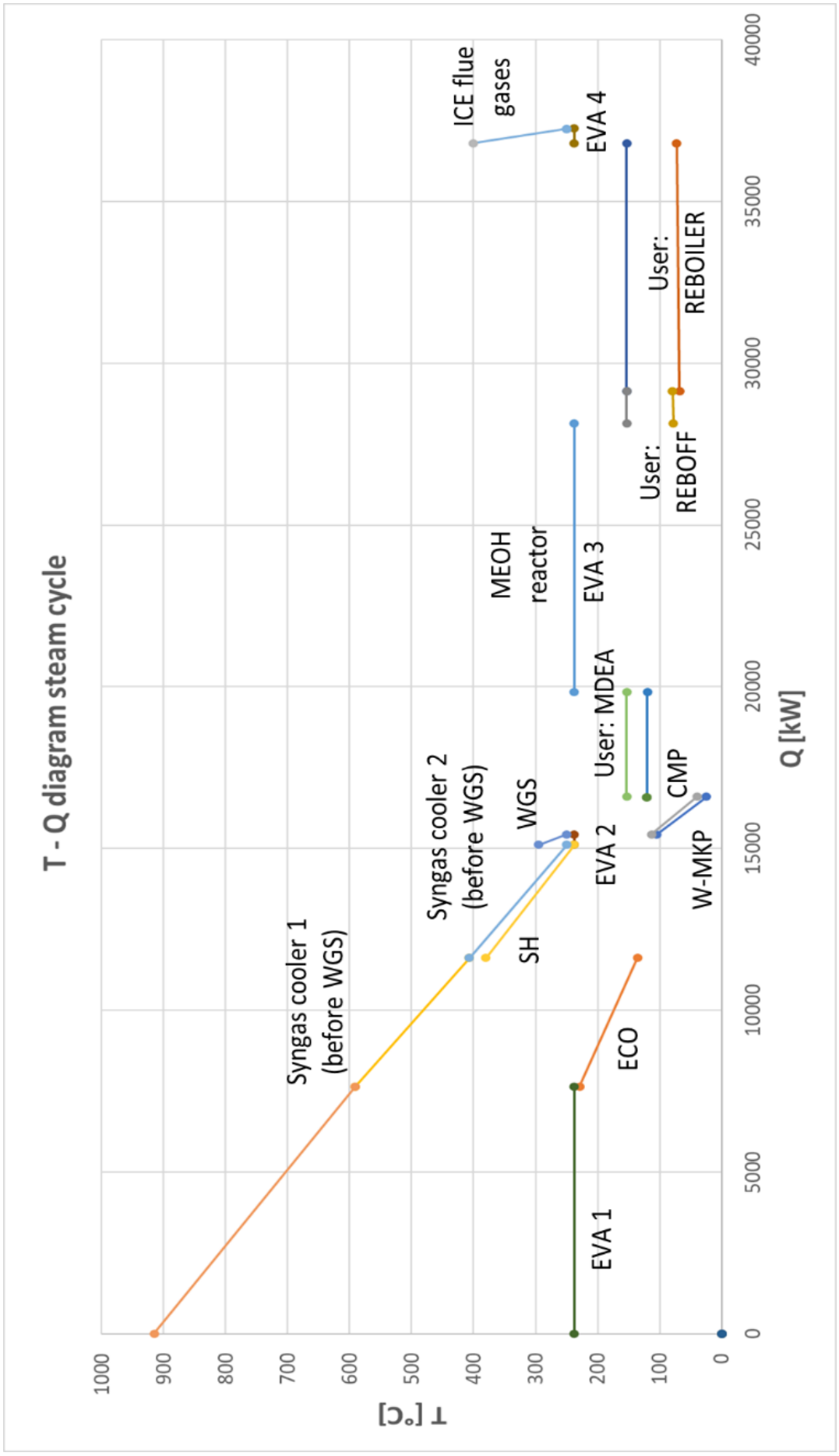

Figure 5-3: full electric configuration steam cycle layout scheme

5.1.4. Off-design: hybrid modes

During off-design operations, a progressive starting of the electrical resistance is realized; 3 intermediate cases are considered, in which a specific flow of oxygen is delivered in the oxygen blown gasifier. The remaining thermal power needed to keep the reactor at its temperature is obtained by partial switch-on of the electrical resistors (25%, 50%, 75% of accension cases are modelled). With the progressive starting of the resistors, a considerable part of raw material is not completely oxidized: the result obtained at the exit of the reactor is a syngas stream of lower mass flow and different composition. The lower mass flow is justified with the reduction of oxygen; nevertheless, the lack of oxidation of part of the biomass causes the syngas leaving the gasifier to be richer in CO and poorer in CO_2. As a consequence, after CO_2 removal, the new stream entering the methanol hierarchy presents a higher mass flow rate.

The net consequences of hybrid off-designs on the steam cycle are the following:

- Recoverable heats, originated before CO_2 are reduced
- Recoverable heats, originated after CO_2 removal are increased.

In all three hybrid cases, the following trade-off related to heat streams entails minimal cycle operative points changes. The HRSC layout remain the same reported in *Figure 5-1* and a comparison between the main operative points of the hybrid modes HRSCs is reported in *Table 5-3*.

Table 5-3: comparison of main operative HRSC points between direct, hybrid and electric mode

Description	Direct	DIR_EL_25%	DIR_EL_50%	DIR_EL_75%	Model 2	Model 1
Inlet turbine pressure [bar]	28.5	28.97	29.66	30.34	31.02	26.98
Discharge pressure [bar]	6	6	6	6	6	6
Evaporation temperature [°C]	237.8	237.8	237.8	237.8	237.8	237.8
Superheated steam temperature [°C]	378.8	379	379.4	379.8	379.9	376.3
Net Power [kW]	2929	3002	3074	3145	3214	2639
Steam mass flow rate [kg/s]	9.42	9.65	9.88	10.11	10.34	9.2

As one can note, the turbine inlet pressure decreases during hybrid modes operations due to a higher steam mass flow rate production of the HRSC. Since the turbine is designed to operate at constant reduced mass flow rate, the increase of steam production leads to an increase in the regulation of turbine inlet pressure, as can be

noticed from Equation (5-5). Instead, in Model 1, the steam production decrease hence the must be regulated to a lower value.

5.2. Indirect gasifier steam cycle

5.2.1. Heat Sources

In this configuration the hot streams available are the following:

- Syngas cooling:-reformed syngas exits gasification section at 800 °C and can be cooled down up to 250°C. In this case, only one syngas cooler is sufficient for cooling purposes since heat stream is fully cooled down in an evaporator heating up saturated water at 32.2 bar till steam. Therefore, metal dusting risk for superheater exchanger does not subsist.

- Gasifier combustor flue gases cooling: biomass combustion process, occurring to satisfy gasifier energy need, produces a stream of flue gases, that are vented at the stack. This stream is cooled down from 915°C to 300 °C, heating up steam from 237.8 °C to 480 °C. After this first cooling, the stream is exploited to preheat the air flow into the gasifier with a further cooling from 300°C to 140 °C.

- Methanol reactor cooling: reactor cooling process, as mentioned in *section 5.1.1.*, is made by heating up subcooled water at 229 °C generating saturated steam at 237.8 °C used in the HRSC.

- ICE flue gases cooling: light gases, coming from methanol distillation column, are burned in an internal combustion engine. The latter is modelled as described in *section 5.1.* The flue gases stream can be cooled down to 100°C recovering thermal power and increasing the efficiency of the plant. To perform this flue gas cooling a HRSC liquid water exchanger is used.

- Multistage compressor cooling: compression is performed in two stages as described in *section 5.1* for the direct gasifier.

5.2.2. Steam Cycle

In the indirect configuration, *Figure 5-4*, water at 3.9 bar is collected from the utilities and conveyed to the feedwater pump; pressure is increased to 34.3 bar to handle pressure losses occurring in economizer and evaporators heat-exchangers. Pressure losses were considered constant at the value -1.4 bar for the economizers and -0.7 bar the superheaters. The use of the syngas stream is preferred for the evaporator to avoid metal dusting. Instead, flue gases cooling is used for economization, superheating and to heat up turbine outlet steam for the gasifier.

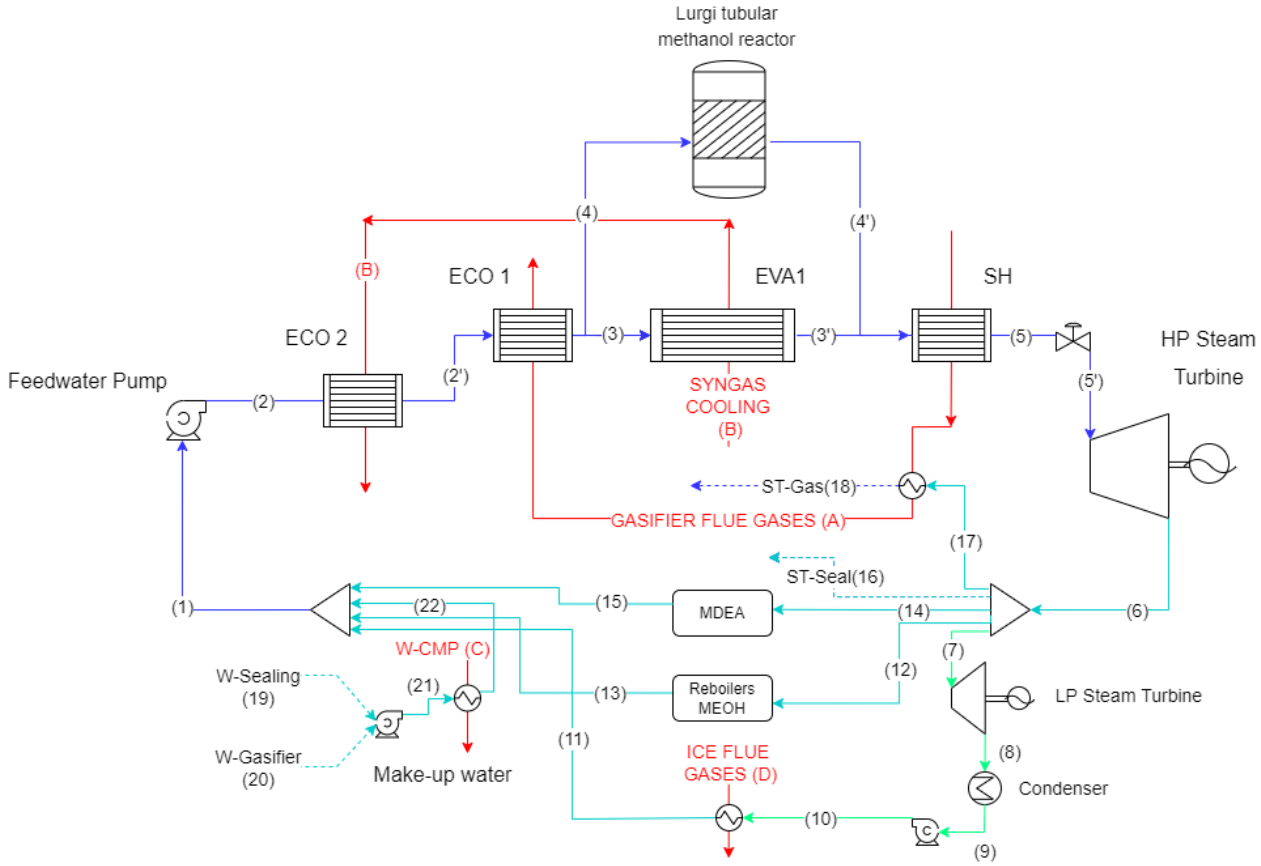

Figure 5-4: indirect gasifier configuration steam cycle

The management of thermal resources is realized in the following way:

- Economization is achieved through the use of two economizers. The first one employs syngas cooling to heat up water from 131 °C to 209.9 °C. The second one, in series, employs flue gases cooling to heat up liquid water from 209.9 °C to 229 °C. It is considered a subcooling temperature delta of 10°C to prevent the formation of a vapor phase within the economizer.

- The evaporation phase is achieved by syngas stream cooling that allows the evaporation of 5.45 kg/s saturated water at 32.2 bar. In parallel, a flow rate of saturated liquid is directed towards the methanol reactor to ensure its cooling.

- The superheater, made with the flue gases cooling, provides a flow rate of 9.23 kg/s at the temperature of 480 °C and 31.5 bar pressure. In contrast with the directive for the direct gasification superheater, in the indirect cycle superheating is achieved exploiting the flue gases cooling. For this reason, the maximum operative temperature is increased up to 480 °C.

The steam flow, prior entering the steam turbine, is partially laminated to the pression of 30.6 bar. The latter process is realized to keep constant the reduced mass flow rate at the inlet of the turbine as described in *section 5.1.2*.

The steam turbine is able to produce 3.998 MW of net electric power in counter-pressure configuration.

Then, low-pressure steam exiting the turbine at the pressure of 4 bar is divided between 4 different users:

- MDEA: the process operates as described in *section 5.1.2*; 1.17 kg/s of superheated steam heat up the solution in the column reboiler condensing from 251.9 °C to 137.7 °C with a 10 degree of subcooling.

- Methanol distillation section: as described in *section 5.1.2* a consistent portion of steam flow is employed in the distillation columns of methanol synthesis section. The thermal duties of the respective reboilers are satisfied by 2.78 kg/s steam coming out of the turbine in counter pressure and condensing from 251.9 °C to 137.7 °C.

- Gasifier: to ensure the optimal steam to carbon ratio (S/C) a 400°C steam import is required; part of the thermal power recovered from the flue gases is used to heat up of turbine outlet steam from 251.9 to 400 °C.

- Sealing: to satisfy gasifier sealing operations, 0.69 kg/s of steam are taken at the turbine outlet.

In on design operations the volumetric steam flow rate is enough to meet the needs of the users, exceeding for a residual quantity of 1.97 kg/s at 4 bar and 251.9 °C. In presence of other separated utilities, the excess can represent, as a steam export, a new

stream of revenues for the plant. In the current study is instead simulated the opposed case: steam flow is valorised as energy in a low-pressure turbine. Indeed, a complete sub atmospheric cycle is modelled: it's hence possible to extract 0.967 MW_{el} extra from the source. The condensed water is then reheated up to 154.8 °C exploiting ICE flue gases.

Steam deployed for gasification activities need a reintegration: two stream of makeup water are then arranged; a pump and a heat exchanger (powered by second stage of syngas compressor heat rejection) are used to pressurize and preheat the streams.

Water loop is then closed with the mixing of the 4 pressurized water flows exiting the utilities and a reheated water coming from the condenser.

In *Figure 5-5*, it's shown the T-q diagram of the indirect plant. In *Table 5-4* the operative points of the HRSC are reported.

Table 5-4: HRSC operative points for indirect gasifier configuration

Description	**T**	**P**	**Gm**	**Xvapor**
Material flows	°C	bar	kg/s	%
Water (1)	130.7	3.90	9.23	-
Water (2)	131.2	34.3	9.23	-
Water (2')	209.9	34.3	9.23	-
Steam (3,4)	229	32.9	9.23	-
Steam (3',4')	237.8	32.2	9.23	1
Steam(5)	480	31.5	9.23	1
Steam(5')	479.5	30.6	9.23	1
Steam(6)	251.9	4	9.23	1
Steam(7)	251.9	4	1.97	1
Steam(8)	45.8	0.1	1.97	1
Water(9)	45.8	0.1	1.97	-
Water (10)	45.8	3.9	1.97	-
Water (11)	154.8	3.9	1.97	-
Water (12)	251.9	4	2.78	-
Water (13)	137.7	4	2.78	-
Water (14)	251.9	4	1.17	-
Water (15)	137.7	4	1.17	-
Water (16)	251.9	4	0.7	1
Water (17)	251.9	4	2.62	1
Water (18)	400	4	2.62	1
Water (19)	25	1.01	0.7	-
Water (20)	25	1.01	2.62	-
Water (21)	25	3.9	3.32	-
Water (22)	107.7	3.9	3.32	-

Heat streams	**Qth**
	kW
GASIFIER FLUE GASES-SH(A)	5603
GASIFIER FLUE GASES-ST-GAS (A)	799
GASIFIER FLUE GASES-ECONOMIZER(A)	3175
SYNGAS – EVAPORATOR (B)	9912
SYNGAS - ECONOMIZER (B)	810
W-CMP (C)	1145
MEOH REACTOR COOLING	6856
FLUE GASES ICE (D)	908
TOT	29208

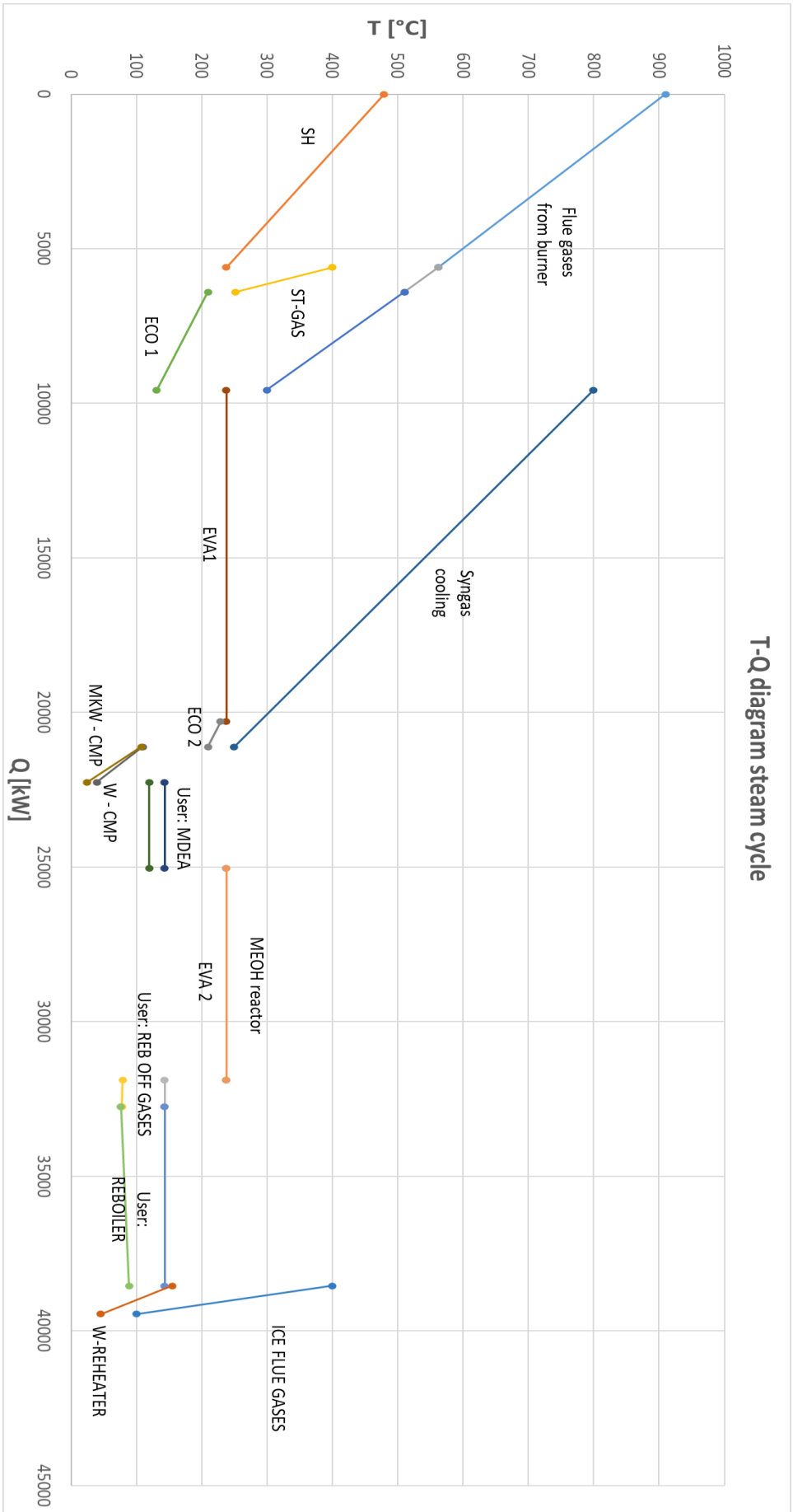

Figure 5-5: indirect gasifier configuration T-q diagram

5.2.3. Off-design: electric mode

Under nominal conditions (i.e., in the absence of resistances) the indirect gasifier reaches the nominal temperature thanks to the partial recirculation of solids that, together with an olivine flow, is heated by means of a biomass combustor. Under electrification mode, recirculation remains to keep the inventory of solids constant; however, the combustor is turned off and the thermal energy is supplied to the gasifier by joule effect. In this operational mode, the biomass previously destined to combustion is considered an avoided cost; operatively, composition, temperature and pressure of the syngas flow exiting the gasifier is kept constant. The result is that, from a heat recovery point of view, heat streams and users' requirements are unchanged. Indeed, from a heat sources perspective, resistances activation only results in the loss of combustor flue gases as a heating source.

In on design operation, flue gases account for a total thermal power of 9.578 MW_{th} (calculated cooling the flue gases from 915°C to 300°C) and they are responsible of superheating, economization and gasifier steam import heating. The absence of the latter source results in a complete redesign of the steam cycle.

5.2.3.1. Steam cycle redesign

The logic chosen for the implementation of the new cycle is to give priority to steam users (crucial for the plant operations). In this case, reduction or total absence of power generation is accepted.

In the first instance, superheating is not pursued as a solution due to the lack of thermal power. Avoiding superheating 4 MW_{th} are saved and used for steam production. As a second occurrence, the role of heat recovered from the syngas cooler is reconfigured to support economization and gasifier steam import heating. As a consequence, evaporation becomes closely dependent on the Lurgi methanol reactor as primarily heating source; the cycle is then fixed at the evaporation temperature set by the reactor. Since the superheater has been abandoned and users require saturated steam at a pressure of 4 bar, the adoption of a turbine bypass with the presence of a throttled valve is necessary.

From a preliminary calculation made with International Association for the Properties of Water and Steam (IAPWS), it is clear that even with these changes the goal cannot be reach. The thermal utilities require a flow rate of about 7.82 kg/s, while the resources available to the plant are at most able to provide 7.36 kg/s. The draft calculations are reported in Equation (5-6) and the results are reported in *Table 5-5*.

Table 5-5: draft calculations for energy balance verify

Heat source	Q_{th} [kW]
Syngas	10700
Methanol	6700
Gasifier	-1250
ICE	700
TOT	16850

Water/steam	Δh [kJ/kg]
Inlet	**512.41**
Outlet	**2803.27**
TOT	**2290.85**

$$\dot{m}_{steam} = \frac{\dot{Q}_{th,available}}{\Delta h_{eva} + \Delta h_{eco} + \Delta h_{superheating}} \quad (5\text{-}6)$$

Applying the Equation (5-6) it is evident that the maximum steam production is 7.36 kg/s and it is not enough to satisfy the aforementioned user request; hence, an alternative heat source is researched.

After a critical process analysis, to cover the steam request of the plant thermal users and to achieve a higher power production, a configuration with a larger boiler that burns all the methanol synthesis light gases is investigated. This solution foreseen the shutdown of the ICE that leads to a loss of 2 MW_{el}. The electrical power is compensated by the higher steam production thanks to the boiler and, hence, the possibility to superheats and expands steam into the turbine.

The idea behind the engine shutdown is to obtain an extra source of heat to be used for overheating, evaporation and economization of water in order to avoid the adoption of a dissipative element such as the throttled valve and turbine bypass system.

In *Figure 5-6* the new plant configuration is shown. The analysis of the following configuration is possible starting from the base case: it is possible to note the lack of thermal power from the flue gases of the combustion engine (now replaced) and the presence of a new flow: the flue gases of the implemented boiler.

In *Figure 5-7*, it is reported the T-q diagram of the indirect electric mode plant.

It is possible to note the choice of arrangement of superheater and evaporator working through the boiler flue gases cooling: the latter avoid superheater creep phenomenon and at the same time becomes a source of thermal inertia during off-design operations.

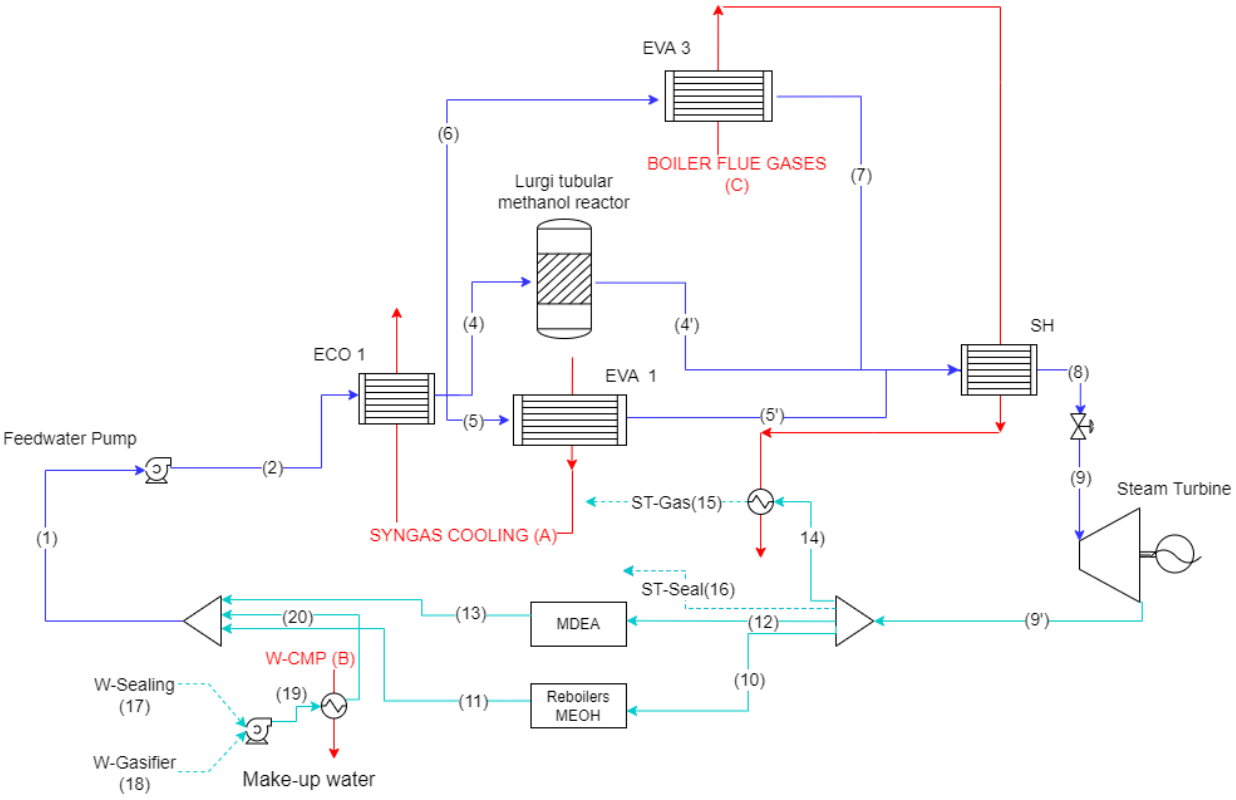

Figure 5-6: indirect full electric gasifier configuration steam cycle

Ideally the presence of the additional boiler could be avoided: during the operation of the plant in resistances could be interesting to investigate in the possibility of burning the light-gases in the same combustor active in conditions of on-design and dedicated to the burning of biomass. The considerable advantage obtained would be the reduction of the transients from the classical mode of gasification to the resistance mode since the combustor would be kept at the nominal temperature in any case. The drawback of this configuration would be the imposition of exchange surfaces (probably undersized).

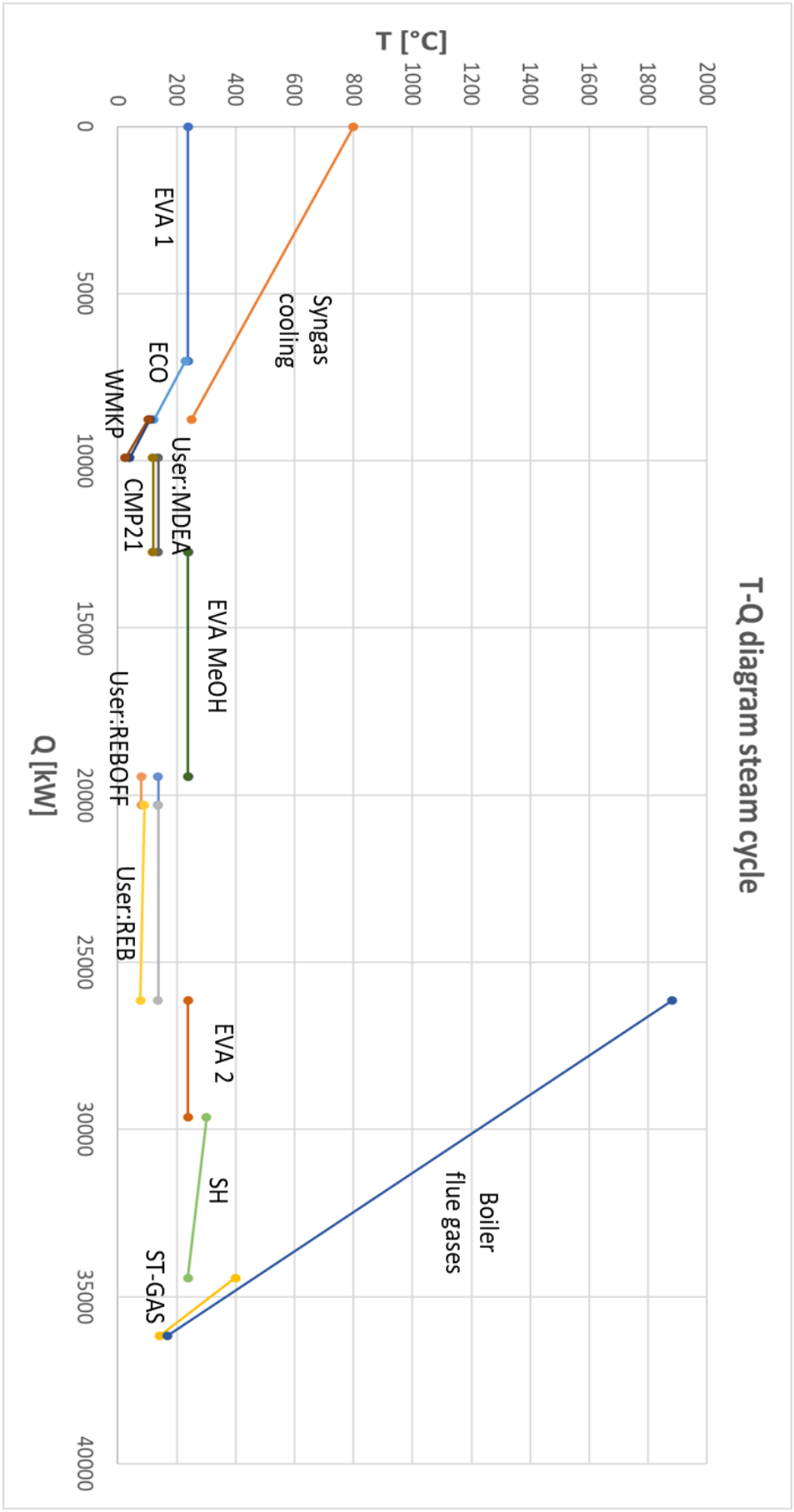

Figure 5-7: full electric indirect gasifier configuration steam cycle T-q diagram

5.2.4. Off-design: hybrid modes

During off-design operations, a progressive starting of the electrical resistance is realized; 5 intermediate cases are considered, in which a decreasing biomass flow rate is sent to the combustor. The combustion process, lacking so of fuel, is not able to bring in temperature the inventory of solids being part of the recirculation (olivine). The remaining thermal energy needed is obtained by the partial switch-on of the electrical resistors. In this operational mode, biomass previously destined to combustion is considered an avoided cost; 5 case of increasing biomass saving are simulated.

Operatively, downstream gasifier, syngas flow rate composition, temperature and pressure are kept constant: the result is that, from a heat recovery point of view, heat streams and user's requirements are unchanged. Indeed, resistances activation only results in reducing the thermal potential of flue gases.

In on design operation, flue gases account for a total heating potential of 9.575 MW_{th} (computed cooling the source from 915°C to 300°C) and they are responsible of superheating, economization and gasifier steam import heating. The partial absence of the latter leads to an off-design functioning of the steam cycle with a decrease of the electrical power production. This trend is verified until the 53% electrification hybrid mode while from 53% hybrid mode the full electric steam cycle configuration is adopted. In *Table 5-6* and *Table 5-7* , the recap of the main operative HRSC points is reported.

Table 5-6: comparison of steam cycle main operative points between hybrid modes

Description	Indirect	INDIR_EL_12%	INDIR_EL_26%	INDIR_EL_39%	INDIR_EL_53%
Inlet turbine pressure [bar]	30.59	29.27	27.94	26.41	25.10
Discharge pressure [bar]	4	4	4	4	4
Evaporation temperature [°C]	237.8	237.8	237.8	237.8	237.8
TIT [°C]	479.5	478.8	478.1	477.27	374.73
Net Power [kW]	4965	4503	4046	3622	3025
Steam mass flow rate [kg/s]	9.22	8.83	8.43	8.04	8.14

Table 5-7:comparison of steam cycle main operative points between biochar and full electric mode

Description	INDIR_EL_77%	INDIR_EL_100%
Inlet turbine pressure [bar]	26.92	24.15
Discharge pressure [bar]	4	4
Evaporation temperature [°C]	237.8	237.8
TIT [°C]	376.2	301
Net Power [kW]	3502	2949
Steam mass flow rate [kg/s]	8.73	8.28

6 Results

In this section the main thermodynamic results of each plant configuration and mode are reported and critically discussed. The trend of Key performance indicators (KPIs), defined in *section 3.3*, is reported to compare the performance of each plant.

6.1. Direct gasifier configurations

The diagrams shown in this section report trends compliant with Model 2. However, as mentioned in *section 4.2.2.*, the results and considerations associated with the Model 1 are reported to provide a critical comparison, highlighting the differences that can arise from two different sets of assumptions. The model 1 results are reported in a different colour since do not follow the Model 2 trend.

6.1.1.1. Fuel efficiency

In *Figure 6-1* fuel efficiency trend, Equation (3-8), is reported. It is possible to notice a linear increase switching from the direct gasification to the 100% hybrid mode. This trend is related to the increasing methanol production described in *section 4.2.2.* As far as the oxygen injected in the gasifier is reduced, an extra part of syngas, not oxidized, is produced and is available for methanol production.

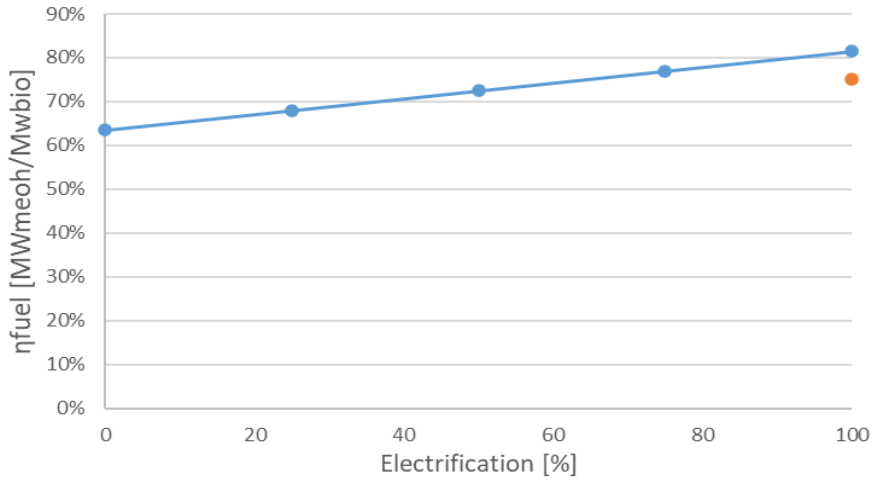

Figure 6-1: Fuel efficiency with respect to the electrification of the gasifier

Model 1 fuel efficiency is slightly lower because of the lower methanol production with the same biomass inlet flow rate, as mentioned in *section 4.1.*

6.1.1.2. Power-to-methanol efficiency

Exploring gasifier hybridization mode, it is interesting to calculate the incremental effect of resistances implementation. As depicted in *paragraph 4.1.*, the electrification of a direct gasifier leads to higher methanol production and, as consequence, higher electricity consumptions.

It is possible to highlight what is the punctual net effect of electrification on final product yield, with Power-to-methanol efficiency parameter, calculated as reported in Equation (6-1).

$$Power - to - Methanol\ [-] = \frac{d\dot{m}_{MeOH} * LHV}{d\dot{P}_{el}} \tag{6-1}$$

The formula reports the differential variation of produced methanol chemical potential, LHV based, with respect to incremental electrical power requested, $d\dot{P}_{el}$.

To extrapolate the parameter, that is a differential value, a discretisation process is realized: a set of discretized Power-to-methanol efficiencies are computed, as reported in Equation (6-2), between two sequential levels of electrification, i.e., between DIR_EL_[x]% and DIR_EL_[x-offset] %. For this analysis, an offset value of 12.5% is considered.

$$Power - to - Methanol\ [-] = \frac{\Delta\dot{m}_{MeOH} * LHV}{\Delta\dot{P}_{el}} \tag{6-2}$$

The obtained results, reported in *Figure 6-2*, show an almost constant trend, with an efficiency ranging between 87.5% and 88%. In this case the result associated with Model 1 is not considered of interest and, hence, is not reported.

In the context of Biomass to Methanol plants, Power-to-methanol efficiency can be incremented through different paths. In the work of Poluzzi et al [78], electricity withdrawn from the grid is used to feed an electrolyser that produces hydrogen from water. The resulting stream of hydrogen is mixed with cleaned syngas to increase methanol production (the presence of methanol synthesis reagents increases). Conversely, in the current thesis work, electricity is exploited to supply thermal power to gasification reactors; in this way inlet carbon is saved from oxidation.

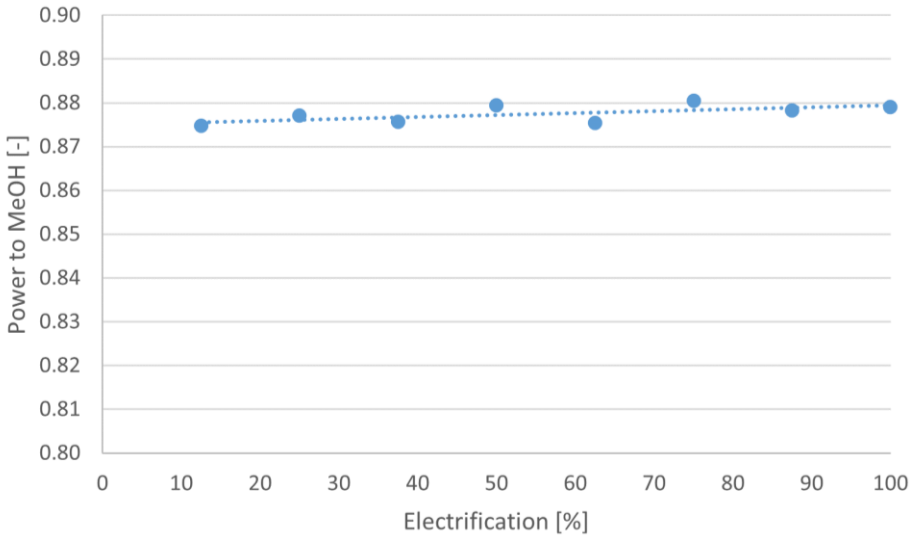

Figure 6-2: Power-to-Methanol efficiency with respect to electrification

It is interesting to note that the value of 88%, obtained in the current research study, outweighs the corresponding value obtained with the addition of H_2 [78]. From this outcome, it can be concluded that for this type of plant, electrify through electrical resistances is preferable to electrify through electrolysers thanks to the greater energy efficiency.

6.1.1.3. Global yield & single passage yield

As one can note from *Figure 6-3*, methanol reactor yields show an increasing trend justified by the different syngas compositions that enter the methanol section in each functioning mode as depicted in *paragraph 4.1.1.*

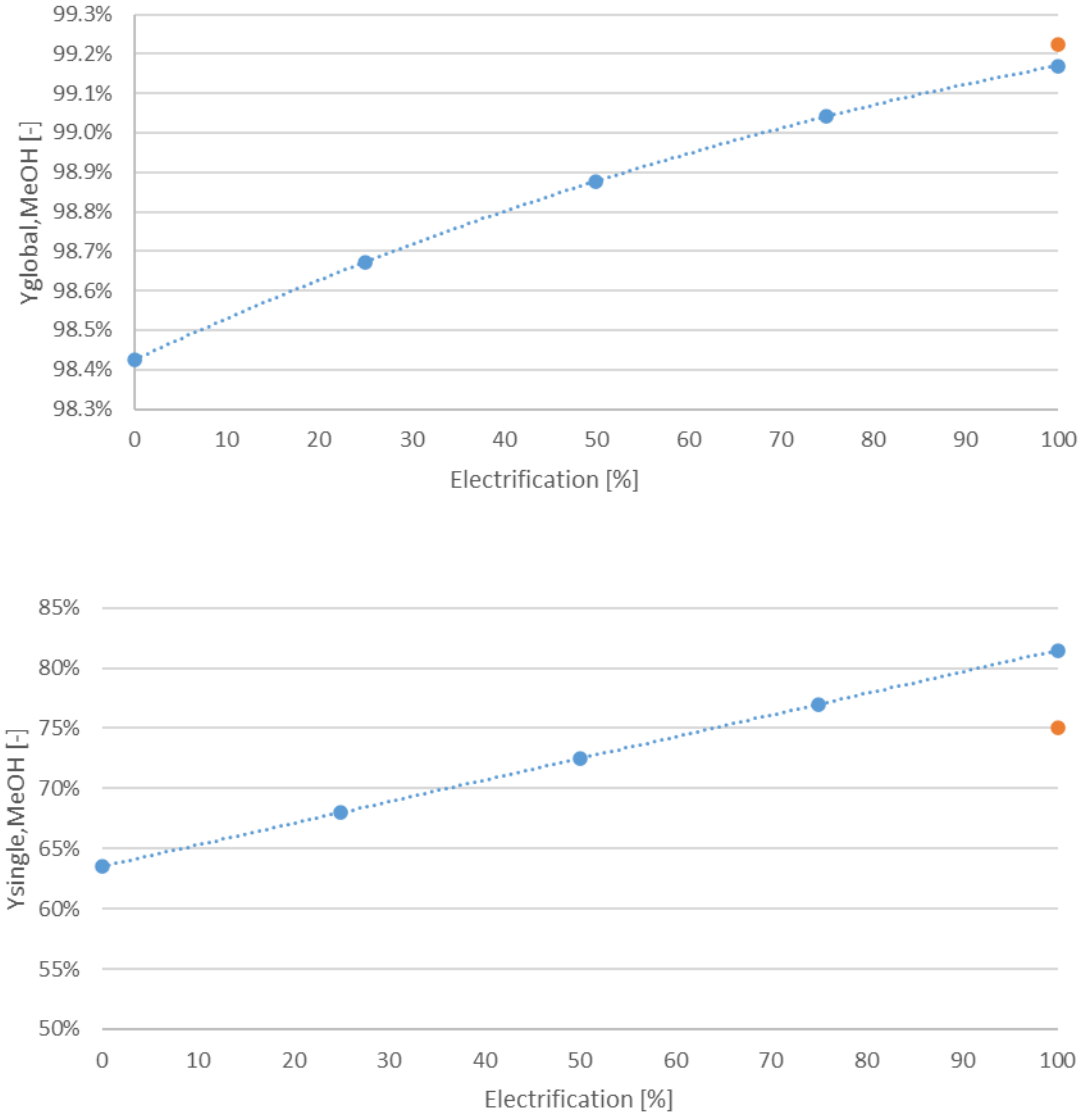

Figure 6-3: global and single methanol reactor yield

6.1.1.4. CO_2 emissions

In *Figure 6-4*, it is possible to note the linear decrease of the CO_2 emissions, depicted in Equation (3-15), with the progressive use of the electric resistances. The trend is explained considering the lower carbon oxidizable that is sent to the internal combustion engine in the light–gases stream as the gasifier is electrified.

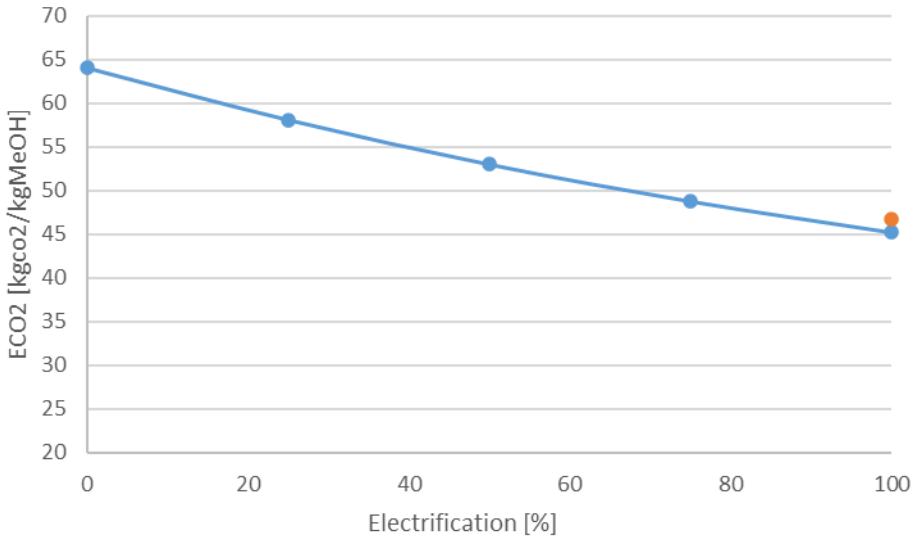

Figure 6-4: CO_2 emissions with respect to the electrification of the gasifier

Moreover, since the emissions are normalized with respect to methanol production, the increase of the latter leads to a decrease of the specific emissions. For this reason, Model 1 emission point is slightly higher with respect with the 100% hybrid mode one; even though the absolute value of CO2 emissions is lower, since methanol production further decrease, the overall result is higher.

6.1.1.5. Carbon efficiencies

In *Figure 6-5*, the carbon efficiencies trends are reported.

The green line, which represents the overall carbon efficiency, reported in Equation (3-12), is almost constant at the value of 82%. Nonetheless, it is interesting to report and analyse the three considered carbon efficiency, Equations (3-9), (3-10), (3-11), that together forms the above trend, i.e., biochar, methanol, and CO_2 captured carbon efficiency.

Methanol carbon efficiency increase due to the higher methanol production, while it is possible to notice that the biochar carbon efficiency remains constant because the gasification model is the same, hence, the biochar extracted.

It is possible to notice a decrease in the CO_2 captured by switching on the electric resistances. The phenomenon stems from the CO_2 capture system implemented; the capture percentage is fixed at 95% of the mass flow rate of CO_2 presents in syngas for all the plants. Low oxygen presence in the gasifier results in a lower CO_2 concentration in the syngas; from a relative point of view, the capture system continues to operate in

the same way, but from an absolute point of view it captures more CO_2 where a greater oxidation has occurred.

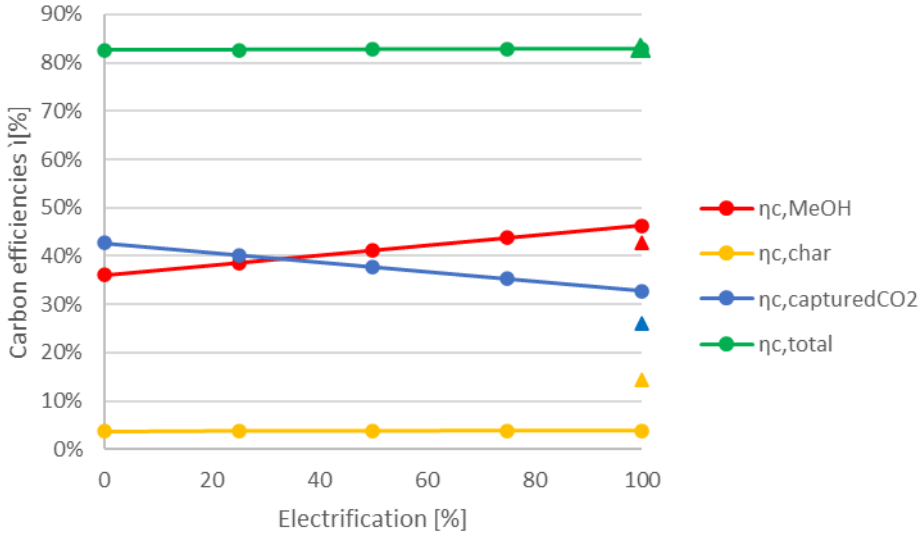

Figure 6-5: carbon efficiencies with respect to electrification of the gasifier

Finally, it is interesting to observe Model 1 data. Even though a larger part of carbon is directed to biochar (due to higher residual recoverable char hypothesis) the overall carbon efficiency is aligned with Model 2 data; Indeed, carbon is only redistributed according to a different logic and hence the overall sum is almost constant.

6.1.1.6. CGE gasifier

In *Figure 6-6* the trend of Cold Gas Efficiency (CGE) and net gasifier efficiency (NGE), computed in Equation (3-16) and (3-17), are reported.

CGE increasing trend is due to the higher LHV of the outlet syngas. The latter is related to the lower presence of inert components (i.e., nitrogen and argon) and lower presence of water and carbon dioxide, in favour of a higher H_2 presence (LHV=120 MJ/kg).

CGE does not take in account the thermal power given by the implemented electrical resistances; therefore, a modified version of the CGE, the net gasifier efficiency (NGE), Equation (3-17), is defined to analyse this effect.

NGE parameter is reported to separate the increase in CGE (characteristic of a decrease in oxidized carbon) from the incremental effect of electrical resistances. NGE parameter, reported on the same diagram, shows a less pronounced increasing trendline; it can therefore be stated that the hybrid gasifier does not work that far better

(as can be derived from CGE trend) but simply that CGE does not account for the power from the resistances which is an important source of power entering the gasifier.

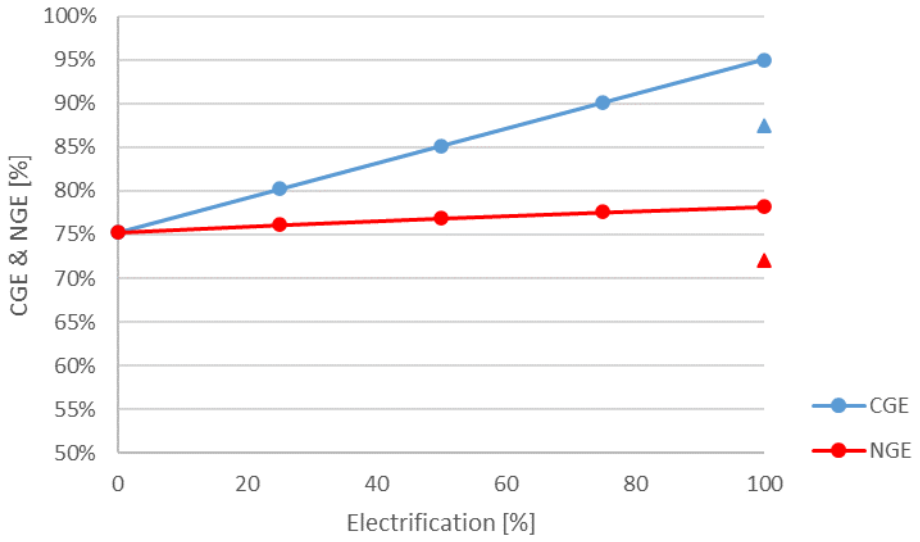

Figure 6-6: CGE and NGE with respect to the electrification of the gasifier

6.1.1.7. CGE WGS

In *Figure 6-7*, the trend of the water gas shift reactor CGE is reported. The slightly increase is related to the higher LHV of the syngas at the WGS outlet because of the lower CO_2 presence in favour of H_2.

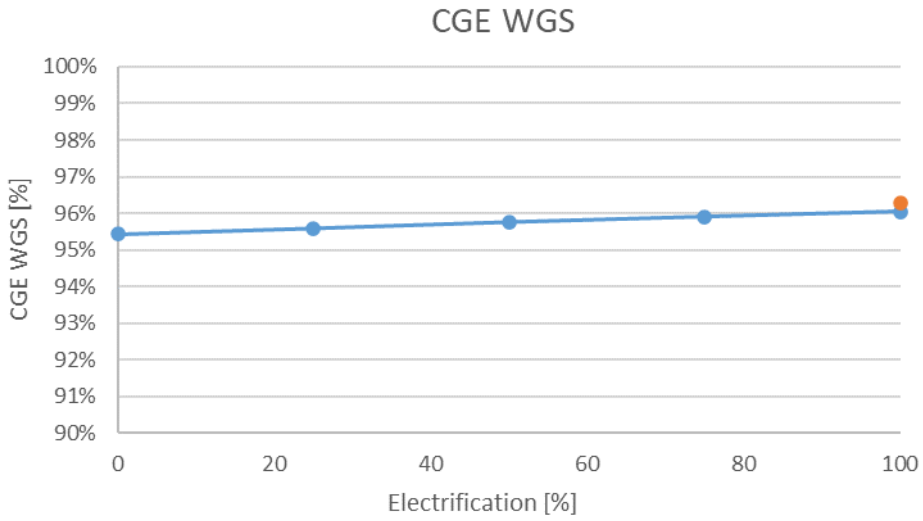

Figure 6-7: WGS CGE with respect to the electrification the gasifier

6.1.1.8. CGE methanol reactor

The trend reported in *Figure 6-8* belongs to the methanol reactor CGE, defined in Equation (3-16) applied for methanol reactor. The value is constant since the reactor works almost in the same conditions (i.e., same syngas module M and same recirculation ratio RR).

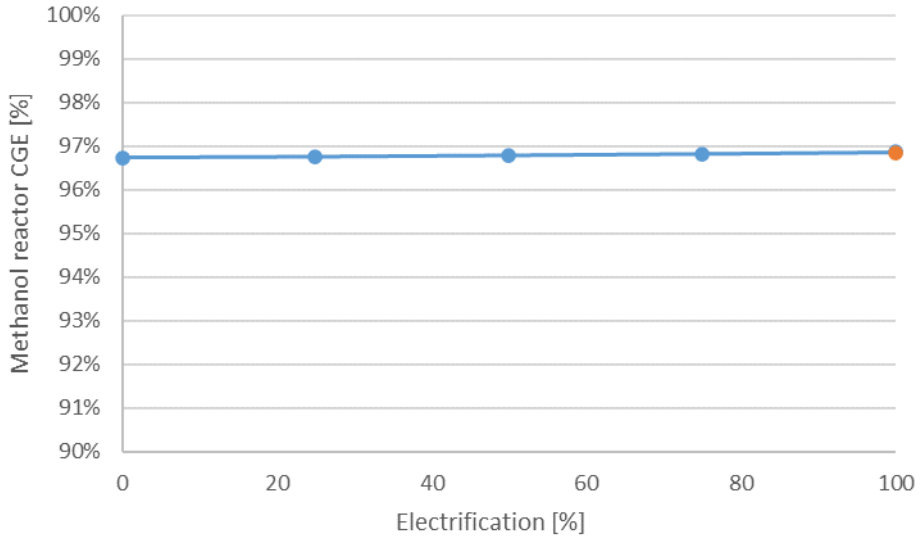

Figure 6-8: CGE of the methanol reactor with respect to the electrification of the gasifier

6.2. Indirect gasifier configurations

Contrary to the direct configurations, indirect hybrid modes adopt all the same gasification model, i.e., the indirect one described in *section 3.2.2* and *section 4.3*.

From an electric point of view, every hybrid mode corresponds to an achieved grade of electrification. The hybrid modes used to extrapolate the following trends belong to two different categories, although they are realised from the same basic assumptions: the first group belong to "biomass saving modes" (i.e., 12%, 26%, 39%, 53% of electrification), whereas the second, in addition to saving biomass, produces biochar as an extra product (i.e., 77%, 100% of electrification). As a result, trends dependent by biomass utilization varies up to the level of electrification correspondent to 53% of electrification.

Furthermore, it is important to highlight that plant off-design is not present as the electrification level increase. Indeed, the inlet streams into the gasifier do not change in their quantity or composition; hybridization is achieved through a different

alimentation to the combustor but does not directly affect the gasifier (unless physical presence of electrical resistances in it).

For this reason, gasifier downstream components of the plant do not change their operational functioning and, hence, their parameters.

6.2.1.1. Fuel efficiency

In Figure 6-9, fuel efficiency trend, Equation (3-8), is reported; it is possible to notice an increasing trend switching from indirect to full electric configuration until 53% of electrification. Indeed, the growth is related to biomass consumption reduction; methanol production is constant for each case. After 53% of electrification, numerator and denominator of the formula are constant and, hence, the trendline.

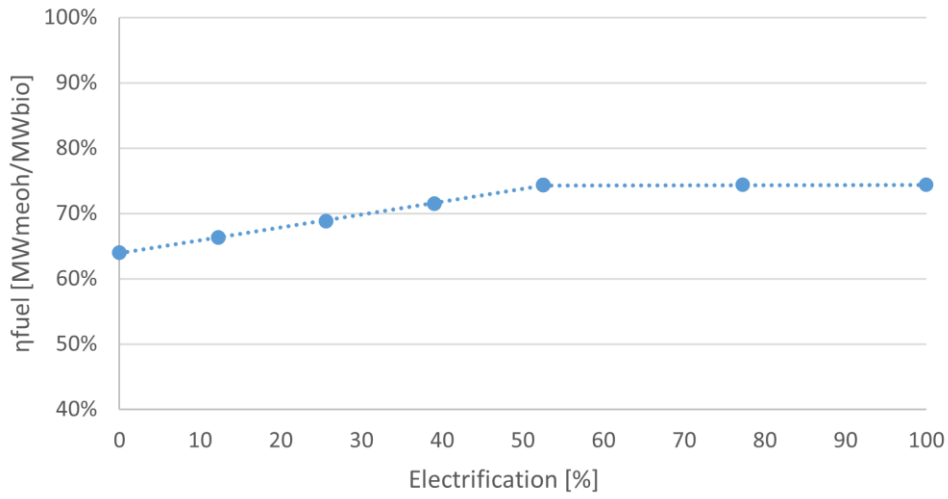

Figure 6-9: fuel efficiency with respect to the electrification of the gasifier

6.2.1.2. Global yield & single passage yield

As explained in *section 4.3.1*, the indirect configurations do not present off-design conditions for gasifier and methanol reactor. This phenomenon results in constant yields of the reactor varying the hybridization percentage as shown in *Figure 6-10*.

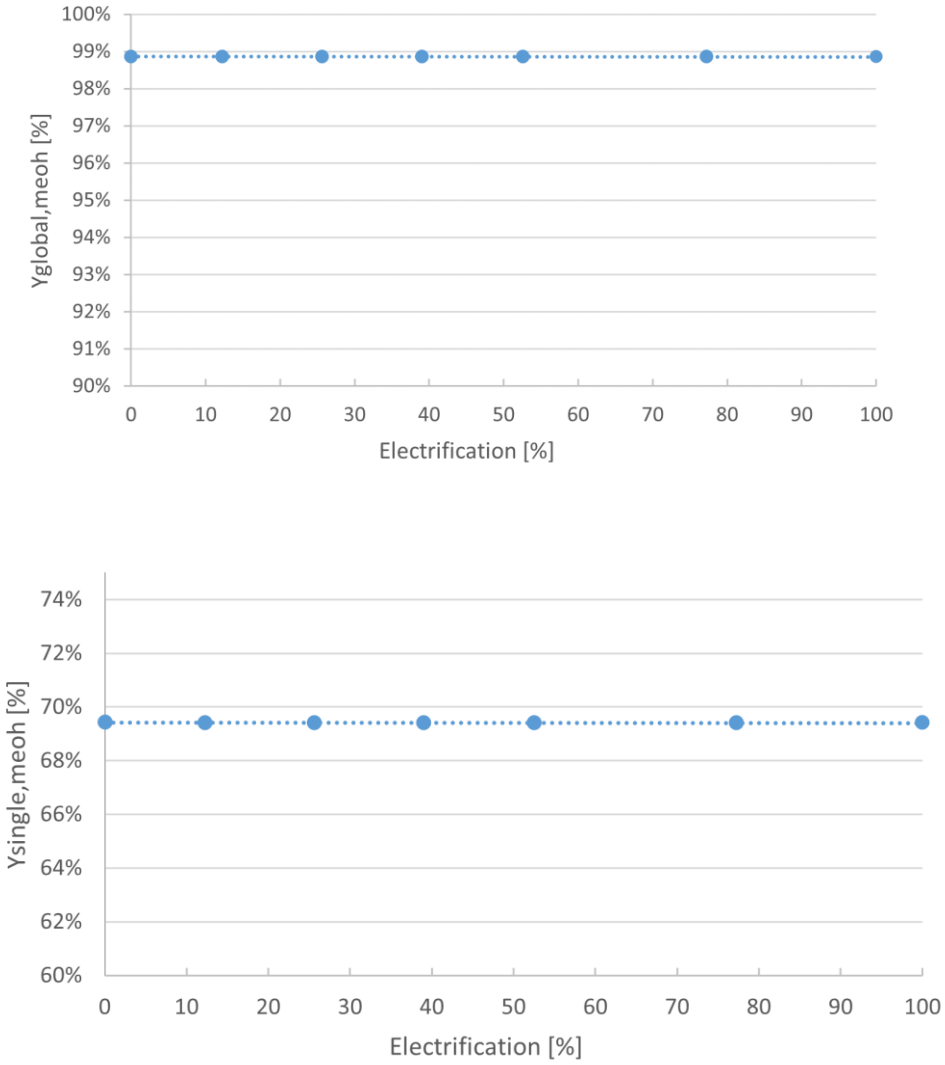

Figure 6-10: global and single passage methanol reactor yields with respect to the electrification of the gasifier

6.2.1.3. CO_2 emissions

As one can note in *Figure 6-11*, CO_2 emissions, Equation (3-15), are drastically higher with respect to the direct configurations since in the baseline case a considerable part of the biomass is burned to satisfy gasifier thermal load. With the progressive electrification, the combustor is alimented with less biomass and, after 53% of electrification, les char. The decreasing trend is then justified by the less carbon-based fuel used to cover the gasifier thermal supply.

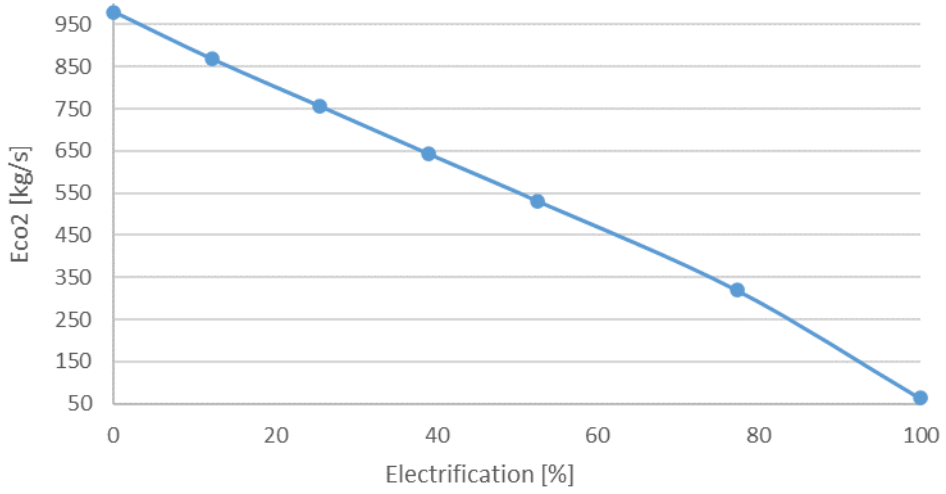

Figure 6-11: CO_2 emissions with respect of the electrification of the gasifier

6.2.1.4. Carbon efficiencies

In *Figure 6-12*, the carbon efficiencies trends are reported.

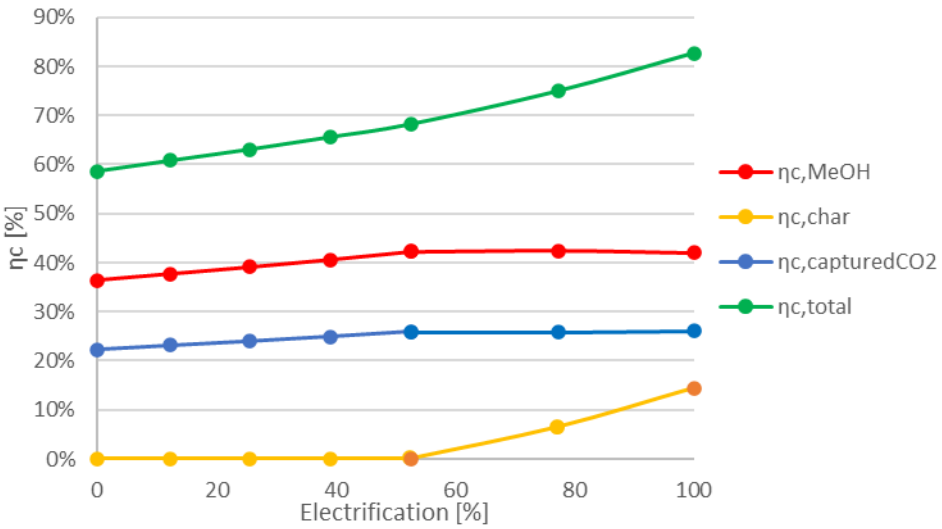

Figure 6-12: carbon efficiencies with respect to the electrification of the gasifier

The green trendline, which represents the overall carbon efficiency, reported in Equation (3-12), is increasing from a value of 59% to a value of 82%. Indeed, as the gasifier is electrified, less carbon-based fuel is used to cover the gasifier thermal load. It is noted that the value reached at the maximum electrification is close to that one reached in direct cases.

It is also interesting to report and analyse the three considered carbon efficiency that together forms the above trend, i.e., biochar, methanol, and CO_2 captured carbon efficiency.

Methanol and captured CO_2 carbon efficiencies show the same trend. Indeed, due to the lack of off-design of indirect modes, methanol production and carbon storage is constant, whereas burnt biomass is progressively reduced; from 53% of electrification on, the trend is constant since also saved biomass is fixed.

Conversely, biochar carbon efficiency is null until 53% of electrification; from that point on biochar is progressively stocked and sell as commercial product.

6.2.1.5. CGE gasifier and methanol reactor

As explained in *section 4.3.1*, the indirect configurations do not present off-design conditions for gasifier and methanol reactor; hence, CGE of methanol and gasifier reactor are unchanged as shown in *Figure 6-13*.

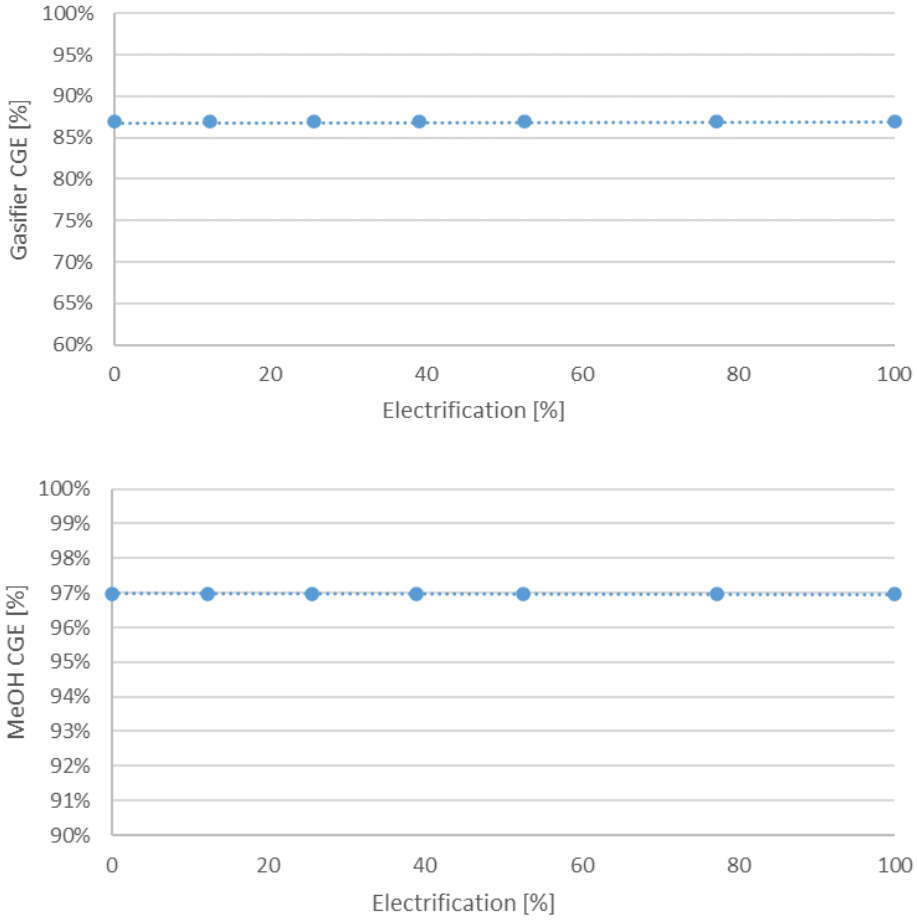

Figure 6-13: gasifier and methanol reactor with respect to the electrification of the gasifier

6.3. Indirect emissions from electric grid

The exploitation of electricity from the grid involves importing emissions from the network to which the plant is connected. The benefit related to the increase in carbon efficiency is less justified if to achieve this result is used electricity that carries a significant share of emissions.

Hence, the condition a priori of the current study is to consider as a source of electricity a future grid with high penetration of renewable and low gCO_2/kWh ratio.

As an alternative, the feasibility of the application of a solar field coupled with plant is studied; in this way a renewable source for electricity is ensured.

Nonetheless, it is interesting to highlight the effect of the indirect emissions from a current electricity grid on the final product. In this way it is possible to stress the intrinsic trade-off between carbon efficiency and indirect emissions. This purpose is reached varying the electrical grid and hence varying the CO_2 impact associated to each configuration. Grid emissions are varied with continuity; three specific thresholds are highlighted, i.e., Finland, Italy and Poland grid emissions, which are chosen as a representative case of a grid with high renewable penetration (Finland), high fossil fuel dominance (Poland) and average renewable penetration (Italy). Grid emissions trend, obtained from the IEA site for the year 2021 [79], are reported below.

$$Finland_{grid\ emissions} = 135 \frac{gCO_2}{kWh_{el}}$$

$$Italy_{grid\ emissions} = 226 \frac{gCO_2}{kWh_{el}}$$

$$Poland_{grid\ emissions} = 332 \frac{gCO_2}{kWh_{el}}$$

6.3.1. Grid effect on emissions

Bioenergy is a versatile renewable energy source that may be used in a variety of industries, and it can make use of existing transmission and distribution networks as well as end-user equipment. However, there are restrictions to extending bioenergy supplies, as well as potential trade-offs with sustainable development goals, such as avoiding conflicts at the local level with other land uses, particularly for food production and biodiversity protection. For these reasons, in the scientific community, is still under discussion how to classify CO_2 emissions from biogenic sources [80].

In the following analysis two schools of thought are followed; for each configuration, CO_2 emissions are reported both considering biomass carbon emissions as accountable or as net zero.

The first logic considers only the net emissions caused by flue gas venting in the atmosphere. In the Equation (6-4) is reported the trend of CO_2 direct and indirect emissions in grams per kilograms of produced methanol.

$$E_1[\frac{gCO_2}{kgMeOH}] = \frac{\dot{m}_{CO_2,emitted}}{\dot{m}_{MeOH}} + GridEm * \frac{El_{Power}}{\dot{m}_{MeOH}} \quad (6\text{-}4)$$

The first term, $\frac{\dot{m}_{CO_2,emitted}}{\dot{m}_{MeOH}}$ $[\frac{gCO_2}{kgMeOH}]$, is derived from equation (3-15) and accounts for CO_2 direct emissions. The second one is the product between grid greenhouse gas impact, i.e. $GridEm$ $[\frac{gCO_2}{kWh_{el}}]$, and the ratio between electrical power required by the plant and consequent methanol production i.e. $\frac{El_{Power}}{\dot{m}_{MeOH}}$ $[\frac{kW_{el}}{kgMeOH/h}]$.

Conversely, with the second logic, emissions caused by flue gas venting are neglected (as the source is considered biogenic and, hence, net zero). Furthermore, as one can note in Equation (6-5), the positive action of carbon dioxide sequestration (with CCS or with a profitable by-product, i.e., biochar) is accounted as negative emissions (first term of the equation).

$$E_2\ [\frac{gCO_2}{kgMeOH}] = -\frac{\dot{m}_{CO2\ stored} + \frac{MM_{CO2}}{MM_C}\dot{m}_{Produced\ biochar}}{\dot{m}_{MeOH}} + GridEm * \frac{El_{Power}}{\dot{m}_{MeOH}} \quad (6\text{-}5)$$

As depicted for Equation (6-4), the second term considers the indirect emissions, carried by the grid.

6.3.1.1. Direct plants

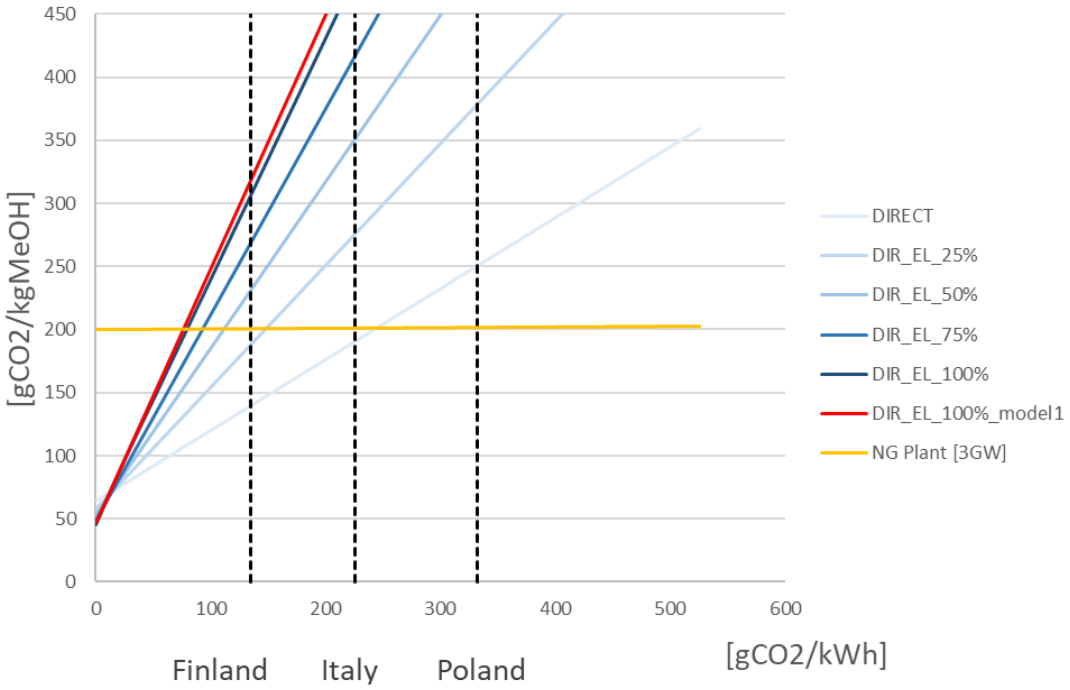

Figure 6-14: plants specific CO_2 emissions with respect to the grid emissions

In *Figure 6-14* a comparison of CO_2 emissions with respect to the carbon dioxide impact of the grid emissions [gCO_2/kWh] is reported.

As highlighted in *section 6.1.1.4*, for direct gasifier modes the impact of CO_2 vented in atmosphere is not as significant as for indirect ones. For these reasons, the full electrified plant outweighs the baseline configuration only for grid emissions level below 12.5 gCO_2/kWh. To have a comparison term, a fossil fuel-based methanol power plant is considered in the diagram as reference for the CO_2 emissions (yellow trendline) [81]. Since these diagrams do not account the biomass as net zero source, CO_2 emissions are considered equal to the fossil fuels one and a comparison can be realized. Full electrified plant results to be convenient for grid emissions value lower than 57 gCO_2/kWh, far below Finland reference value.

Conversely, considering every biogenic source as net zero, a completely different set of trendlines can be reported. CO_2 plant emissions are negative and, hence, there's no competition for conventional natural gas plant as one can note in *Figure 6-15*.

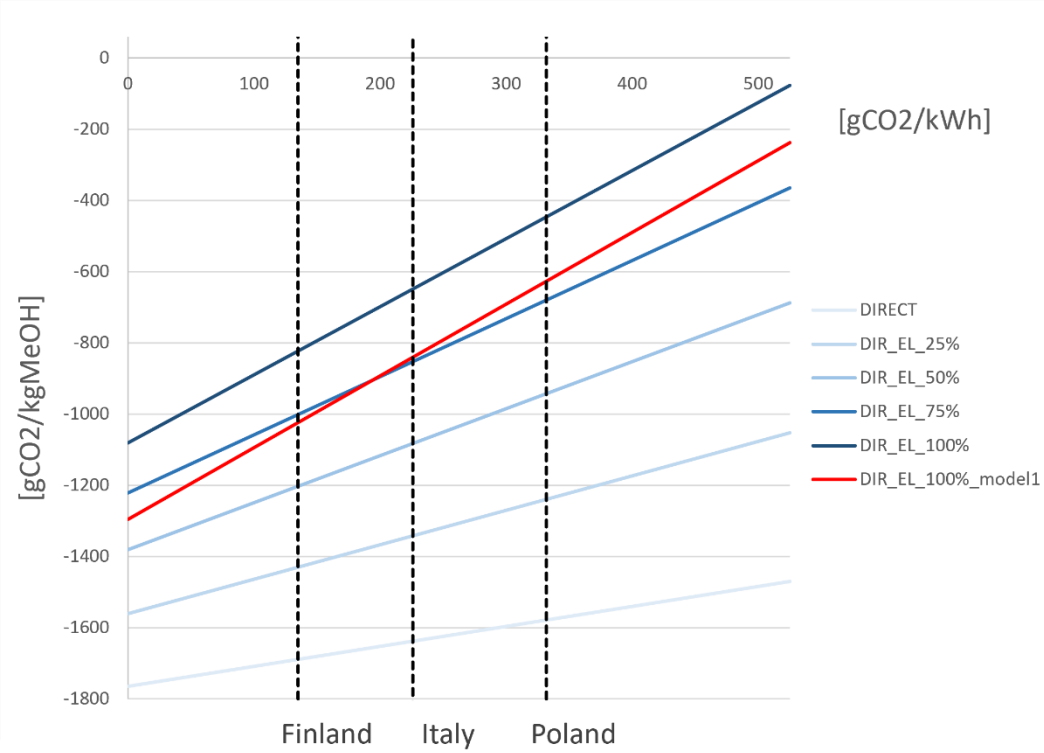

Figure 6-15: plants specific CO emissions with respect to grid emissions considering biomass as biogenic source

Furthermore, less electrified plants appear to be more interesting from an emission point of view. This is related to CCS section, which, as stated before, capture 95% of syngas CO_2. Hence, from a syngas flows richer in carbon dioxide (i.e., less electrified modes) CO_2 captured absolute value is higher.

The latter phenomenon can be distortional if not explicated. Renewable biomass is a limited resource: replacing a significant portion of fossil fuels with biofuels entails transferring as much renewable carbon into biofuels as possible. Electrifying has a higher value since it allows to increase the carbon efficiency of the plant and exploits a scarce resource more efficiently.

6.3.1.2. Indirect plants

In *Figure 6-17*, a comparison of CO_2 emissions with respect to the carbon dioxide impact of the grid between each investigated plant is reported.

For indirect gasifier modes the impact of CO_2 vented in atmosphere is significant; hence, these plants are not able to compete with a conventional fossil fuel-based methanol power plant (blue trendline) [65]. Since these diagrams do not account the biomass as net zero source, CO_2 emissions are considered equal to the fossil fuels one.

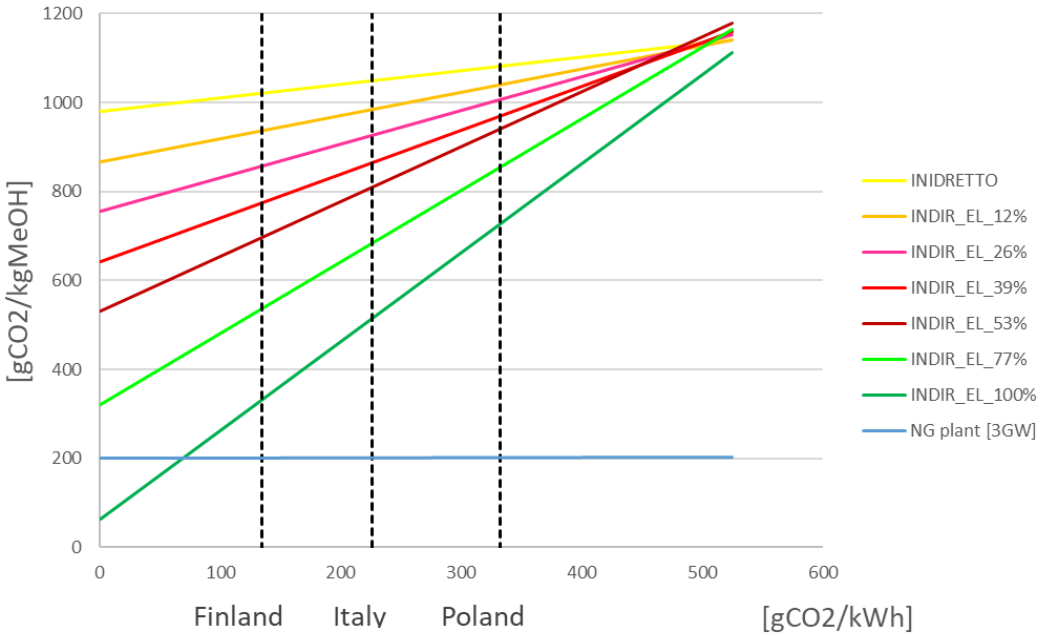

Figure 6-17: plants specific CO2 emissions with respect to the grid emissions

Conversely, considering every biogenic source as net zero, a completely different set of trendlines is reported in *Figure 6-16*. CO_2 plant emissions are negative and, hence, there's no competition for conventional natural gas plant.

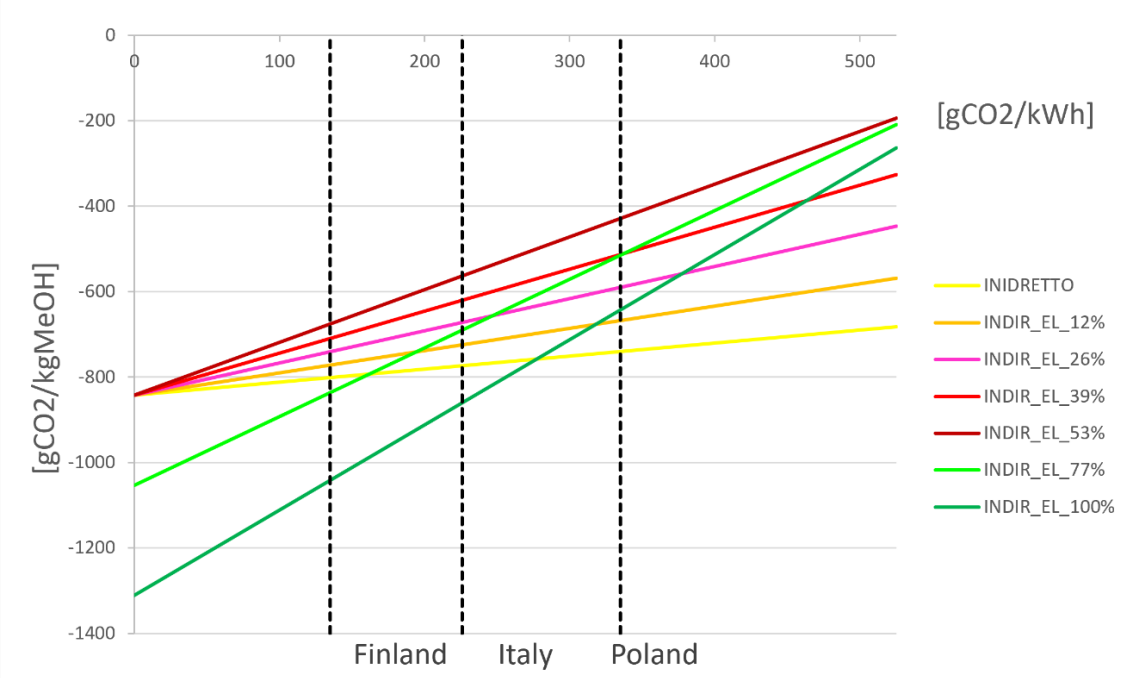

Figure 6-16: plants specific CO emissions with respect to grid emissions considering biomass as biogenic source

Furthermore, the distortional phenomenon described in *section 6.3.1.1* for direct plants is less pronounced in this case. Every hybrid mode from 1% to 53% of electrification starts with the same off-set, result of same CO_2 captured (no off-design); however, from the configuration with 53% of electrification on, biochar is sequestrated. The new term $\frac{MM_{CO2}}{MM_C}\dot{m}_{Produced\ biochar}$ is then accounted in Equation (6-5) and hence the starting offset decreases; the latter reduction compensates the increasing in slope and makes full electric case the more competitive also considering Italian grid.

7 Economic analysis

The target of the current study is to assess the feasibility of the implementation of electrical resistances in existing plants to perform gasification with an alternative source of heating. Hence, the economic analysis is based on a differential form which considers only the variations of costs and revenues between the analysed case and the reference one assessing in which framework of hypotheses the implementation of electric resistances can be profitable.

The reference cases chosen are the non-electrified gasifiers described in *section* 3.2.1 and 3.2.2. As consequence, in this study only costs related to the implementation of resistances, solar field and battery are considered.

As depicted in *section 4.2.2.* and *4.3.2.*, a resistances integrated plant is able to operate at any percentage of electrification, simply increasing or reducing the amount of electricity that flows in the resistors. The economic analysis defines criteria and parameters that determine when it is convenient to power the electrical resistances and in which percentage.

The simulation is run over the 8760 hours of the year and aims to determine the amount of:

- Commercial items produced
- CO_2 emissions
- Energy consumed
- Operative hours of each mode

7.1. Assumptions

The main cost assumptions on which this study is based are reported in *Table 7-1.*

Table 7-1: prices assumptions for economic analysis

Specific Costs	Assumed value	Reference
INVESTMENT		
Resistances [€/kW]	100	[HP]
Total installed solar field [€/kW]	855	[13]
Battery [€/kWh]	150	[82][83]
CONSUMPTION GOODS		
Methanol [€/ton]	400-600	[30]
Biomass [€/ton]	46-100	[46][87]
Biochar [€/ton]	300	[84][85][86]
CO2 captured [€/ton]	50	[88]

From a design point of view, the electrification procedure could result in the implementation of resistive or inductive cylindrical electrical elements immersed in the fluid beds horizontally (in case of boiling fluid beds) or vertically (in case of circulating fluid beds). There is no literature about electrification of gasifier or chemical reactors where specific costs for electrical resistances are reported. In this thesis study the resistances specific cost is assumed 100 €/kW.

Furthermore, in the current study it is considered important to access the feasibility of the application of a solar field coupled with the production plant to ensure a renewable source of electricity. In the sensitivity analysis, the size of the solar field is increasingly varied from a minimum load of 30 MW (insufficient for the electrical demands of the plant) up to a size of 100 MW. A total installed solar field specific cost of 855 €/kW is assumed, in accordance with 2021 IRENA report for renewables technologies [13].

As the solar field scale increases, an increasing share of electric power is sold back to the grid at peak production times; it is assumed to resell the energy on the grid at a sale price equal to 40% of the purchase price. To overcome this phenomenon (which is economically detrimental) the adoption of a battery is considered as a strategy to operate energy time-shifting. During overcapacity hours, energy is stored in the battery; conversely, during night hours, energy is prevailed from the battery and feeds

plant energy loads. For what concern battery cost, a value of 150 €/kWh with 4 hours storage capacity is assumed; the value reflects future trend costs projections to 2030 reported by the U.S. department of energy [82]. The assumption is confirmed in the article of Curry et al [83] published in 2017 by Bloomberg which foresees for 2030 a price even lower 100 €/kWh. Methanol price, as reported in *Table 7-1*, is assumed as 600 €/ton according to September 2022 MMSA price [30]. This price is largely affected by the current crisis. Hence, a specific cost of 400 €/ton (pre-war value) is also reported with the intent of performing a sensitivity analysis between the two reported values.

For what concern biochar price, a world commercial market to refer to does not exist yet; hence, biochar selling price is assumed starting from research literature. In the work of Meyer et al [84] a wide variety of statistics on char production costs report price values ranging from 51 US$/ton (pyrolysis biochar) to 386 US$/ton (retort charcoal). According to Galinato et al [85], a price of 350.74 US$/ton can be assumed for biochar obtained by crop production and carbon sequestration. According to these references and envisaging a further expansion of biochar market [86], a price of 300 €/ton is considered reasonable and is assumed.

For the biomass price two values are reported in *Table 7-1;* the first one is referred to "as received" biomass (49 €/ton), the second one to dry biomass (100 €/ton) respectively according to [46] and [87] .

For captured and stored CO_2, a commercial value of 100 €/ton is assumed [88]; to account for CO_2 compression and transportation, a cost of 50 €/ton is considered. The result of these hypotheses is a net CO_2 value equal to 50 €/ton, which is finally accounted. It is important to highlight that this price is calculated relying on the actual commercial value of CO_2 certificates and, hence, is underestimated with respect to future enviable trends. In Boyce et al [89] , it is shown that the carbon prices required to limit global warming to below 2°C by the end of the century [2] are in the order of magnitude of 200-250 US$/ton.

7.1.1. Grid assumptions

In this economic analysis two different electric grid prices are analysed: 2019 Italian, grid and November 2021 – October 2022 Italian grid.

In the first electric network renewable sources account for 42.77% of the overall electricity produced [79] and the average price of electricity is 52 €/MWh [90]. In a context of future sustainable development, it is possible to assume for European electricity networks a progressive decrease in electricity prices as a result of an increase of renewable penetration [41].

The second reference grid is considered as a "crisis condition" reference case. Indeed, between November 2021 – October 2022, the electric grid prices are affected by two macro events: covid-19 pandemic and Ukraine – Russia war (February 24th, 2022). More in details, after covid outbreak at the end of 2021 the electricity prices increased due to post-pandemic economic recovery. Furtherly, war and blackmail policies implemented by Russia against Europe countries have led to a shortage of natural gas, that represent the main fuel adopted in Italy for power production [79]. The effect of this shortage in the first and second quarter of the year has led to a dramatically increase of the electricity price that has touched during summer the maximum value of 871 €/MWh [90].

These two completely different sets of prices are taken in consideration in the current study to make the resulting analysis more resilient. The first one represents a precautionary starting point for a future electric grid, whereas the second is reported to record the effect on an investment of unpredictable events, i.e., Black Swans [91].

7.2. Methodology

7.2.1. Willingness to pay prices

To perform an hourly simulation, it is necessary to understand what is the reference price that makes it profitable to switch on a larger share of resistors, i.e., the incremental Break-Even Prices (BEP) of electricity. BEP parameter assesses the trade-off between a higher product yield (larger incomes) and higher purchased electricity; it ultimately represents the "willing to pay" electricity price that results an instantaneous income equal to zero.

The general differential BEP function can be obtained from the equilibrium of the incremental differential revenues and costs, as depicted in Equation (7-1) where $Price_{el}$ is the grid hourly electricity price, $d\dot{P}_{el}$ is the power consumption differential between each plant operative point, $Price_i$ is the price of the i-product of the plant and $d\dot{m}_i$ is the i-product differential between each plant operative point. For the considered plant configurations, the only differential cost is represented by electricity, whereas differential revenues derive from the selling of the streams of valuable products obtained.

$$Price_{el}\, d\dot{P}_{el} = \sum Price_i\, d\dot{m}_i \tag{7-1}$$

The latter equilibrium equation can be rearranged into Equation (7-2), where Break-Even Price of electricity ($BEP_{Price,el}$) is highlighted. The BEP represent the minimum price of electricity that make the profits of the plant equal to 0.

$$BEP_{Price,el} = \sum Price_i \frac{d\dot{m}_i}{d\dot{P}_{el}} \quad (7\text{-}2)$$

According to the shape of incremental BEP function different scenarios can arise:

- Scenario 1- linear increase of incremental BEP: the progressive switch on of the resistances (i.e., a larger electricity purchase) results in increasing production yields which outweigh costs. In this case, if the grid price is lower than maximum value of BEP, the plant is always operated in full electric mode.

- Scenario 2- constant trend for incremental BEP: the trade-off between yields and electricity is zero. Since there's no economical difference in operating in direct mode or in full electric mode, if the grid price is lower than maximum value of BEP, it is chosen to operate the plant in full electric mode. In this way a larger quantity of useful product is obtained and, as consequence, the plant operator is able to control a larger share of product market.

- Scenario 3- linear decrease of incremental BEP: the incremental switch on of the resistances results in a low increasing production yields which are outweighed by increasing costs. In this case the plant is always operated without resistances and, hence, the investment is not envisaged.

- Scenario 4 – incremental BEP trend is a non-linear function: in this case a functional study is conducted to identify the areas, between relative minimum and maximum values, in which it is profitable to operate the plant.

7.2.1.1. Willing to pay direct configurations

For the direct configuration, incremental BEP function is computed as reported in Equation (7-3).

$$BEP_{el} = \frac{d\dot{m}_{MeOH}}{d\dot{P}_{el}} Price_{MeOH} + \frac{d\dot{m}_{CO2}}{d\dot{P}_{el}} Price_{CO2} \quad (7\text{-}3)$$

The formula is derived from the general BEP differential equilibrium, Equation (7-1), which is rearranged in Equation (7-4); CO_2 and Methanol price are assumed as constant.

$$Price_{CO2}\, d\dot{m}_{CO2} + Price_{MeOH}\, d\dot{m}_{MeOH} = Price_{el}\, d\dot{P}_{el} \qquad (7\text{-}4)$$

The characterization of BEP differential form is made through a discretisation process in which a set of incremental $Price_{el}$ are computed, as reported in Equation (7-5), between two sequential levels of electrification, i.e., between DIR_EL_[x]% and DIR_EL_[x-offset]%. For this analysis, an offset value of 12.5% is considered.

$$Price_{el,discretized} = \frac{\Delta\dot{m}_{MeOH}}{\Delta\dot{P}_{el}}\, Price_{MeOH} + \frac{\Delta\dot{m}_{CO2}}{\Delta\dot{P}_{el}}\, Price_{CO2} \qquad (7\text{-}5)$$

In *Figure 7-1* incremental electricity BEP trends are shown.

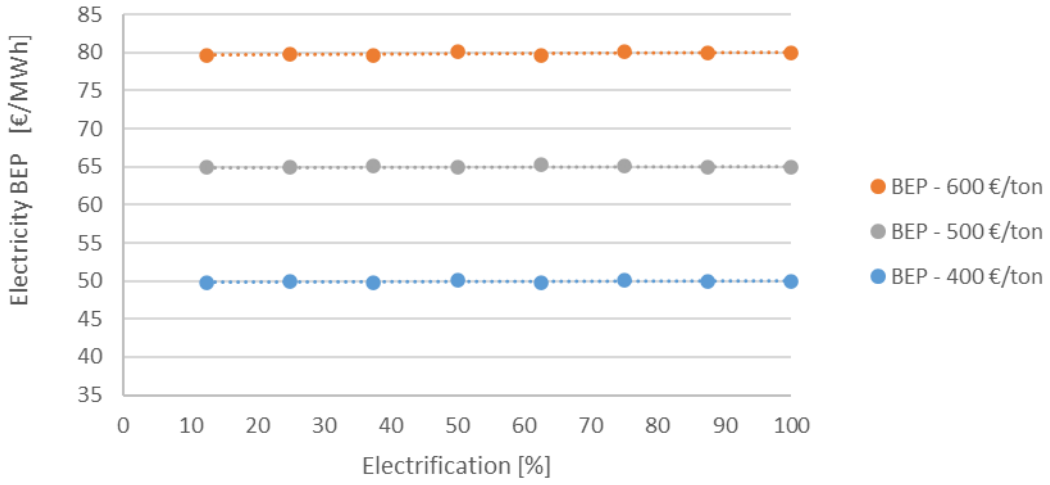

Figure 7-1: BEP with respect to the electrification of the direct gasifier

It is possible to notice that BEP trends are constant and strongly depend on methanol price. The computed values of 50 €/MWh, 65 €/MWh and 80 €/MWh are considered as "willing to pay" electricity prices.

Furthermore, as the incremental BEP function is constant, scenario 2 depicted in *paragraph 7.2.1* is realised. Hence, whenever the grid price is lower than 50 €/MWh, 65 €/MWh or 80 €/MWh (depending on methanol cost current assumption), it is chosen to operate the plant in full electric mode. In the other case, with higher grid prices, the switch-on of the resistances is not profitable and, hence, the gasifier is operated in the baseline mode.

7.2.1.2. Willing to pay indirect configurations

For the indirect configuration, incremental BEP function is computed as reported in Equation (7-6).

$$Price_{Biochar}\, d\dot{m}_{Biochar} + Price_{BioDry}\, d\dot{m}_{BioSaved} = Price_{el}\, d\dot{P}_{el} \qquad (7\text{-}6)$$

Comparing Equation (7-6) with Equation (7-4), it is interesting to highlight the absence of methanol and captured CO_2 terms; these products are fixed in quantity as the electrification is increased and therefore have an incremental delta of production equal to zero. Conversely, biochar and biomass production vary with the increasing electrification and, hence, are reported in Equation (7-6).

Furthermore, for indirect configurations, two areas of operation can be defined: between 0% and 53% of electrification (where an increasing part of biomass is saved) and between 53% and 100% (where an increasing part of biochar is sequestrated).

Consequently, for the first range BEP function assumes the expression reported in Equation (7-7).

$$BEP_{el} = \frac{d\dot{m}_{BioSaved}}{d\dot{P}_{el}}\, Price_{BioDry} \qquad (7\text{-}7)$$

whereas, for the second range, Equation (7-8) takes in consideration only biochar production.

$$BEP_{el} = \frac{d\dot{m}_{Biochar}}{d\dot{P}_{el}}\, Price_{Biochar} \qquad (7\text{-}8)$$

The characterization of BEP differential form is made through a discretisation process in which a set of incremental $Price_{el}$ are computed between two sequential levels of electrification, i.e., between DIR_EL_[x]% and DIR_EL_[x-offset]%.

In *Figure 7-2*, incremental electricity BEP trend, divided in the two ranges, is shown.

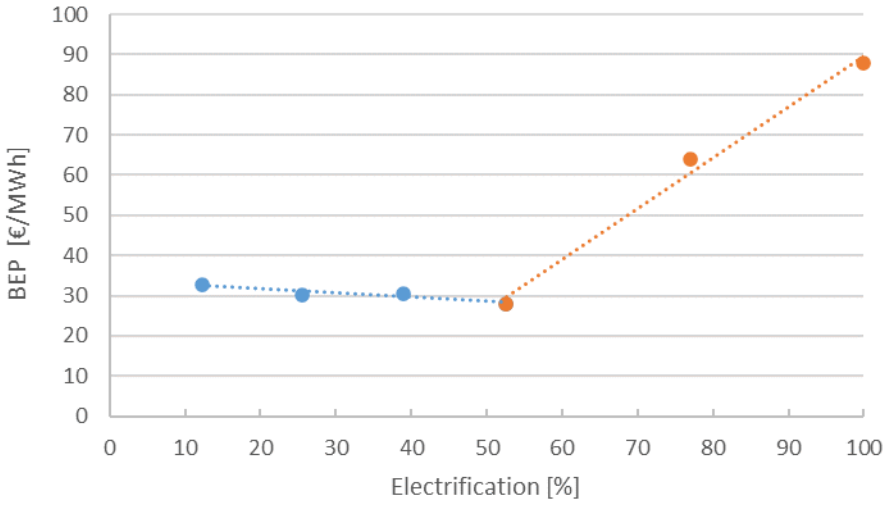

Figure 7-2: BEP with respect to the electrification of the indirect gasifier

It is possible to notice that BEP trend is a decreasing function until the change of range, where the trend is reversed; scenarios 3 and 1 depicted in *paragraph 7.2.1* are respectively realised. However, since BEP price of INDIR_EL_100% configuration outweighs the other relative minimum (INDIRECT case) the overall scenario can be assumed as 1; hence, in this case, plant is always operated in full electric whenever possible.

Since the piecewise-defined function has a local minimum and it is decided to operate only between two points (minimum and maximum electrification), the calculation of the BEP must be redone taking in account only the two chosen operating points. From the final Equation (7-9) a BEP value of 53 €/MWh is calculated.

$$BEP_{Price,el}[IND_{EL_{100\%}} - IND] = \frac{\Delta\dot{m}_{char}}{\Delta\dot{P}_{el}} Price_{char} + \frac{\Delta\dot{m}_{BioSaved}}{\Delta\dot{P}_{el}} Price_{BioDry} \quad (7\text{-}9)$$

7.2.2. Hourly simulation algorithms

In the previous section, BEP prices are identified as:

- 50 €/MWh, 65 €/MWh or 80 €/MWh for direct configuration (depending on methanol cost assumption)
- 53 €/MWh for indirect configuration

The aim of this section is to use BEP information to shape the algorithms for plant simulation.

Two different algorithms, shared by both direct and indirect configuration, are identified:

- the first one concern grid simulation (i.e., the case in which the plant is operated only in connection with the grid)
- the second one involves the adoption of a solar field and a battery

For simplicity in this paragraph, algorithm considerations are based on the direct configurations, even though they are still completely valid for indirect one

First case algorithm, synthetized in *Table 7-2*, is derived by considerations on BEP prices made in *paragraph 7.2.1* on BEP electricity prices and scenarios.

Table 7-2: direct configuration simulation algorithm logic

	Price > BEP	Price < BEP
Active configuration	DIRECT	DIR_EL_100%

Second case algorithm, depicted in *Table 7-3* is less trivial since has to deal with solar field regulation. If the solar production is not sufficient to satisfy plant baseload, second algorithm falls into the first one: if price is lower with respect to BEP it is profitable to switch on all installed resistance power, otherwise the plant is operated baseline case.

Table 7-3: solar field case direct configuration simulation algorithm logic

Solar field \ BEP	Price > BEP	Price < BEP
Solar production < plant baseload	DIRECT	DIR_EL_100%
Solar production > plant baseload	DIR_EL_[x]%	DIR_EL_100%

Conversely if solar production is higher than plant baseload two cases arise:

- if price is higher than BEP it is not convenient to withdraw energy from the grid. Hence only internal energy coming from the solar field is exploited to satisfy

resistances load. In this way, only a fraction [x], ranging from 1% to 100% of resistance power is switched on, i.e., DIR_EL_[x]%.

- Conversely, if grid price is convenient, solar field energy is used for full resistance powering; missing extra energy is bought from the grid.

The instance "Solar production > plant baseload" also includes the case in which solar production exceeds maximum plant energy consumption. Whenever the solar field is over-dimensioned, a higher share of electricity produced is sold back to the grid at peak production times at a selling price lower than purchase one. In these cases, as depicted in *section 7.1*, the adoption of a battery is considered as a strategy to operate energy time shifting.

A charge-discharge efficiency (round-trip efficiency) of 90% is assumed for battery management [92].

Price selling to grid is assumed to be equal to 40% of purchase price.

7.2.2.1. Example of plant operation

In this section an example of the current functioning of the plant is reported in *Figure 7-3*. Direct plant simulation: first day of the year (01/01/2019, first 24 hours)

Assumptions:

- 2019 Italian Grid
- Methanol price: 400 €/ton
- BEP of electricity: 50 €/MWh
- Solar field size: 80 MW [93]
- Battery size: 20 MWh of storage

In the first hour of the year, electricity price is equal to 51 €/MWh with no energy production from the solar field; hence, the plant is operated (in accordance with algorithm 2) in DIRECT configuration (6.6 MWh are withdraw from the grid to satisfy plant baseload). From the hour 2 to 6, price is below BEP and no energy is produced from the solar field; hence the plant is operated in DIR_EL_100% configuration. From the hour 7 to 16, the solar field is active and hence an increasing part of the load is satisfied by it. With a size of 80 MW, the solar field is over dimensioned: during hour 9,10,11 extra energy flows from the solar field to the battery till battery capacity is saturated; from that point on extra energy is sold on the grid. During hour 15, since solar field energy is not enough to sustain full electrification, residual energy is taken from the battery. During hour 16, DIR_EL_3% configuration is active, as consequence

of a solar production higher with respect to baseload and a grid price higher than BEP. From hour 17 to 24, electricity price is higher than BEP with no energy production from the solar field; hence, plant is operated in DIRECT configuration with part of the energy that is prevailed in hour 17 and 18 from the battery.

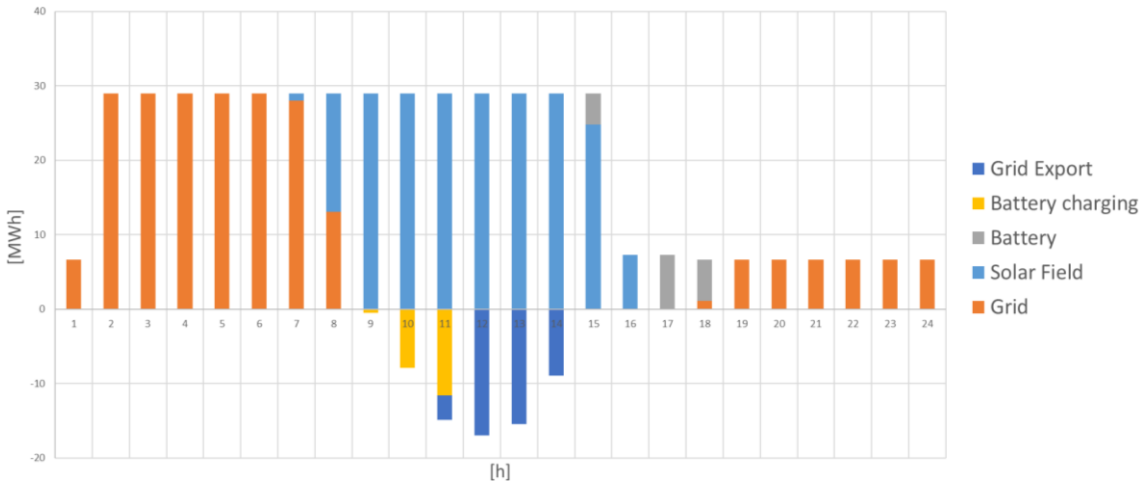

Figure 7-3: 24 hours example of simulation results. In the diagram the power absorbed by the plant in each hour and the sources of that power.

7.2.3. Economic model

The economic analysis is based on a differential form which consider only the variations of costs and revenues between the analysed case and the reference one.

The following assumptions are taken:

- Discount rate=8%
- Inflation= 2%
- Yearly plant OPEX = 3%CAPEX

For every simulation the following quantities are calculated.

Net present value (NPV), depicted in Equation (7-10), is the net present value of the cash flows (CF) compared to the initial investment and accounting a discount rate (r). The value is calculated over an estimated 20-year time horizon (t), equal to supposed plant service life [46]. This parameter is positive whenever it is convenient to undergo the investment.

$$NPV\ [€] = \sum_{t=0}^{20} \frac{CF_t}{(1+r)^t} \tag{7-10}$$

The internal rate of return (IRR) is calculated in Equation (7-11). It represents the discount rate (r) that nulls the NPV and indicates the profitability of the investment.

$$0 = \sum_{t=0}^{20} \frac{CF_t}{(1 + IRR)^t} \tag{7-11}$$

The revenues/costs of material products/inlets of the plant computed as reported in Equation (7-12), where n is the number of configuration used during the year, while i is the products/inlets of the plant that correspond to:

- Methanol
- Biochar
- CO_2 captured
- Saved biomass
- Inlet biomass
- Emitted CO_2

$$C_i \left[\frac{€}{y}\right] = \sum_{n=0}^{n} \dot{m}_{i,n} * 3.6 * h_n * price_i \tag{7-12}$$

The cost of electricity is computed as depicted in Equation (7-13).

$$C_{el} \left[\frac{€}{y}\right] = \sum_{h=0}^{8760} Grid\_consumption_h * Hourly\_Electricity\_price_h \tag{7-13}$$

For every hour of the year the product between $Grid\_consumption_h[kWh]$ and $Hourly\_Electricity\_price$ $[^{€}/_{kWh}]$ is computed and finally summed.

7.2.4. Sensitivity analysis

In this current study the following sensitivity analysis are performed:

- 2019 Italian grid vs 2021/2022 Crisis condition" Italian grid
- Methanol price: 400 €/ton or 600 €/ton
- Solar field size: 30 MW – 50 MW – 65 MW – 80 MW – 100 MW
- Battery size: 1 – 2 – 3 – 4 equivalent hours of storage

Grid and methanol price sensitivities are performed to make the resulting analysis more robust against Black Swan events such as Covid-19 outbreak or Russo-Ukrainian War. Solar field and battery sizes are varied to identify the most profitable operating combination depending on the assumptions.

7.3. Results

In this section simulation results are reported and critically discussed.

The value of the following parameters is reported.

- NPV

Net present value is calculated as reported in Equation (7-10) assuming a discount rate equal to 8% as stated in *paragraph 7.2.3.*

- IRR

Internal Rate of Return is calculated through numerical methods by setting to zero Equation (7-11).

- Capacity Factor of Resistances, reported in Equation (7-14).

$$CF_{Resistances} = \frac{EE_{resistances}\ [MWh/y]}{P_{nominal\ resistances}\ [MW] * 8760\ [h/y]} \tag{7-14}$$

The numerator shows the total annual energy that, given a certain configuration, flows into the resistors. The denominator instead shows the nominal power of the resistances multiplied by the annual hours of operation.

This dimensionless parameter accounts for the electrification level of the simulated plant. Since the economic analysis carried out is differential and compares the simulated case with respect to the baseline case, a high parameter value entails high operating hours in resistances and, therefore, high differential revenues.

Given the logic of operation of the system, $CF_{Resistances}$ is independent from the size of the battery. Indeed, according to the chosen algorithm, battery operations are limited to energy time-shifting action and doesn't change the operating points of the plant.

- PV usage, depicted in Equation (7-15).

$$PV\ usage_{Net} = PV\ usage = \frac{EE_{PV-to-Plant}\ [MWh/y]}{P_{nominal\ solar\ field}[MW] * 8760\ [h/y]} \tag{7-15}$$

The numerator shows the total annual energy that, given a certain configuration, directly flows from solar field to the plant. The denominator instead shows the nominal power of the solar field multiplied by the annual hours of operation. Since the simulation operation algorithm requires that the battery is charged only during overcapacity periods, PV usage parameter does not vary with the battery size.

To account also energy coming to the plant from the battery, $EE_{Battery-to-Plant}$ $[MWh/y]$, which is ultimately produced by the solar field itself, a new term is added at the numerator of the formula, obtaining the Equation (7-16).

$$PV\ usage_{Gross} = \frac{EE_{PV-to-Plant} + EE_{Battery-to-Plant}\ [MWh/y]}{P_{nominal\ solar\ field}[MW] * 8760\ [h/y]} \quad (7\text{-}16)$$

In this way it is also possible to account for battery energy time-shifting action.

- Battery yearly equivalent hours of storage, reported in Equation (7-17).

$$Heq_{battery}[h/y] = \frac{EE_{stored}\ [MWh/y]}{P_{nominal\ resistances}\ [MW]} \quad (7\text{-}17)$$

The numerator shows the total annual energy that, given a certain configuration, is stored in the battery and then given back to the plant during under-capacity periods; a round-trip efficiency of 90% is assumed as reported in *paragraph 7.2.2*. The denominator instead shows the nominal power of the resistances multiplied by the annual hours of operation.

The parameter accounts for the yearly equivalent hours of utilization of the battery.

7.3.1. Direct Simulation Results

In this section, simulation results regarding direct configurations are reported and critically discussed. In the diagrams of the following section, the different solar sizes are reported in legend as 30, 50, 65, 80 and 100 MW.

Battery yearly equivalent hours of storage and PV usage (net and gross one) change in accordance with the sizes of the solar field and battery, but they are independent from grid and price choices. Hence, it is chosen to report their diagram in this separate section as they are shared between all the cases.

In *Figure 7-4*, Net PV usage is reported in correspondence with *x=0;* the parameter is then increased accounting the effect of the battery to obtain Gross PV usage parameter.

Net PV usage ranges from a value of 100% (in case of a 30 MW solar field) to 60% (for a 100 MW one).

Net PV usage obtained from a solar field of 30 MW is saturated at 100% since a field of that size is not able at any time of the year to meet the maximum rated power of the

fully electrified plant (the solar field, sized on 30MW, produces a peak 27.5MW [93], lower than 29 MW requested).

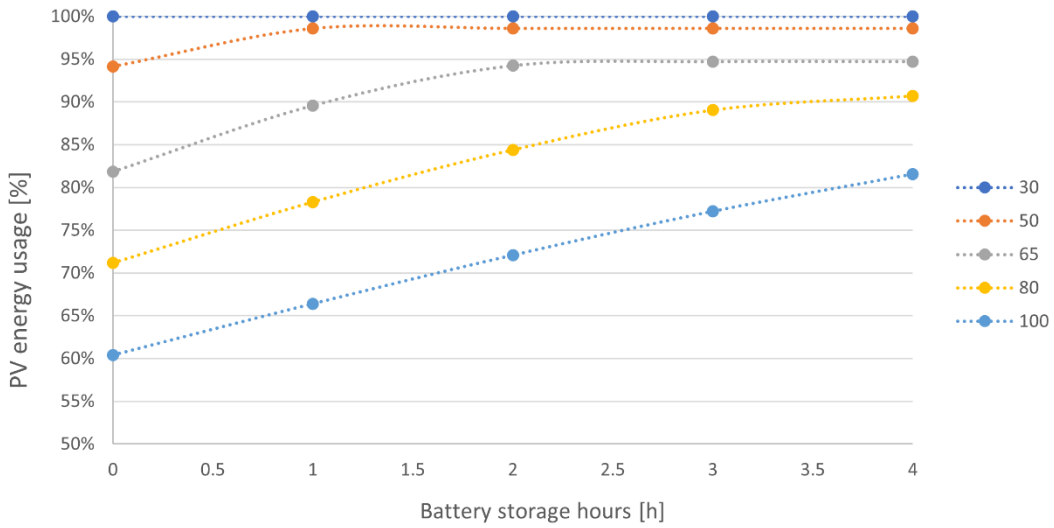

Figure 7-4: PV energy usage with respect to the battery storage hours

The addition of the battery allows to save energy in times of overcapacity and return it during times of under-capacity. Gross PV trends increase as the size of the battery increases; however, they don't reach 100%, since a battery round-trip efficiency of 90% is assumed (this is not valid for 30 MW solar field case, which is an exception since Net PV Usage is already saturated to 100%). The trend of Battery yearly equivalent hours of storage is reported in *Figure 7-5*.

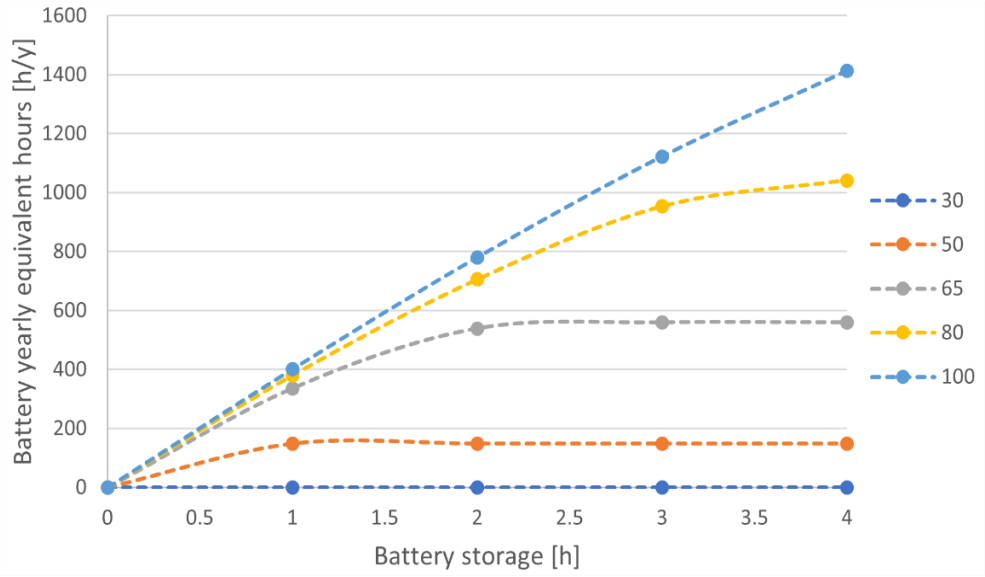

Figure 7-5: battery equivalent hours with respect to the battery storage hours

From the diagram, it can be stated that battery reach an interest number of yearly hour of utilization (i.e., higher than 1000 h_{eq}/y) only for over-dimensioned solar fields (80-100 MW) and 3 to 4 hours of storage of nominal plant load (i.e., 87MWh and 116MWh).

Furthermore, for solar sizes of 30MW, 50MW and 65MW, the trend is saturated at 0h, 2h and 3h storage respectively. The reason is related to the fact that for these combinations of solar size and battery, the battery is oversized compared to the solar field; the combinations thus obtained have therefore no techno-economic relevance.

In this way, the parameter allows to eliminate unnecessary cases. In the following analysis, these combinations are highlighted in grey to distinguish them from the others.

7.3.1.1. Grid 2019 - MeOH price 600€/ton

The case dealt with in this section considers a high price of methanol and an assumed grid, that one of 2019, whose average electricity price is around 52 €/MWh. Such a set of prices, far lower with respect to BEP of electricity price (80€/MWh), in principle allows a very high number of operating hours in resistance mode, with high profits from the sale of methanol. As one can see in *Figure 7-6*, CF Resistances parameter shows an almost constant trend around the value of 98.25%.

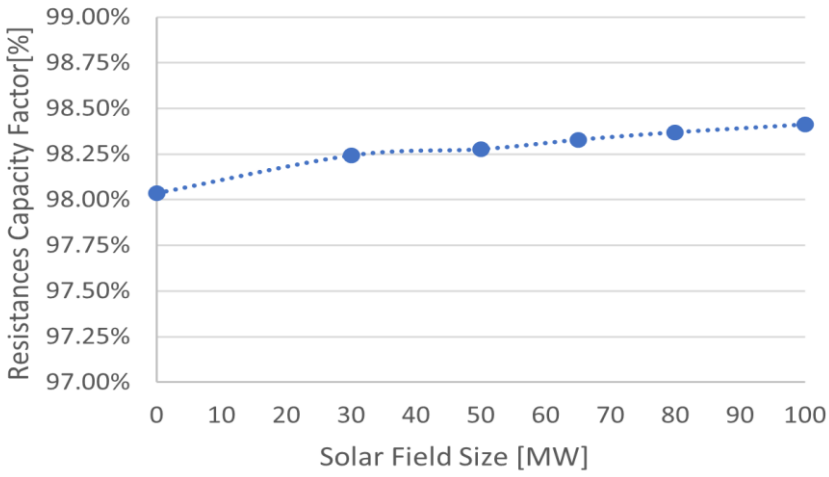

Figure 7-6: resistances capacity factor with respect to the size of the solar field

The high value is explained by the fact that, given the favourable set of assumptions, the plant has a great advantage in powering the resistances already without a solar field. The addition of the latter does not bring the parameter to saturation since times with peak energy prices (night-time) during which plant operate in baseline mode are decoupled from those of maximum solar energy generation (daytime).

For IRR and NPV trends, it is chosen to also report the table of values with conditional formatting (blue to red) in order to highlight the topical cases (in grey, over-dimensioned battery cases).

As one can note in *Table 7-4* and in *Figure 7-7*, the trend of the IRR rewards the configuration with no solar field as the most profitable one.

Table 7-4: 2019-600 €/ton IRR with respect to the size of the solar field

IRR						
Battery storage hours	***Solar size [MW]***					
	0	**30**	**50**	**65**	**80**	**100**
0	227.7%	25.0%	16.4%	12.7%	10.0%	7.3%
1		21.0%	14.5%	11.6%	9.2%	6.8%
2		17.8%	12.7%	10.4%	8.4%	6.3%
3		15.2%	11.1%	9.2%	7.6%	5.7%
4		13.0%	9.7%	8.0%	6.6%	5.1%

This plant simulation, operating almost exclusively in resistances and benefiting from a favourable price of methanol, is able to recover the total investment of 2,345 M€ already in the first year (annual profit not discounted of 5.5 M€). Hence, IRR calculation exceed 100% (in the graph this value is not reported).

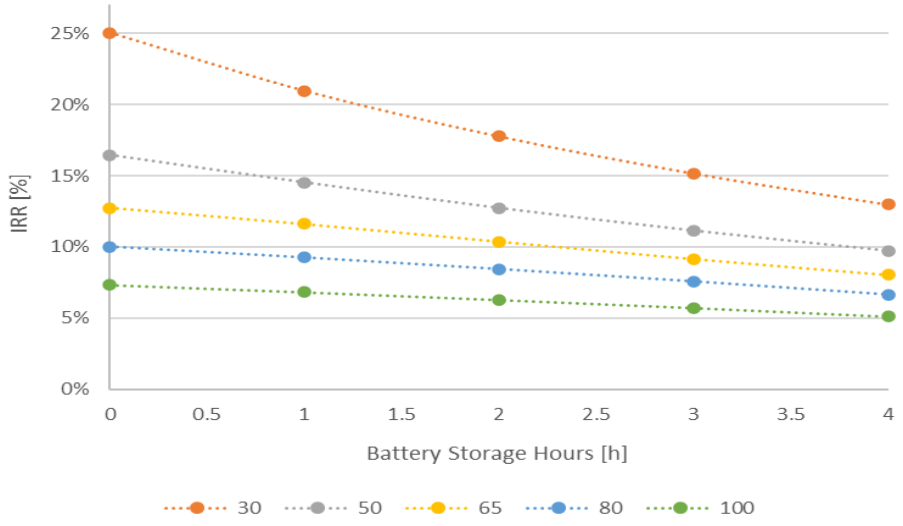

Figure 7-7: 2019-600 €/ton IRR with respect to the battery storage hours

For what concern the other cases, it is evident that the high cost of solar field and battery is not balanced by the internal benefit of plant decoupling from the grid. The trend is confirmed by CF resistances parameter, which barely change passing from no solar field case to a 100MW solar field.

As reported in *Figure 7-8* and *Table 7-5*, NPV trend is almost aligned IRR one. Being calculated by placing discount rate equal to 8%, the trend is negative for each configuration that presents IRR<8%.

Table 7-5: 2019-600 €/ton NPV with respect to the size of the solar field

NPV [M€]						
Battery	***Solar size [MW]***					
storage hours	**0**	**30**	**50**	**65**	**80**	**100**
0	50.0	41.0	30.7	21.3	10.6	-4.2
1		35.1	25.6	17.2	6.9	-7.7
2		29.3	19.7	11.9	2.5	-11.7
3		23.5	13.9	6.1	-2.6	-16.1
4		17.6	8.1	0.2	-8.5	-21.0

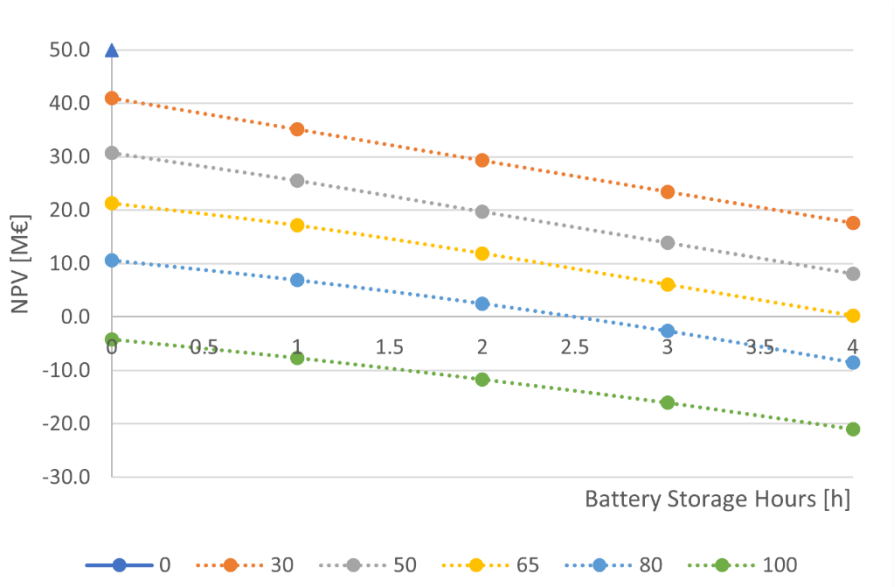

Figure 7-8: 2019-600 €/ton NPV with respect to the battery storage hours

7.3.1.2. Grid 2019 - MeOH price 400€/ton

The case considered in this section takes into account a low price of methanol and a grid, that of 2019, whose average electricity price is around 52 €/MWh. Such a set of prices, slightly higher than BEP of electricity price (50€/MWh), in principle allows an average number of operating hours in resistance mode, but with scantly profits from the sale of methanol. As can be noticed in *Figure 7-9*, CF Resistances diagram shows an increasing trend from 45% to 65%.

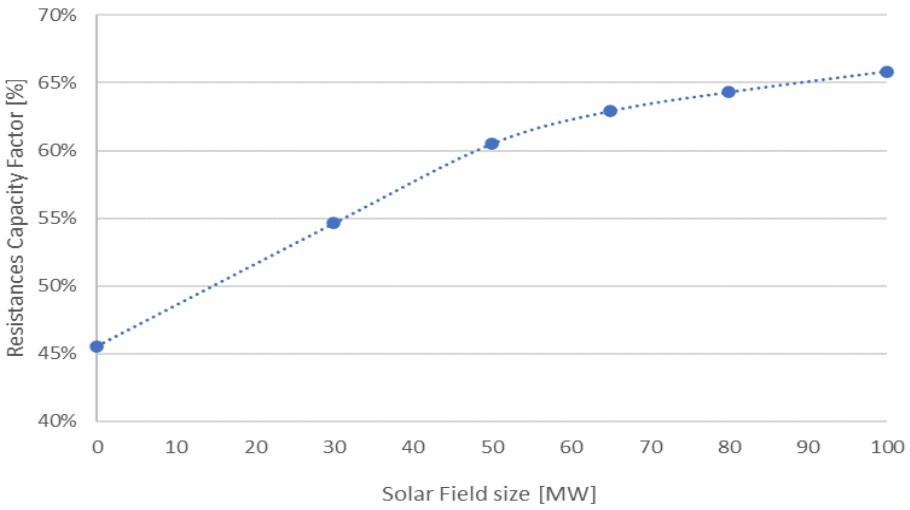

Figure 7-9: resistances capacity factor with respect to the size of the solar field

The proximity between average price on the grid and BEP contributes to an average utilization factor when the system is only connected to the grid. The value is than increased as the solar field is oversized. The growth, initially linear, soon becomes logarithmic; the reason is linked to the fact that the price of electricity is low in conjunction with the daytime hours due to the presence of solar energy dispatched on the network with priority. Hence, since daytime hours are partially just accounted in the case with no solar field, the effect of solar field on this parameter is limited.

As mentioned in *paragraph 7.3.1.1*, IRR and NPV values are reported in *Table 7-6* and *Table 7-7* with conditional formatting (blue to red) in order to highlight the topical cases (in grey, over-dimensioned battery cases).

Table 7-6: 2019-400 €/ton IRR with respect to the size of the solar field

IRR						
Battery	***Solar size [MW]***					
storage hours	**0**	**30**	**50**	**65**	**80**	**100**
0	28.4%	4.7%	2.0%	0.3%	NPV<0 IRR = 0	NPV<0 IRR = 0
1		2.2%	0.6%	NPV<0 IRR = 0	NPV<0 IRR = 0	NPV<0 IRR = 0
2		0.1%	NPV<0 IRR = 0	NPV<0 IRR = 0	NPV<0 IRR = 0	NPV<0 IRR = 0
3		NPV<0 IRR = 0	NPV<0 IRR = 0	NPV<0 IRR = 0	NPV<0 IRR = 0	NPV<0 IRR = 0
4		NPV<0 IRR = 0	NPV<0 IRR = 0	NPV<0 IRR = 0	NPV<0 IRR = 0	NPV<0 IRR = 0

The trend of the IRR rewards the configuration with no solar field as the most profitable one. This configuration operates 45% of the hours in resistances mode, being able to recover the total investment of 2,345 M€ in 5 years (annual profit not discounted of 0.7 M€). For the other cases, it is evident that the high cost of solar field and battery is not balanced by the internal benefit of plant decoupling from the grid. Furthermore, the effect obtained by their addition is to completely erode the profit (NPV<0 with IRR=0). For this reason, IRR trend is not reported in a graph.

Table 7-7: 2019-400 €/ton NPV with respect to the size of the solar field

NPV [M€]						
Battery	***Solar size [MW]***					
storage hours	**0**	**30**	**50**	**65**	**80**	**100**
0	4.2	-6.2	-17.5	-27.5	-38.5	-53.8
1		-12.1	-22.8	-32.0	-42.6	-57.6
2		-17.9	-28.6	-37.6	-47.9	-62.7
3		-23.7	-34.5	-43.5	-54.1	-68.6
4		-29.6	-40.3	-49.4	-60.4	-75.0

The NPV trend is almost aligned with that of the IRR. As explained in *paragraph 7.3.1.1*, the trend is negative for each configuration that presents IRR<8%, being calculated by placing discount rate equal to 8%, and it is reported in *Figure 7-10*.

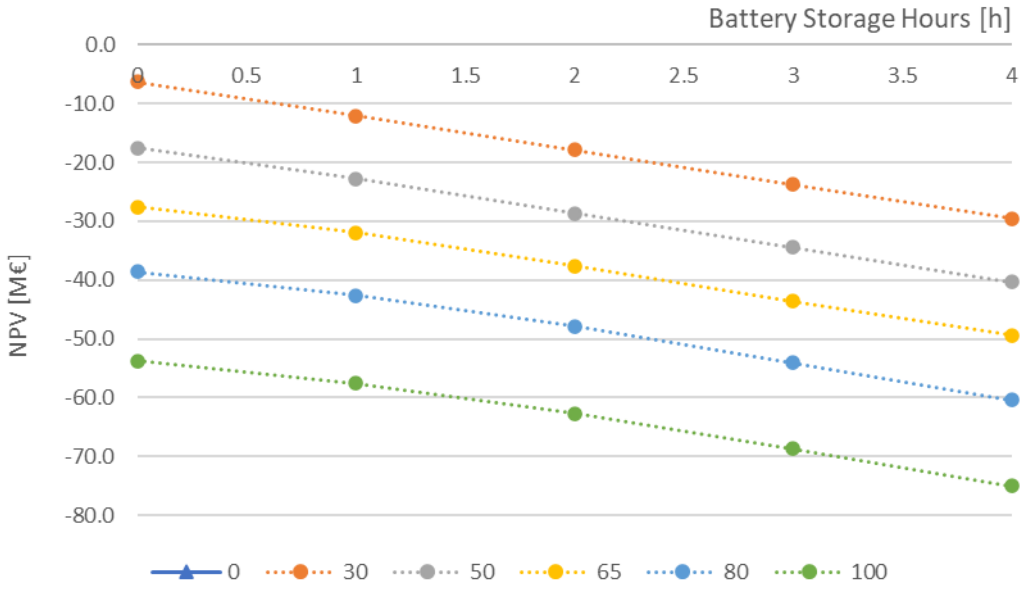

Figure 7-10: 2019-400 €/ton NPV with respect to the battery storage hours

7.3.1.3. Grid 21/22- MeOH price 600€/ton

The case studied in this section considers a high price of methanol and an assumed grid, "crisis one", whose average electricity price is around 300 €/MWh.

Such a set of prices, definitely higher than BEP electricity price (80€/MWh), in principle does not allow the system to operate in resistances; in this case the importance of solar field and battery rises.

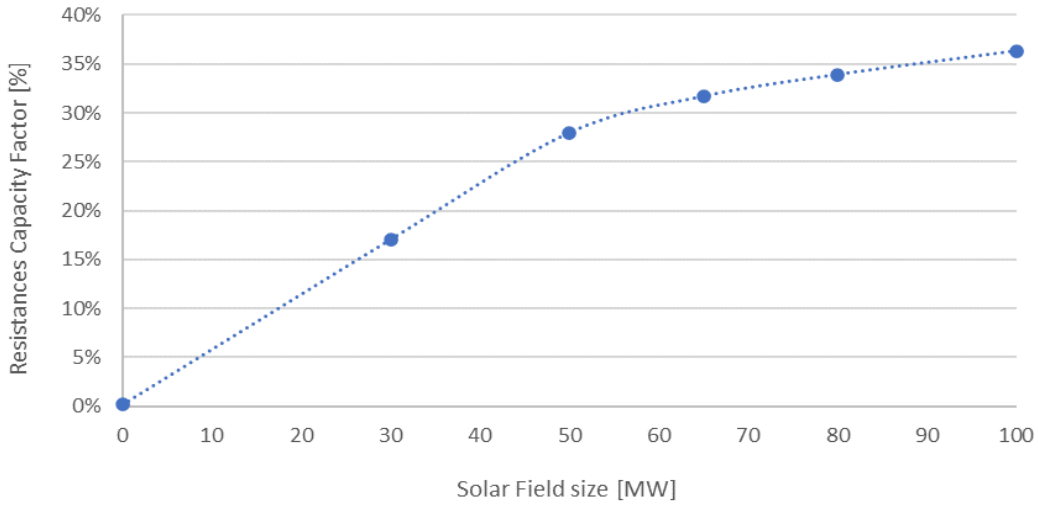

Figure 7-11: resistances capacity factor with respect to the size of the solar field

As one can note in *Figure 7-11*, CF parameter shows an increasing trend from almost 0% to 35%. Grid prices are too high to allow resistances powering; in this case the only way to gain access to the resistance modes is to rely on solar field energy. Comparing *Figure 7-11* with that of the previous *section 7.3.1.2* (grid case 2019-400 €/ton) it is possible to appreciate the action of the solar field. In the previous case its addition, spoiled by an initial offset of 45%, raised the parameter value by 20 points; in this case, instead, contributes to a delta of 35%, being decoupled by the grid effect.

In *Table 7-8* and *Figure 7-12*, IRR trends are reported.

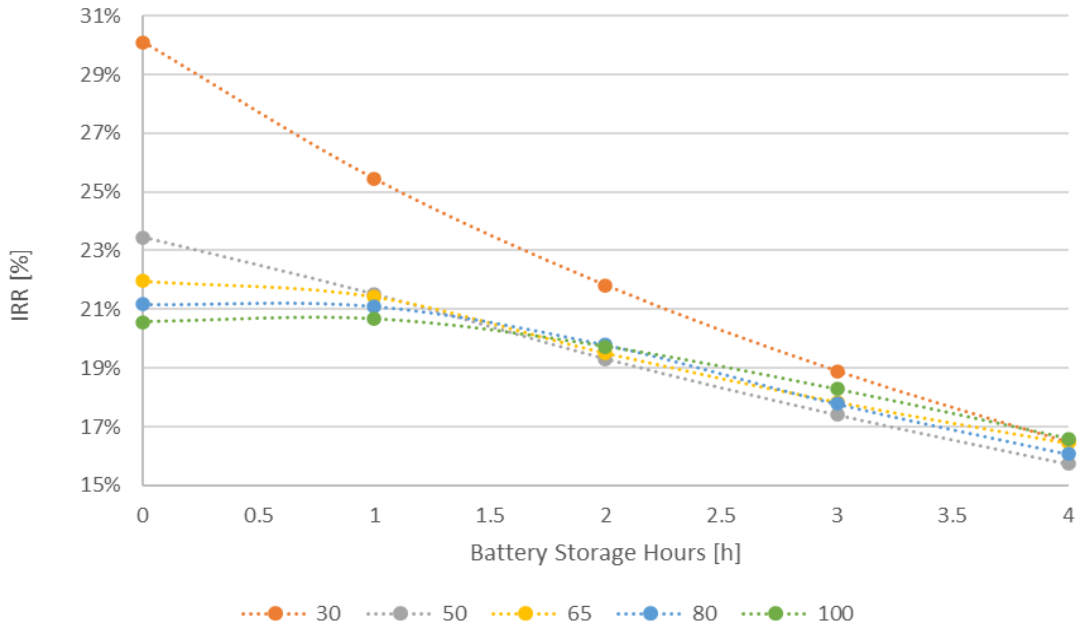

Figure 7-12: 2021-600 €/ton IRR with respect to the battery storage hours

In opposition with cases based on 2019 Italian grid, the configuration with no solar field is not profitable (NPV<0 with IRR=0). This configuration operates almost exclusively without resistances, given the high prices of electricity, and hence is not able to recover the total investment of 2,345 M€.

Conversely, solar field adoption permits to decouple the plant from the grid; in this way it is possible to hedge against high prices and obtain large differential revenues. However, the high investment cost penalizes the IRR, which reach higher values for lower solar field sizes.

If for the previous cases the energy time-shifting benefits linked to the increase in size of the battery were not sufficient to recover the investment cost of the latter, in this framework there is a case (100MW) in which IRR trend has a maximum for 1h of storage (battery size=29MWh).

Table 7-8: 2021-600 €/ton IRR with respect to the size of the solar field

IRR						
Battery	***Solar size [MW]***					
storage hours	**0**	**30**	**50**	**65**	**80**	**100**
0	NPV<0 IRR=0	30.1%	23.5%	22.0%	21.2%	20.6%
1		25.4%	21.5%	21.4%	21.1%	20.7%
2		21.8%	19.3%	19.5%	19.8%	19.7%
3		18.9%	17.4%	17.8%	17.8%	18.3%
4		16.5%	15.7%	16.4%	16.1%	16.6%

In *Table 7-9* and *Figure 7-13*, NPV trends are reported.

Table 7-9: 2021-600 €/ton NPV with respect to the size of the solar field

NPV [M€]						
Battery	***Solar size [MW]***					
storage hours	**0**	**30**	**50**	**65**	**80**	**100**
0	-3.1	54.4	59.4	68.2	78.3	92.3
1		48.6	56.2	70.3	82.6	97.7
2		42.7	50.4	63.6	77.9	94.1
3		36.9	44.5	57.1	67.1	85.1
4		31.1	38.7	51.3	57.3	73.1

In this case, the NPV trend is not perfectly aligned with the one of the IRR. If the highest values for IRR are reached for low solar field size, instead the best configurations in term of NPV are the ones which adopt large solar fields. Indeed, the higher the solar field the higher are the differential revenue that can be obtain with respect to a base case with no resistances and no solar field in which it is necessary to buy electricity on an expensive grid. Furthermore, NPV trends show a local maximum as the battery size varies, highlighting the beneficial effect of the latter.

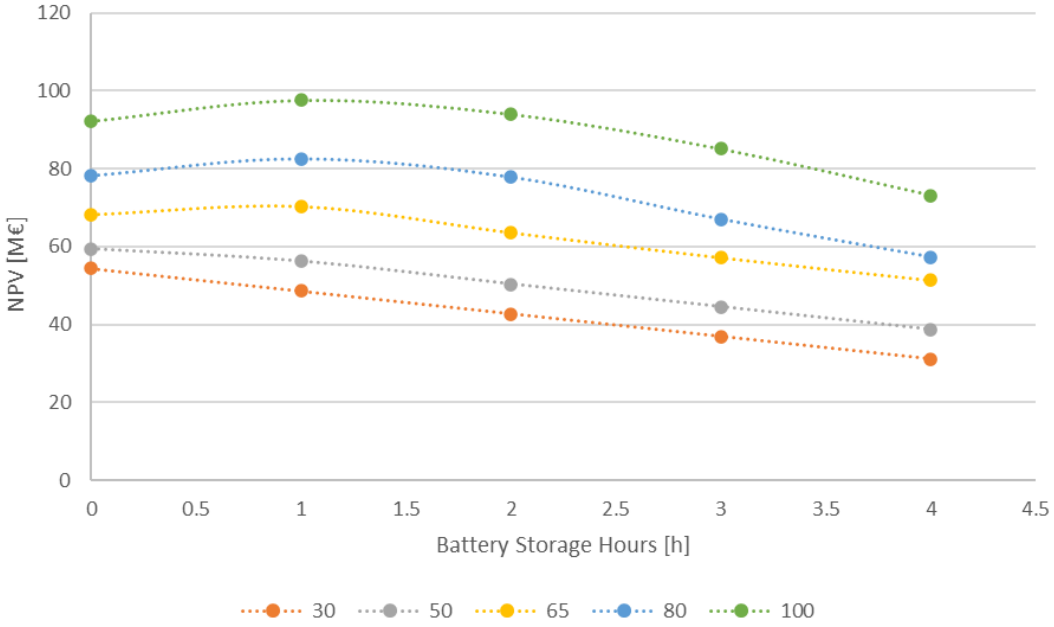

Figure 7-13: 2021-600 €/ton NPV with respect to the battery storage hours

7.3.1.4. Grid 21/22- MeOH price 400€/ton

The case investigated in this section is the most critical one, since takes into account a low price of methanol and an assumed grid, "crisis one", whose average electricity price is around 300 €/MWh. Such a set of prices, definitely higher BEP electricity price (50€/MWh), in principle does not allow the system to operate in resistances; in this case the importance of solar field and battery rises.

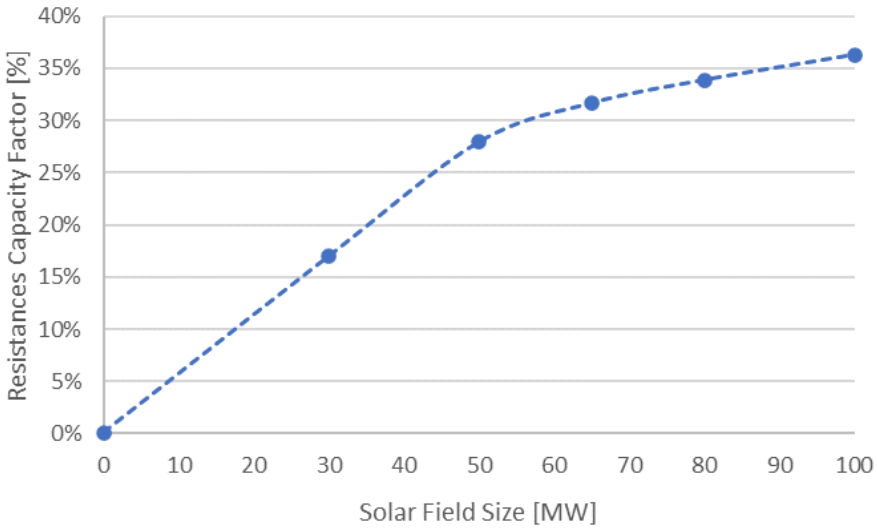

Figure 7-14: resistances capacity factor with respect to the size of the solar field

As depicted in *Figure 7-14*, CF Resistances shows an increasing trend from almost 0% to 35%. Note how the graph presents the same trend of grid case 2019-400 €/ton, *section 7.3.1.3*. Indeed, the effect of the solar field is independent of the selling price of methanol; hence, in the cases in which the only way to gain access to the resistance modes is to rely on solar field energy, the trend is the same.

In *Table 7-10* and *Figure 7-15*, IRR trends are reported. As depicted in *section 7.3.1.3*, the configuration with no solar field is not profitable (NPV<0 with IRR=0) whereas solar field adoption permits to decouple the plant from the grid.

Table 7-10: 2021-400 €/ton IRR with respect to the size of the solar field

	IRR					
Battery	***Solar size [MW]***					
storage hours	**0**	**30**	**50**	**65**	**80**	**100**
0	NPV <0 IRR=0	27.1%	20.0%	18.7%	18.3%	18.0%
1		22.8%	18.3%	18.4%	18.4%	18.3%
2		19.4%	16.3%	16.6%	17.2%	17.4%
3		16.7%	14.5%	15.1%	15.3%	16.0%
4		14.4%	12.8%	13.8%	13.6%	14.4%

If for the previous cases the energy time-shifting benefits linked to the increase in size of the battery were not sufficient to recover the investment cost of the latter, in this set of assumptions there are two cases (80MW and 100MW) in which IRR trend has a maximum for 1h of storage (battery size=29MWh).

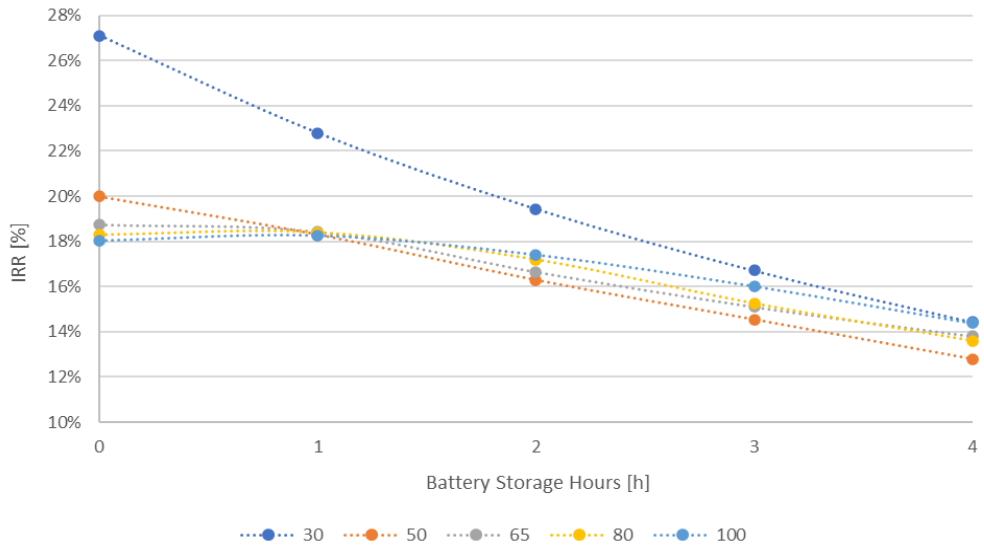

Figure 7-15: 2021-400 €/ton IRR with respect to the battery storage hours

In *Table 7-11* and *Figure 7-16*, NPV trends are reported. The qualitative considerations depicted in *section 7.3.1.3*. for NPV trends are valid for the current case; from a quantitative point of view lower values of NPV are shown, as a lower methanol price assumed.

Table 7-11: 2021-400 €/ton NPV with respect to the size of the solar field

	NPV [M€]					
Battery	***Solar size [MW]***					
storage hours	**0**	**30**	**50**	**65**	**80**	**100**
0	-3.1	46.4	45.0	51.2	59.7	72.2
1		40.6	41.8	53.3	64.1	77.6
2		34.8	36.0	46.5	59.3	74.0
3		28.9	30.1	40.1	48.5	65.0
4		23.1	24.3	34.3	38.7	53.1

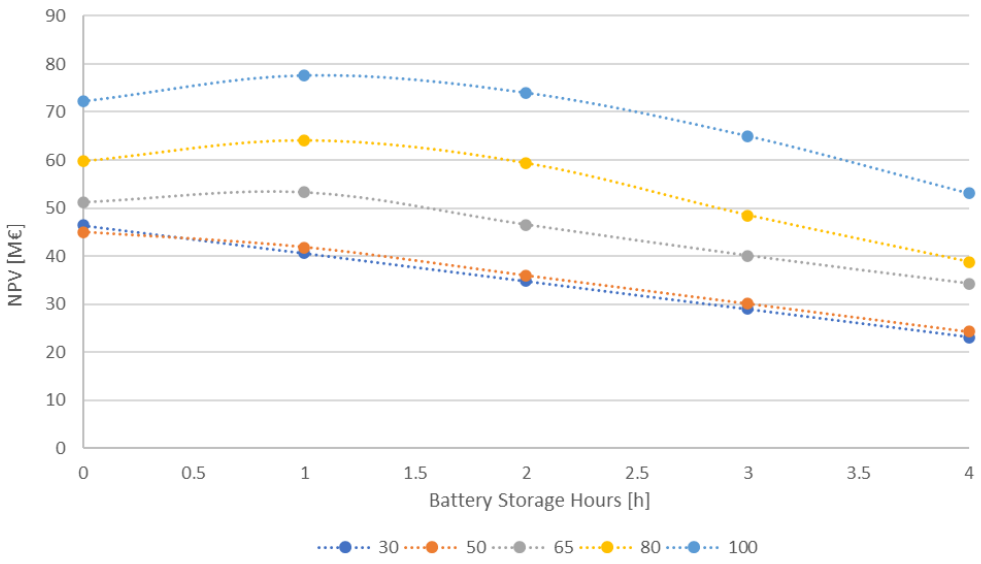

Figure 7-16: 2021-400 €/ton NPV with respect to the battery storage hours

7.3.2. Indirect Simulation Results

In this section simulation results regarding indirect configurations are reported and critically discussed. As stated in the introduction of *section 7.3.1*, Battery yearly equivalent hours of storage and PV usage trends are reported in this separate section as they are shared between all the cases.

In *Figure 7-17*the trends of Net and Gross PV usage for indirect configurations are reported. The same considerations illustrated in *section 7.3.1* for direct plants are valid for the indirect case; indeed, the qualitative trends are unchanged, whereas the quantitative results slightly vary and, hence, are reported.

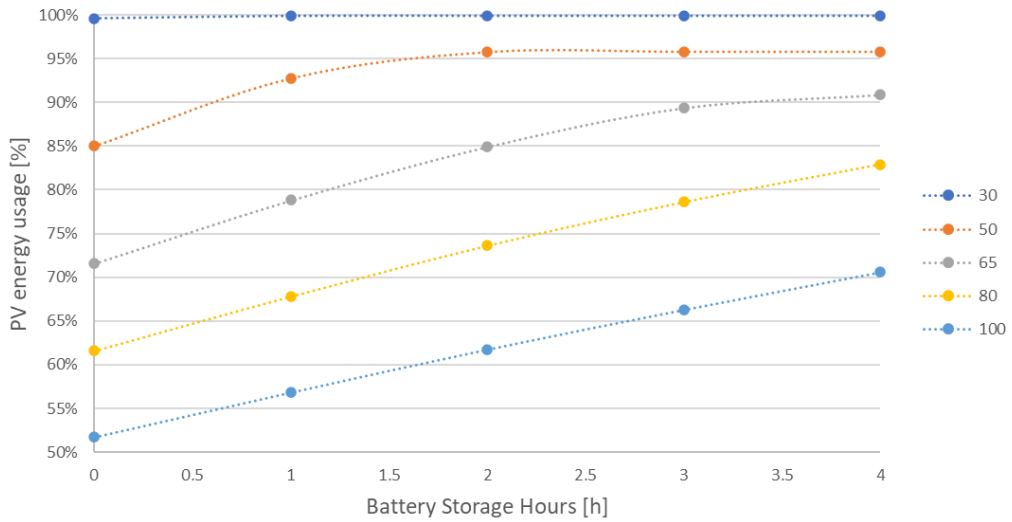

Figure 7-17: PV energy usage with respect to the battery storage hours

PV usage ranges from a value of 100% (in case of 30MW solar field) to 52% (for 100MW one). Gross PV trends increase as the size of the battery increases; however, they do not reach 100%, since a round-trip efficiency of 90% is assumed. As one can note in *Figure 7-18*, the trends of Battery yearly equivalent hours of storage are reported. From the diagram, it can be stated that battery reach an interest number of yearly hour of utilization (i.e., higher than 1000 heq/y) only for over-dimensioned solar fields (65-80-100 MW) and 3 to 4 hours of storage of nominal plant load (i.e., 71MWh and 95MWh).

Furthermore, for solar sizes of 30MW and 50MW, the trend is saturated at 1h and 3h storage respectively; as stated in *paragraph 7.3.1*, the parameter allows to eliminate unnecessary cases, i.e., the cases where the battery is over dimensioned with respect to the solar field size.

In the following analysis, these cases are highlighted in grey to distinguish them from the others.

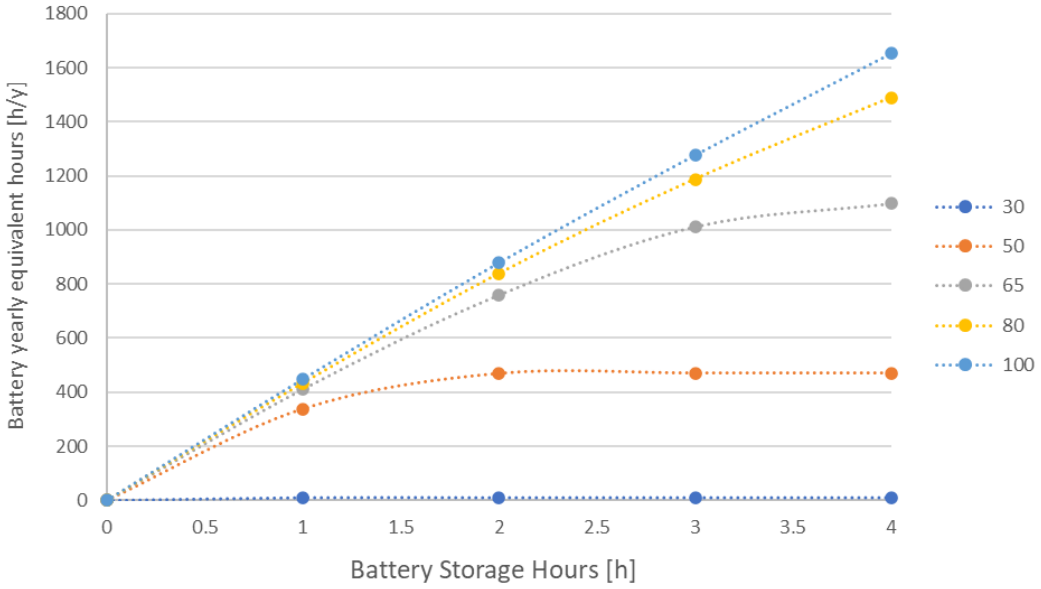

Figure 7-18: battery equivalent hours with respect to the battery storage hours

7.3.2.1. Grid 2019

The case addressed in this section assumed 2019 Italian grid as reference electricity grid; its average electricity price is around 52 €/MWh. Such a set of prices, that is perfectly aligned with BEP electricity price (set at 53€/MWh), in principle allows an average number of operating hours in resistance mode.

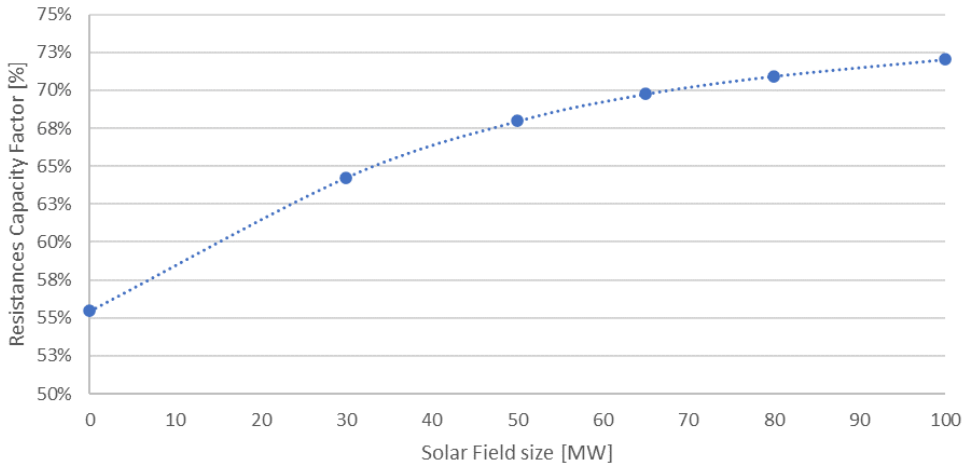

Figure 7-19: resistances capacity factor with respect to the size of the solar field

CF Resistances diagram, reported in *Figure 7-19*, shows an increasing trend from 55% to 72%. Average grid price and BEP values are closed one to each other; this reason

generates an average utilization factor when the system is only connected to the grid. The evolution trend of the parameter follows the considerations stated in *paragraph 7.3.1.2* for the correspondent CF parameter.

In *Table 7-12* and *Figure 7-20,* IRR trends are reported.

Table 7-12: indirect gasifier 2019 IRR with respect to the size of the solar field

IRR						
Battery storage hours	***Solar size [MW]***					
	0	**30**	**50**	**65**	**80**	**100**
0	50.6%	19.6%	12.3%	9.0%	6.7%	4.3%
1		16.6%	11.0%	8.2%	6.1%	3.9%
2		14.2%	9.6%	7.2%	5.3%	3.3%
3		12.2%	8.3%	6.2%	4.5%	2.7%
4		10.3%	7.2%	5.2%	3.7%	2.0%

The trend of the IRR rewards the configuration with no solar field as the most profitable one. This configuration operates 55% of the hours in resistances mode, being able to recover the total investment of 1.789 M€ in 3 years (annual profit not discounted of 0.89 M€). For the other cases, it can be stated that the high cost of solar field and battery is not balanced by the internal benefit of plant decoupling from the grid.

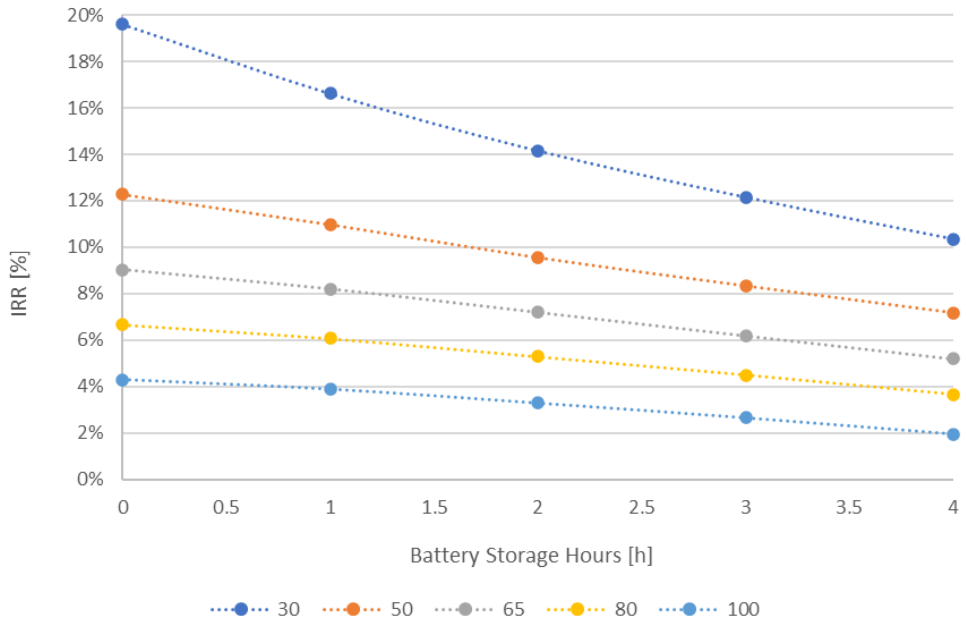

Figure 7-20: indirect gasifier 2019 IRR with respect to the battery storage hours

In *Table 7-13* and *Figure 7-21*, NPV trends are reported.

Table 7-13: indirect gasifier 2019 NPV with respect to the size of the solar field

	NPV [M€]					
Battery	***Solar size [MW]***					
storage hours	**0**	**30**	**50**	**65**	**80**	**100**
0	12.9	26.4	14.7	4.4	-6.6	-21.9
1		21.6	10.8	0.9	-10.0	-25.1
2		16.8	6.0	-3.7	-14.5	-29.5
3		12.2	1.3	-8.6	-19.3	-34.3
4		7.4	-3.5	-13.8	-24.5	-39.5

The NPV trend is almost aligned with that of the IRR. Being calculated by placing discount rate equal to 8%, the trend is negative for each configuration that presents IRR<8%. However, it is interesting to note that the maximum value of the NPV is reached for the case with a 30MW solar field and not with the case only connected to the grid (which instead returns the highest IRR).

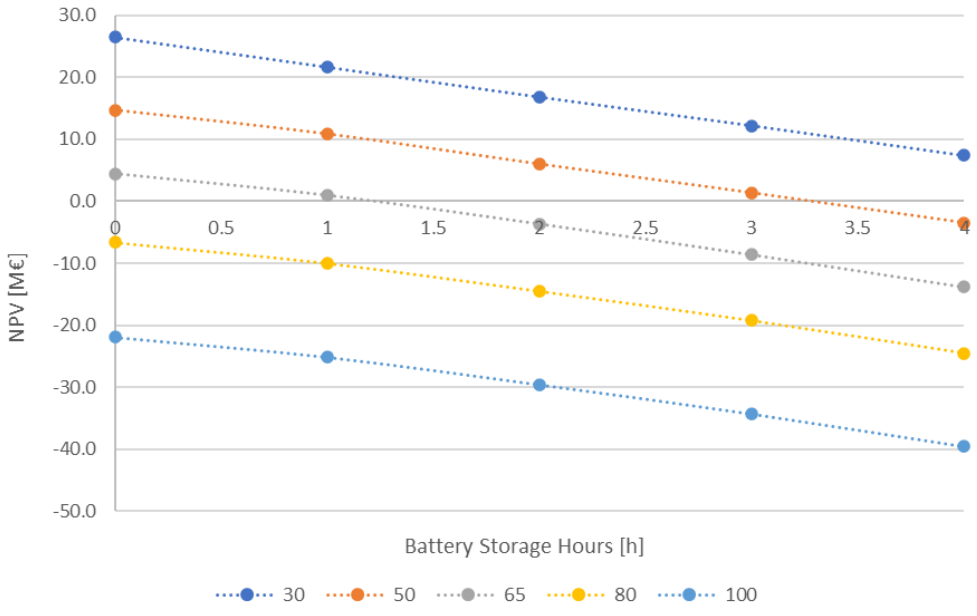

Figure 7-21: indirect gasifier 2019 NPV with respect to the battery storage hours

7.3.2.2. Grid 21/22

The case handled in this section assumed "grid crisis" as reference electricity grid; its average electricity price is around 300 €/MWh. Such a set of prices, definitely higher than BEP electricity price (set at 53€/MWh), in principle does not allow the system to operate in resistances; in this case the importance of solar field and battery rises.

AS one can note in *Figure 7-22*, CF Resistances parameter shows an increasing trend from almost 0% to 35%. Grid prices are too high to allow resistances powering; in this case the only way to gain access to the resistance modes is to rely on solar field energy. For the reasons cited in *paragraph 8.3.1.3*, the diagram is the same obtained for directed cases with 21/22 grid.

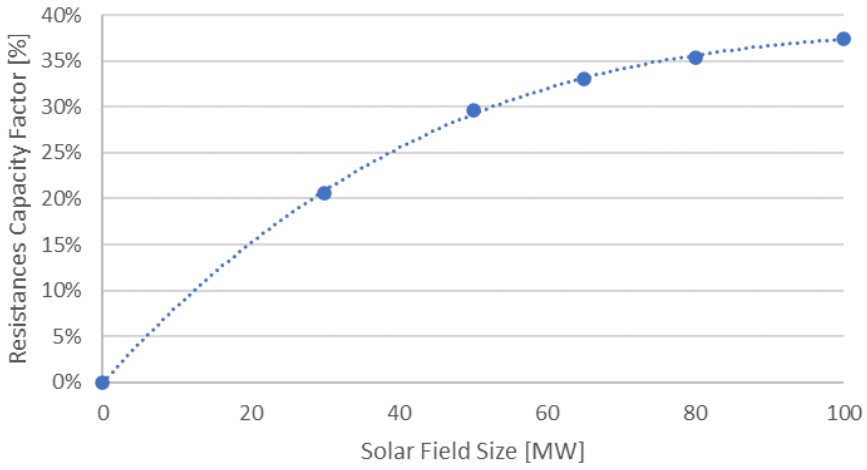

Figure 7-22: resistances capacity factor with respect to the size of the solar field

In *Table 7-14* and *Figure 7-23*, IRR trends are reported.

Table 7-14: indirect gasifier 2021 IRR with respect to the size of the solar field

	IRR					
Battery	***Solar size [MW]***					
storage hours	**0**	**30**	**50**	**65**	**80**	**100**
0	NPV<0 IRR = 0	24.0%	19.3%	18.7%	18.4%	18.3%
1		20.6%	18.5%	18.5%	18.3%	18.1%
2		17.8%	16.4%	16.7%	16.9%	17.1%
3		15.6%	14.9%	14.6%	15.2%	15.7%
4		13.6%	13.6%	12.9%	13.4%	14.1%

As depicted for direct plant based on the "crisis grid", *sections 7.3.1.3* and *section 7.3.1.4*, the configuration with no solar field is not profitable (NPV<0 with IRR=0). The latter

operates almost exclusively without resistances, given the high prices of electricity, and hence is not able to recover the total investment of 1.789 M€.

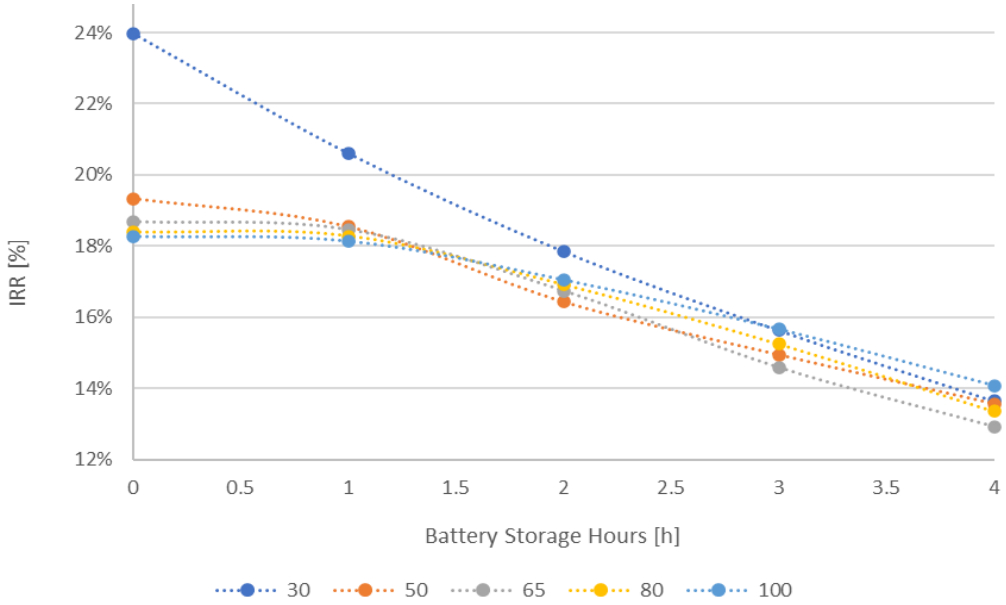

Figure 7-23: indirect gasifier 2021 IRR with respect to the battery storage hours

Conversely, solar field adoption permits to decouple the plant from the grid; in this way it is possible to hedge against high prices. However, the high investment cost penalizes the IRR, which reach higher values for lower solar field sizes.

Table 7-15 and *Figure 7-24*, NPV trends are reported.

Table 7-15: indirect gasifier 2021 NPV with respect to the size of the solar field

	NPV [M€]					
Battery	***Solar size [MW]***					
storage hours	**0**	**30**	**50**	**65**	**80**	**100**
0	-2.4	37.5	41.8	50.4	59.9	73.6
1		32.7	41.8	52.4	62.3	75.6
2		27.9	35.2	45.7	56.0	69.5
3		23.3	30.5	35.5	46.7	60.1
4		18.4	25.7	27.4	35.4	48.6

In this case, the NPV trend is not perfectly aligned with the one of the IRR. If the highest values for IRR are reached for low solar field size, instead the best configurations in term of NPV are the ones which adopt large solar fields. Indeed, at higher the solar field sizes correspond higher differential revenues that can be obtain

with respect to a base case with no resistances and no solar field which is obliged to buy electricity on an expensive grid. Furthermore, NPV trends show a local maximum as the battery size vary, highlighting the beneficial effect of the battery.

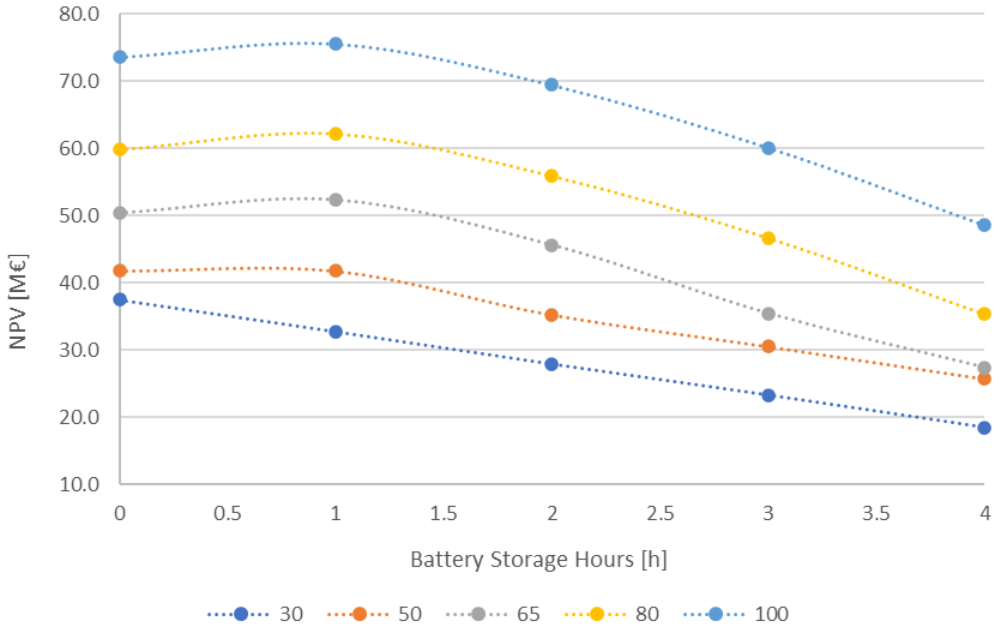

Figure 7-24: indirect gasifier 2021 NPV with respect to the battery storage hours

7.3.3. Result analysis

From this analysis several conclusions can be stated:

- Where the electricity grid has favourable set of prices, it is suggested to adopt only electrical resistances, without installation of the solar field, since it is possible to obtain a high number of hours of operation of the plant and consequently wide differential revenues.

- On the contrary, in the event of the adoption of a disadvantageous grid, the solar field allows to cover the investment costs of the resistances. In these cases, it is necessary to deal with the trade-off between the maximization of NPV, obtained by increasing the size of the solar field, and the maximization of the IRR, which provides greater values for smaller sizes.

- The investment cost of the battery in almost all cases exceeds the economic advantage that is derived by its adoption; accordingly, the adoption of the latter is discouraged. The only cases where implementing a battery allows to raise

IRR and NPV are those where the solar field is over-sized and consequently a sufficient range of hours of annual operation is guaranteed to the battery.

- For both direct and indirect configuration, the most robust solution is the one that adopts a 30MW solar field without battery since it is the only one capable of obtaining IRR>0 under every set of assumptions.

8 Conclusions

The current Thesis Work studied and analysed two biomass to methanol plants, respectively operating with an oxy-blown gasifier and a bubbling fluidized dual-bed gasifier. The purpose of the study was to find a profitable alternative to biomass oxidation for gasifier reactor heating by exploiting electrical resistances inside gasification reactor. The resulting plants were studied and modelled using *Aspen Plus*® software to perform mass and energy balances and, from the obtained results, depict the changes of plants Key Performance Parameters.

In the second chapter, the literature review on biomass to fuel plant was presented; the various possible arrangements for unit operations were discussed, focusing on the state-of-the-art of biomass gasifiers. In chapter three, a peculiar insight on *Aspen Plus*® gasifier models was presented highlighting the kinetic model. To design electric gasifiers, the lack of literature regarding electrified reactors was addressed selecting hypotheses and assumptions, which were critically discussed in chapter four. The off-design data were obtained from the simulation of the plants in *Aspen Plus*®; it has been shown that it is possible to replace the heating of the reactor with electric elements exploiting Joule effect with an extra consumption of 23.45 MW for the direct case and 17.89MW for the indirect one.

To perform a real case simulation of the electrified plant, hybrid gasifier models, able to contemporary rely on two sources of reactor heating, were modelled in chapter five; from the obtained data it was possible to extrapolate the so-called "hybrid maps that illustrate the trends of peculiar quantities of interest as an increasing share of resistances is switched on. To improve energy performance of the plants, in every off-design configuration a recuperative steam cycle was introduced, in chapter five.

Finally in chapter six the main technical results are presented and discussed; a comparison on the functioning of each plant was possible thanks to the adoption of the key performance indicators.

Electrified direct gasifier, obtained by partializing the oxygen input in the gasifier, was able to elevate fuel efficiency from 63.51% up to 81.5% with methanol production that has passed from 3.28 to 4.21 kg/s. The incremental effect of resistances implementation

was shown through Power-to-Methanol efficiency parameter; it is interesting to note that the value of 88%, obtained for this parameter, outweighs the corresponding value obtainable pursuing plant electrification through hydrogen addition [78]. From this outcome, it can be concluded that for this type of plant, electrify through electrical resistances is preferable to electrify through electrolysers thanks to the greater energy efficiency.

For what concern electrified indirect gasifier, the thermal load, that was previously supplied through the inert carrier (olivine) heated in the combustor, was replaced by electric heating. Since the inlet streams into the gasifier resulted unchanged, no off-design of the gasifier downstream components was appreciated. Hence, electrification didn't directly affect methanol production but mainly target carbon efficiency. The effort was focused on a more efficient employment of biomass (previously burned), since renewable biomass is a limited resource and hence it is fundamental to transfer as much as possible renewable carbon into biofuels. Fuel efficiency resulted to be increased from 63.95% to 74.36%; likewise, total carbon efficiency has been raised from 58.69% to 82.63%. In this way it was possible to reduce plant specific emissions from 979.8 down to 63.43 gCO_2/kg of methanol, save a stream of 0.91 kg/s of dry biomass and obtain an extra production of 0.42 kg/s of biochar.

The economic validation of the technical analysis was provided in chapter eight; the latter was performed in a differential form that considered only the variations of costs and revenues between a yearly simulation of an electrified plant and the one of the reference case, assessing in which framework of hypotheses the implementation of electric resistances could be profitable. To perform this hourly simulation, differential Break-Even Prices (BEP) of electricity were derived for direct and indirect configurations resulting in the following "willing to pay prices": 50 €/MWh, 65 €/MWh or 80 €/MWh (respectively associated to a methanol price of 400 €/ton, 500 €/ton and 600 €/ton) for direct case and 53 €/MWh for indirect plant. With the information of the break-even electricity prices was possible to frame an algorithm for the powering of electrical resistances as well as to access the technoeconomic impact of the adoption of a solar field and a battery, of variable sizes.

The following sensitivity analysis were performed:

- 2019 Italian grid vs 2021/2022 "Crisis condition" Italian grid
- Methanol price: 600 €/ton vs 400 €/ton
- Solar field size: 30 MW – 50 MW – 65 MW – 80 MW – 100 MW
- Battery size: 1 – 2 – 3 – 4 equivalent hours of storage

From these analyses it was possible to derive the following conclusions. The adoption of electrical elements for gasifier heating in biomass to methanol plants is profitable if the average electrical price of grid electricity is comparable with break-even electricity price of the plants. Taking the 2019 Italian grid as a reference case (average electricity price of 52 €/MWh), it was demonstrated that, thanks to a high number of hours of operation in electric mode, it is possible to obtain wide differential revenues with respect to the baseline case. On the contrary, in the event of the adoption of a disadvantageous grid (average electricity price of 300 €/MWh for 21/22 grid), the solar field allows to cover the investment costs of the resistances. In these cases, it is necessary to deal with the trade-off between the maximization of NPV, obtained by increasing the size of the solar field, and the maximization of IRR, which provides greater values for smaller sizes. For both direct and indirect configuration, the most robust solution is the one that adopts a 30MW solar field without battery since it is the only one capable of obtaining IRR>0 under every set of assumptions. The investment cost of the battery is discouraged since in almost all cases its cost exceeds the economic advantage that is derived by its adoption.

Bibliography

[1] E. Michel-Guillou and G. Moser, "Commitment of farmers to environmental protection: From social pressure to environmental conscience," *J Environ Psychol*, vol. 26, no. 3, pp. 227–235, 2006, doi: 10.1016/j.jenvp.2006.07.004.

[2] UNFCCC, "Paris Agreement," 2015.

[3] Commissione Europea, "Il Green Deal europeo," 2019. [Online]. Available: https://sustainabledevelopment.un.org/post2015/transformingourworld

[4] Jim Skea, "Roadmap 2050: a practical guide to a prosperous, low-carbon Europe Volume I: technical and economic assessment Full documentation," 2010.

[5] I. energy Agency, "Statistics report Key World Energy Statistics 2021," 2021.

[6] "Global energy-related CO2 emissions by sector – Charts – Data & Statistics - IEA." https://www.iea.org/data-and-statistics/charts/global-energy-related-co2-emissions-by-sector (accessed Oct. 29, 2022).

[7] I. Renewable Energy Agency, "Renewable Power Generation Costs in 2021 - Executive Summary."

[8] C. Thiel, J. Schmidt, A. van Zyl, and E. Schmid, "Cost and well-to-wheel implications of the vehicle fleet CO<inf>2</inf> emission regulation in the European Union," *Transp Res Part A Policy Pract*, vol. 63, pp. 25–42, 2014, doi: 10.1016/j.tra.2014.02.018.

[9] Ł. Sobol and A. Dyjakon, "The influence of power sources for charging the batteries of electric cars on CO2 emissions during daily driving: A case study from Poland," *Energies (Basel)*, vol. 13, no. 6, 2020, doi: 10.3390/en13164267.

[10] A. Alaswad, A. Baroutaji, H. Achour, J. Carton, A. al Makky, and A. G. Olabi, "Developments in fuel cell technologies in the transport sector," *Int J Hydrogen Energy*, vol. 41, no. 37, pp. 16499–16508, 2016, doi: 10.1016/j.ijhydene.2016.03.164.

[11] C. Cunanan, M.-K. Tran, Y. Lee, S. Kwok, V. Leung, and M. Fowler, "A Review of Heavy-Duty Vehicle Powertrain Technologies: Diesel Engine Vehicles, Battery Electric Vehicles, and Hydrogen Fuel Cell Electric Vehicles," *Clean Technologies*, vol. 3, no. 2, pp. 474–489, 2021, doi: 10.3390/cleantechnol3020028.

[12] O. Awogbemi, D. V. von Kallon, E. I. Onuh, and V. S. Aigbodion, "An overview of the classification, production and utilization of biofuels for internal

combustion engine applications," *Energies (Basel)*, vol. 14, no. 18, 2021, doi: 10.3390/en14185687.

[13] I. Renewable Energy Agency, "Renewable Power Generation Costs in 2021 - Executive Summary."

[14] S. Kim *et al.*, "Carbon-Negative Biofuel Production," *Environ Sci Technol*, vol. 54, no. 17, pp. 10797–10807, 2020, doi: 10.1021/acs.est.0c01097.

[15] A. Molino, V. Larocca, S. Chianese, and D. Musmarra, "Biofuels production by biomass gasification: A review," *Energies (Basel)*, vol. 11, no. 4, 2018, doi: 10.3390/en11040811.

[16] K. Göransson, U. Söderlind, J. He, and W. Zhang, "Review of syngas production via biomass DFBGs," *Renewable and Sustainable Energy Reviews*, vol. 15, no. 1, pp. 482–492, Jan. 2011, doi: 10.1016/J.RSER.2010.09.032.

[17] F. Dalena, A. Senatore, A. Marino, A. Gordano, M. Basile, and A. Basile, *Methanol Production and Applications: An Overview*. 2018. doi: 10.1016/B978-0-444-63903-5.00001-7.

[18] M. E. Dry, "The Fischer-Tropsch process: 1950-2000," *Catal Today*, vol. 71, no. 3–4, pp. 227–241, 2002, doi: 10.1016/S0920-5861(01)00453-9.

[19] Y. H. Choi *et al.*, "Carbon dioxide Fischer-Tropsch synthesis: A new path to carbon-neutral fuels," *Appl Catal B*, vol. 202, pp. 605–610, 2017, doi: 10.1016/j.apcatb.2016.09.072.

[20] R. Ramachandran and R. K. Menon, "An overview of industrial uses of hydrogen," *Int J Hydrogen Energy*, vol. 23, no. 7, pp. 593–598, Jul. 1998, doi: 10.1016/S0360-3199(97)00112-2.

[21] "Hydrogen – Analysis - IEA." https://www.iea.org/reports/hydrogen (accessed Oct. 26, 2022).

[22] S. Z. Abbas, J. R. Fernández, A. Amieiro, M. Rastogi, J. Brandt, and V. Spallina, "Lab-scale experimental demonstration of CaCu chemical looping for hydrogen production and in-situ CO2 capture from a steel-mill," *Fuel Processing Technology*, vol. 237, p. 107475, Dec. 2022, doi: 10.1016/J.FUPROC.2022.107475.

[23] I. K. Gjerdingen, "Hydrogen technology experimentation for sustainable mobility A case study of hydrogen fuel cell experimentation in Lower Saxony in Germany," 2020, Accessed: Nov. 24, 2022. [Online]. Available: http://www.duo.uio.no/

[24] M. Brenna, F. Foiadelli, M. Longo, and D. Zaninelli, "Use of Fuel Cell Generators for Cell-Propelled Trains Renovation," in *Proceedings - 2018 IEEE International Conference on Environment and Electrical Engineering and 2018 IEEE Industrial and*

Commercial Power Systems Europe, EEEIC/I and CPS Europe 2018, 2018. doi: 10.1109/EEEIC.2018.8493819.

[25] E. Malmgren, "Towards sustainable shipping: Evaluating the environmental impact of electrofuels," 2021.

[26] IEA, "Global Hydrogen Review 2022," 2022. https://www.iea.org/reports/global-hydrogen-review-2022/executive-summary

[27] N. NOROUZİ, "An Overview on the renewable hydrogen market," *International Journal of Energy Studies*, vol. 6, no. 1, pp. 67–94, Jun. 2021, Accessed: Nov. 11, 2022. [Online]. Available: https://dergipark.org.tr/en/pub/ijes/issue/63190/934518

[28] F. Dalena, A. Senatore, A. Marino, A. Gordano, M. Basile, and A. Basile, *Methanol Production and Applications: An Overview*. 2018. doi: 10.1016/B978-0-444-63903-5.00001-7.

[29] X. Tan and T. Tan, "Biofuels from biomass toward a net-zero carbon and sustainable world," *Joule*, vol. 6, no. 7, pp. 1396–1399, 2022, doi: 10.1016/j.joule.2022.06.005.

[30] "Home - Methanol Market Services Asia." https://www.methanolmsa.com/ (accessed Oct. 23, 2022).

[31] P. R. Yaashikaa, P. S. Kumar, S. Varjani, and A. Saravanan, "A critical review on the biochar production techniques, characterization, stability and applications for circular bioeconomy," *Biotechnology Reports*, vol. 28, p. e00570, Dec. 2020, doi: 10.1016/J.BTRE.2020.E00570.

[32] K. Abhishek *et al.*, "Biochar application for greenhouse gas mitigation, contaminants immobilization and soil fertility enhancement: A state-of-the-art review," *Science of the Total Environment*, vol. 853, 2022, doi: 10.1016/j.scitotenv.2022.158562.

[33] V. Uday, P. S. Harikrishnan, K. Deoli, F. Zitouni, J. Mahlknecht, and M. Kumar, "Current trends in production, morphology, and real-world environmental applications of biochar for the promotion of sustainability," *Bioresour Technol*, vol. 359, 2022, doi: 10.1016/j.biortech.2022.127467.

[34] O. A. Fakayode, E. A. A. Aboagarib, C. Zhou, and H. Ma, "Co-pyrolysis of lignocellulosic and macroalgae biomasses for the production of biochar – A review," *Bioresour Technol*, vol. 297, p. 122408, Feb. 2020, doi: 10.1016/J.BIORTECH.2019.122408.

[35] L. Fryda and R. Visser, "Biochar for Soil Improvement: Evaluation of Biochar from Gasification and Slow Pyrolysis," *Agriculture (Switzerland)*, vol. 5, no. 4, pp. 1076–1115, Dec. 2015, doi: 10.3390/AGRICULTURE5041076.

[36] H. W. Lee, Y.-M. Kim, S. Kim, C. Ryu, S. H. Park, and Y.-K. Park, "Review of the use of activated biochar for energy and environmental applications," *Carbon Letters*, vol. 26, no. 1, pp. 1–10, 2018, doi: 10.5714/CL.2018.26.001.

[37] J. Lehmann *et al.*, "Biochar in climate change mitigation," *Nat Geosci*, vol. 14, no. 12, pp. 883–892, 2021, doi: 10.1038/s41561-021-00852-8.

[38] "Valutazione dell'impatto della Commissione Europea che accompagna la comunicazione del Piano degli obiettivi climatici 2030," 2020.

[39] F. Ueckerdt, C. Bauer, A. Dirnaichner, J. Everall, R. Sacchi, and G. Luderer, "Potential and risks of hydrogen-based e-fuels in climate change mitigation," *Nat Clim Chang*, vol. 11, no. 5, pp. 384–393, 2021, doi: 10.1038/s41558-021-01032-7.

[40] Maciej Serda *et al.*, "IL CONTO ENERGIA 2011-2013," *Uniwersytet śląski*, vol. 7, no. 1, pp. 343–354, 2022, doi: 10.2/JQUERY.MIN.JS.

[41] C. Martin de Lagarde and F. Lantz, "How renewable production depresses electricity prices: Evidence from the German market," *Energy Policy*, vol. 117, pp. 263–277, Jun. 2018, doi: 10.1016/J.ENPOL.2018.02.048.

[42] Z. Dalala, M. Al-Omari, M. Al-Addous, M. Bdour, Y. Al-Khasawneh, and M. Alkasrawi, "Increased renewable energy penetration in national electrical grids constraints and solutions," *Energy*, vol. 246, 2022, doi: 10.1016/j.energy.2022.123361.

[43] A. J. Minchener, "Coal gasification for advanced power generation," *Fuel*, vol. 84, no. 17, pp. 2222–2235, 2005, doi: 10.1016/j.fuel.2005.08.035.

[44] L. Devi, K. J. Ptasinski, and F. J. J. G. Janssen, "A review of the primary measures for tar elimination in biomass gasification processes," *Biomass Bioenergy*, vol. 24, no. 2, pp. 125–140, 2003, doi: 10.1016/S0961-9534(02)00102-2.

[45] J. Yi, X. Li, J. He, and X. Duan, "Drying efficiency and product quality of biomass drying: a review," *Drying Technology*, vol. 38, no. 15, pp. 2039–2054, 2020, doi: 10.1080/07373937.2019.1628772.

[46] "HORIZON 2020 PROGRAMME RESEARCH and INNOVATION ACTION Flexible Dimethyl ether production from biomass gasification with sorption enhanced processes WP 4-Deliverable D4.4: Final process simulations and economic analysis of FLEDGED systems."

[47] K. J. MOŚCICKI, "Commoditization of biomass: dry torrefaction and pelletization - a review," *Journal of Power Technologies*, Oct. 2014, [Online]. Available: https://papers.itc.pw.edu.pl/index.php/JPT/article/view/562

[48] Y. Ueki, T. Torigoe, H. Ono, R. Yoshiie, J. H. Kihedu, and I. Naruse, "Gasification characteristics of woody biomass in the packed bed reactor," *Proceedings of the*

Combustion Institute, vol. 33, no. 2, pp. 1795–1800, 2011, doi: 10.1016/j.proci.2010.07.080.

[49] H. Yu, Z. Zhang, Z. Li, and D. Chen, "Characteristics of tar formation during cellulose, hemicellulose and lignin gasification," *Fuel*, vol. 118, pp. 250–256, 2014, doi: 10.1016/j.fuel.2013.10.080.

[50] M. L. Valderrama Rios, A. M. González, E. E. S. Lora, and O. A. Almazán del Olmo, "Reduction of tar generated during biomass gasification: A review," *Biomass Bioenergy*, vol. 108, pp. 345–370, 2018, doi: 10.1016/j.biombioe.2017.12.002.

[51] T. Kimura *et al.*, "Development of Ni catalysts for tar removal by steam gasification of biomass," *Appl Catal B*, vol. 68, no. 3–4, pp. 160–170, 2006, doi: 10.1016/j.apcatb.2006.08.007.

[52] I. Dimitriou, H. Goldingay, and A. V. Bridgwater, "Techno-economic and uncertainty analysis of Biomass to Liquid (BTL) systems for transport fuel production," *Renewable and Sustainable Energy Reviews*, vol. 88, pp. 160–175, 2018, doi: 10.1016/j.rser.2018.02.023.

[53] H. Boerrigter *et al.*, "'OLGA' TAR REMOVAL TECHNOLOGY Proof-of-Concept (PoC) for application in integrated biomass gasification combined heat and power (CHP) systems," 2005. [Online]. Available: www.ecn.nl/biomass

[54] M. Asadullah, "Biomass gasification gas cleaning for downstream applications: A comparative critical review," *Renewable and Sustainable Energy Reviews*, vol. 40, pp. 118–132, 2014, doi: 10.1016/j.rser.2014.07.132.

[55] J. C. de Deken, E. F. Devos, and G. F. Froment, "STEAM REFORMING OF NATURAL GAS: INTRINSIC KINETICS, DIFFUSIONAL INFLUENCES, AND REACTOR DESIGN.," *ACS Symposium Series*, pp. 181–197, 1982, doi: 10.1021/BK-1982-0196.CH016.

[56] I. Dybkjaer, "Tubular reforming and autothermal reforming of natural gas - an overview of available processes," *Fuel Processing Technology*, vol. 42, no. 2–3, pp. 85–107, 1995, doi: 10.1016/0378-3820(94)00099-F.

[57] S. Ali, K. Sørensen, and M. P. Nielsen, "Modeling a novel combined solid oxide electrolysis cell (SOEC) - Biomass gasification renewable methanol production system," *Renew Energy*, vol. 154, pp. 1025–1034, 2020, doi: 10.1016/j.renene.2019.12.108.

[58] D. S. Newsome, "The Water-Gas Shift Reaction," *https://doi.org/10.1080/03602458008067535*, vol. 21, no. 2, pp. 275–318, Jan. 2006, doi: 10.1080/03602458008067535.

[59] E. G. Baker, M. D. Brown, R. H. Moore, and L. K. Mudge, "Engineering analysis of biomass gasifier product gas cleaning technology," 1986.

[60] T. L. Levalley, A. R. Richard, and M. Fan, "The progress in water gas shift and steam reforming hydrogen production technologies - A review," *Int J Hydrogen Energy*, vol. 39, no. 30, pp. 16983–17000, 2014, doi: 10.1016/j.ijhydene.2014.08.041.

[61] A. de Klerk, "Fischer–Tropsch refining: Technology selection to match molecules," *Green Chemistry*, vol. 10, no. 12, pp. 1249–1279, 2008, doi: 10.1039/b813233j.

[62] T. E. Rufford *et al.*, "The removal of CO <inf>2</inf> and N <inf>2</inf> from natural gas: A review of conventional and emerging process technologies," *J Pet Sci Eng*, vol. 94–95, pp. 123–154, 2012, doi: 10.1016/j.petrol.2012.06.016.

[63] F. Dalena, A. Senatore, A. Marino, A. Gordano, M. Basile, and A. Basile, *Methanol Production and Applications: An Overview*. 2018. doi: 10.1016/B978-0-444-63903-5.00001-7.

[64] K. M. vanden Bussche and G. F. Froment, "A Steady-State Kinetic Model for Methanol Synthesis and the Water Gas Shift Reaction on a Commercial Cu/ZnO/Al 2 O 3 Catalyst," 1996.

[65] C. N. Hamelinck and A. P. C. Faaij, "Future prospects for production of methanol and hydrogen from biomass," *J Power Sources*, vol. 111, no. 1, pp. 1–22, 2002, doi: 10.1016/S0378-7753(02)00220-3.

[66] B. A. B. T. Walid, B. Hassiba, H. Boumediene, and S. Weifeng, "Improved Design of the Lurgi Reactor for Methanol Synthesis Industry," *Chem Eng Technol*, vol. 41, no. 10, pp. 2043–2052, 2018, doi: 10.1002/ceat.201700551.

[67] IMPCA, "Methanol Reference Specifications," 2015. [Online]. Available: www.impca.be-VAT:BE434211194

[68] Inc. Aspen Technology, "Physical_Property_Methods_and_Models," 2001.

[69] A. Poluzzi *et al.*, "Flexible Power and Biomass-To-Methanol Plants With Different Gasification Technologies," *Front Energy Res*, vol. 9, Jan. 2022, doi: 10.3389/fenrg.2021.795673.

[70] J. A. Rodriguez, P. J. Ramírez, and R. A. Gutierrez, "Highly active Pt/MoC and Pt/TiC catalysts for the low-temperature water-gas shift reaction: Effects of the carbide metal/carbon ratio on the catalyst performance," *Catal Today*, vol. 289, pp. 47–52, 2017, doi: 10.1016/j.cattod.2016.09.020.

[71] D. A. Dalrymple, T. W. Trofe, and J. M. Evans, "Liquid redox sulfur recovery options, costs, and environmental considerations," *Environmental Progress*, vol. 8, no. 4, pp. 217–222, 1989, doi: 10.1002/ep.3300080412.

[72] A. Kazemi, M. Malayeri, A. Gharibi kharaji, and A. Shariati, "Feasibility study, simulation and economical evaluation of natural gas sweetening processes – Part

1: A case study on a low capacity plant in iran," *J Nat Gas Sci Eng*, vol. 20, pp. 16–22, Sep. 2014, doi: 10.1016/J.JNGSE.2014.06.001.

[73] H. Thunman *et al.*, "Advanced biofuel production via gasification – lessons learned from 200 man-years of research activity with Chalmers' research gasifier and the GoBiGas demonstration plant," *Energy Sci Eng*, vol. 6, no. 1, pp. 6–34, 2018, doi: 10.1002/ese3.188.

[74] K. M. vanden Bussche and G. F. Froment, "A Steady-State Kinetic Model for Methanol Synthesis and the Water Gas Shift Reaction on a Commercial Cu/ZnO/Al 2 O 3 Catalyst," 1996.

[75] M. Catania and L. Baggi, "Biofuels and hydrogen production plants with biomass gasification and carbon capture : techno-economic analysis and flexibility assessment," Dec. 2021, Accessed: Nov. 16, 2022. [Online]. Available: https://www.politesi.polimi.it/handle/10589/183372

[76] H. Klein *et al.*, "Flexible Operation of Air Separation Units," *ChemBioEng Reviews*, vol. 8, no. 4, pp. 357–374, 2021, doi: 10.1002/cben.202100023.

[77] C. Schlereth, K. Hack, and M. C. Galetz, "Parameters to estimate the metal dusting attack in different gases," *Corros Sci*, vol. 206, Sep. 2022, doi: 10.1016/J.CORSCI.2022.110483.

[78] A. Poluzzi *et al.*, "Flexible Power & Biomass-to-Methanol plants: Design optimization and economic viability of the electrolysis integration," *Fuel*, vol. 310, 2022, doi: 10.1016/j.fuel.2021.122113.

[79] "Countries & Regions - IEA." https://www.iea.org/countries (accessed Nov. 07, 2022).

[80] "Biogenic Emission Sources | US EPA." https://www.epa.gov/air-emissions-modeling/biogenic-emission-sources (accessed Nov. 07, 2022).

[81] C. Arnaiz del Pozo, S. Cloete, and Á. Jiménez Álvaro, "Techno-economic assessment of long-term methanol production from natural gas and renewables," *Energy Convers Manag*, vol. 266, 2022, doi: 10.1016/j.enconman.2022.115785.

[82] W. Cole, A. W. Frazier, and C. Augustine, "Cost Projections for Utility-Scale Battery Storage: 2021 Update," 2021. [Online]. Available: www.nrel.gov/publications.

[83] C. Curry, "Lithium-ion Battery Costs and Market Squeezed margins seek technology improvements & new business models," 2017.

[84] S. Meyer, B. Glaser, and P. Quicker, "Technical, economical, and climate-related aspects of biochar production technologies: A literature review," *Environ Sci Technol*, vol. 45, no. 22, pp. 9473–9483, 2011, doi: 10.1021/es201792c.

[85] S. P. Galinato, J. K. Yoder, and D. Granatstein, "The economic value of biochar in crop production and carbon sequestration," *Energy Policy*, vol. 39, no. 10, pp. 6344–6350, 2011, doi: 10.1016/j.enpol.2011.07.035.

[86] S. K. Thengane *et al.*, "Market prospects for biochar production and application in California," *Biofuels, Bioproducts and Biorefining*, vol. 15, no. 6, pp. 1802–1819, 2021, doi: 10.1002/bbb.2280.

[87] J.-M. Seiler, C. Hohwiller, J. Imbach, and J.-F. Luciani, "Technical and economical evaluation of enhanced biomass to liquid fuel processes," *Energy*, vol. 35, no. 9, pp. 3587–3592, 2010, doi: 10.1016/j.energy.2010.04.048.

[88] "EU Carbon Permits - 2022 Data," 2022. https://tradingeconomics.com/commodity/carbon (accessed Nov. 07, 2022).

[89] J. K. Boyce, "Carbon Pricing: Effectiveness and Equity," *Ecological Economics*, vol. 150, pp. 52–61, 2018, doi: 10.1016/j.ecolecon.2018.03.030.

[90] "GME - Statistiche - dati di sintesi MPE-MGP." https://www.mercatoelettrico.org/it/Statistiche/ME/DatiSintesi.aspx (accessed Nov. 07, 2022).

[91] C. Chendurpandian and P. Pandey, "Performance of volatility asset as hedge for investor's portfolio against stress events: COVID-19 and the 2008 financial crisis," *IIMB Management Review*, Oct. 2022, doi: 10.1016/j.iimb.2022.10.001.

[92] "Lithium Ion – Lithium Ion Battery Test Centre." https://batterytestcentre.com.au/project/lithium-ion/

[93] "Renewables.ninja." https://www.renewables.ninja/

A Appendix A

A.1. DIR_EL_25% Results

Table A-1: main operative points of 25% electrification hybrid mode

	Streams							
Variable	**Biomass**	**Steam**	**Sealing**	**O2 gasifier**	**Syngas raw**	**Syngas raw**	**Syngas**	**Char**
	(1)	**(2)**	**(3)**	**(5)**	**(6)**	**(10)**	**(12)**	**(7)**
T [°C]	80.0	200.0	200.0	108.4	870.0	870.0	915.0	
P [bar]	1.0	5.9	5.9	4.5	4.0	3.8	3.6	
Gm [kg/s]	-	3.06	0.80	1.55	12.07	12.07	12.71	
Gc [kg/s]	-	-	-	-	0.13	-	-	0.129
Gnc [kg/s]	6.64	-	-	-	0.07	-	-	
Qm [kmol/s]		0.17	0.04	0.05	0.59	0.59	0.67	
	Composition							
xCH4	-	-	-	-	4.27%	4.27%	0.38%	-
xC2H4	-	-	-	-	1.92%	1.92%	0.00%	-
xCO	-	-	-	-	14.03%	14.03%	18.97%	-
xCO2	-	-	-	-	16.59%	16.59%	14.75%	-
xH2	-	-	-	-	22.99%	22.99%	31.62%	-
xH2O	-	100.00%	100.00%	-	38.73%	38.73%	32.85%	-
xO2	-	-	-	95.00%	-	-	0.00%	-
xN2	-	-	-	2.00%	1.19%	1.19%	1.11%	-
xAr	-	-	-	3.00%	0.25%	0.25%	0.31%	-
zCaO	-	-	-	-	-	-	-	-
zCaCO3	-	-	-	-	-	-	-	-
zCchar	-	-	-	-	100	-	-	100%
yBio	100	-	-	-	-	-	-	-
yash	-	-	-	-	100	-	-	-

A.2. DIR_EL_50% Results

Table A-2: main operative points of 50% electrification hybrid mode

	Streams							
Variable	**Biomass (1)**	**Steam (2)**	**Sealing (3)**	**O2 gasifier (5)**	**Syngas raw (6)**	**Syngas raw (10)**	**Syngas raw (12)**	**Char (7)**
T [°C]	80.00	200.00	200.00	108.42	870.00	870.00	915.00	-
P [bar]	1.01	5.90	5.90	4.50	4.00	3.80	3.60	-
Gm [kg/s]	-	3.46	0.80	1.17	12.09	12.09	12.75	-
Gc [kg/s]	-	-	-	-	0.13	-	-	0.13
Gnc [kg/s]	6.64	-	-	-	0.07	-	-	-
Qm [kmol/s]		0.19	0.04	0.04	0.62	0.62	2505.32	-
	Composition							
xCH4	-	-	-	-	4.12%	4.12%	0.36%	-
xC2H4	-	-	-	-	1.85%	1.85%	0.00%	-
xCO	-	-	-	-	13.53%	13.53%	18.88%	-
xCO2	-	-	-	-	16.01%	16.01%	13.78%	-
xH2	-	-	-	-	25.81%	25.81%	33.25%	-
xH2O	-	100%	100%	-	37.36%	37.36%	32.42%	-
xO2	-	-	-	95.00%	-	-	0.00%	-
xN2	-	-	-	2.00%	1.11%	1.11%	1.04%	-
xAr	-	-	-	3.00%	0.18%	0.18%	0.25%	-
zCaO	-	-	-	-	-	-	-	-
zCaCO3	-	-	-	-	-	-	-	-
zCchar	-	-	-	-	100%	-	-	100%
yBio	100%	-	-	-	-	-	-	-
yash	-	-	-	-	100%	-	-	-

A.3. DIR_EL_75% Results

Table A-3: main operative points of 75% electrification hybrid mode

	Streams							
Variable	**Biomass (1)**	**Steam (2)**	**Sealing (3)**	**O2 gasifier (5)**	**Syngas raw (6)**	**Syngas raw (10)**	**Syngas raw (12)**	**Char (7)**
T [°C]	80.00	200.00	200.00	108.42	870.00	870.00	915.00	-
P [bar]	1.01	5.90	5.90	4.50	4.00	3.80	3.60	-
Gm [kg/s]	-	3.87	0.80	0.79	12.12	12.12	12.78	-
Gc [kg/s]	-	-	-	-	0.13	-	-	0.13
Gnc [kg/s]	6.64	-	-	-	0.07	-	-	-
Qm [kmol/s]	-	0.21	0.04	0.02	0.64	0.64	0.72	-
	Composition							
xCH4	-	-	-	-	3.98%	3.98%	0.35%	-
xC2H4	-	-	-	-	1.79%	1.79%	0.00%	-
xCO	-	-	-	-	13.07%	13.07%	18.77%	-
xCO2	-	-	-	-	15.46%	15.46%	12.90%	-
xH2	-	-	-	-	28.45%	28.45%	34.82%	-
xH2O	-	100%	100%	-	36.08%	36.08%	31.98%	-
xO2	-	-	-	95.00%	-	-	0.00%	-
xN2	-	-	-	2.00%	1.04%	1.04%	0.98%	-
xAr	-	-	-	3.00%	0.12%	0.12%	0.19%	-
zCaO	-	-	-	-	-	-	-	-
zCaCO3	-	-	-	-	-	-	-	-
zCchar	-	-	-	-	100%	-	-	100%
yBio	100%	-	-	-	-	-	-	-
yash	-	-	-	-	100%	-	-	-

B Appendix B

B.1. INDIR_EL_12% Results

Table B-1: main operative points of 12% electrification hybrid mode

	Streams														
Variable	**Biomass feed (1)**	**Steam - in (2)**	**Steam sealing (3)**	**Burner air (15)**	**Syngas raw (4)**	**Syngas raw (6)**	**Syngas raw (13)**	**Burner biomass (19)**	**Solid recycle (5)**	**Olivine make up (20)**	**Burner recycle (22)**	**Burner out (21)**	**Solid recycle (22)**	**Flue gases (23)**	**Biosave (18)**
T [°C]	80.00	400.00	400.00	270.00	815.00	815.00	799.99	80.00	814.78	25.00	910.00	910.00	910.00	910.00	80.00
P [bar]	1.01	3.90	3.90	1.60	1.43	1.23	1.10	1.01	1.43	1.01	1.43	1.43	1.43	1.43	1.01
Gm [kg/s]	-	2.62	0.69	10.17	8.72	8.72	9.21	-	-	-	-	11.28	-	11.28	-
Gc [kg/s]	-	-	-	-	164.07	-	-	-	164.07	0.28	60.87	224.80	224.57	0.22	-
Gnc [kg/s]	5.71	-	-	-	4.11	-	-	0.70	4.10	-	1.51	5.62	5.56	0.06	0.23
Qm [kmol/s]	-	0.15	0.04	0.35	0.47	0.47	0.55	-	1.02	0.00	0.00	0.37	0.00	0.37	-
	Composition														
xCH4	-	-	-	-	6.07%	6.07%	0.52%	-	-	-	-	-	-	-	-
xC2H4	-	-	-	-	1.61%	1.61%	0.00%	-	-	-	-	-	-	-	-
xCO	-	-	-	-	14.47%	14.47%	17.90%	-	-	-	-	-	-	-	-
xCO2	-	-	-	-	12.48%	12.48%	12.84%	-	-	-	-	16.15%	-	16.15%	-
xH2	-	-	-	-	27.99%	27.99%	40.57%	-	-	-	-	-	-	-	-
xH2O	-	100.00%	100.00%	-	36.25%	36.25%	27.05%	-	-	-	-	7.25%	-	7.25%	-
xO2	-	-	-	20.70%	-	-	0.00%	-	-	-	-	3.00%	-	3.00%	-
xN2	-	-	-	77.30%	1.11%	1.11%	1.01%	-	-	-	-	72.69%	-	72.69%	-
xAr	-	-	-	0.97%	0.00%	0.00%	0.08%	-	-	-	-	0.91%	-	0.91%	-
zCaO	-	-	-	-	-	-	-	-	-	-	-	-	-	-	-
zCaCO3	-	-	-	-	-	-	-	-	-	-	-	-	-	-	-
zCchar	-	-	-	-	100.00%	-	-	-	3.46%	-	-	-	-	-	-
zOlivFE	-	-	-	-	-	-	-	-	39.43%	40.84%	40.84%	40.84%	40.84%	40.84%	-
zOliveMG	-	-	-	-	-	-	-	-	57.11%	59.16%	59.16%	59.16%	59.16%	59.16%	-
yBio	100.00%	-	-	-	-	-	-	100.00%	-	-	-	-	-	-	100.00%
yash	-	-	-	-	100.00%	-	-	-	100.00%	-	100.00%	100.00%	100.00%	100.00%	-

B.2. INDIR_EL_26% Results

Table B-2: main operative points of 26% electrification hybrid mode

	Streams														
Variable	**Biomass feed (1)**	**Steam - in (2)**	**Steam sealing (3)**	**Burner air (15)**	**Gass-Out (4)**	**Syngas raw (6)**	**Syngas raw (13)**	**Burner biomass (19)**	**Solid recycle (5)**	**Olivine make up (20)**	**Burner recycle (22)**	**Burner out (21)**	**Solid recycle (22)**	**Flue gases (23)**	**Biosaved (18)**
T [°C]	80.00	400.00	400.00	270.00	815.00	815.00	800.00	80.00	814.78	25.00	910.00	910.00	910.00	910.00	80.00
P [bar]	1.01	3.90	3.90	1.60	1.43	1.23	1.10	1.01	1.43	1.01	1.43	1.43	1.43	1.43	1.01
Gm [kg/s]	-	2.62	0.69	8.69	8.72	8.72	9.21	-	-	-	-	9.58	-	9.58	-
Gc [kg/s]	-	-	-	-	164.07	-	-	-	164.07	0.28	60.87	224.80	224.57	0.22	-
Gnc [kg/s]	5.71	-	-	-	4.11	-	-	0.46	4.10	-	1.51	5.62	5.56	0.06	0.46
Qm [kmol/s]	-	0.15	0.04	0.30	0.47	0.47	0.55		1.02	0.00	0.00	0.32	0.00	0.32	-
Composition															
xCH4	-	-	-	-	6.07%	6.07%	0.52%	-	-	-	-	-	-	-	-
xC2H4	-	-	-	-	1.61%	1.61%	0.00%	-	-	-	-	-	-	-	-
xCO	-	-	-	-	14.47%	14.47%	17.90%	-	-	-	-	-	-	-	-
xCO2	-	-	-	-	12.48%	12.48%	12.84%	-	-	-	-	16.48%	-	16.48%	-
xH2	-	-	-	-	27.99%	27.99%	40.57%	-	-	-	-	-	-	-	-
xH2O	-	100.00%	100.00%	-	36.25%	36.25%	27.05%	-	-	-	-	5.94%	-	5.94%	-
xO2	-	-	-	20.70%	-	-	0.00%	-	-	-	-	3.00%	-	3.00%	-
xN2	-	-	-	77.30%	1.11%	1.11%	1.01%	-	-	-	-	73.66%	-	73.66%	-
xAr	-	-	-	0.97%	0.00%	0.00%	0.08%	-	-	-	-	0.92%	-	0.92%	-
zCaO	-	-	-	-	-	-	-	-	-	-	-	-	-	-	-
zCaCO3	-	-	-	-	-	-	-	-	-	-	-	-	-	-	-
zCchar	-	-	-	-	100.00%	-	-	-	3.46%	-	-	-	-	-	-
zOlivFE	-	-	-	-	-	-	-	-	39.43%	40.84%	40.84%	40.84%	40.84%	40.84%	-
zOliveMG	-	-	-	-	-	-	-	-	57.11%	59.16%	59.16%	59.16%	59.16%	59.16%	-
yBio	100.00%	-	-	-	-	-	-	100.00%	-	-	-	-	-	-	100.00%
yash	-	-	-	-	100.00%	-	-	-	100.00%	-	100.00%	100.00%	100.00%	100.00%	-

B.3. INDIR_EL_36% Results

Table B-3: main operative points of 36% electrification hybrid mode

	Streams														
Variable	**Biomass feed (1)**	**Steam - in (2)**	**Steam sealing (3)**	**Burner air (15)**	**Gass-Out (4)**	**Syngas raw (6)**	**Syngas raw (13)**	**Burner biomass (19)**	**Solid recycle (5)**	**Olivine make up (20)**	**Burner recycle (22)**	**Burner out (21)**	**Solid recycle (22)**	**Flue gases (23)**	**biosaved (18)**
T [°C]	80.00	400.00	400.00	270.00	815.00	815.00	800.00	80.00	814.78	25.00	910.00	910.00	910.00	910.00	80.00
P [bar]	1.01	3.90	3.90	1.60	1.43	1.23	1.10	1.01	1.43	1.01	1.43	1.43	1.43	1.43	1.01
Gm [kg/s]	-	2.62	0.69	7.22	8.72	8.72	9.21	-	-	-	-	7.87	-	7.87	-
Gc [kg/s]	-	-	-	-	164.07	-	-	-	164.07	0.28	60.87	224.80	224.57	0.22	-
Gnc [kg/s]	5.71	-	-	-	4.11	-	-	0.23	4.10	-	1.51	5.61	5.56	0.06	0.70
Qm [kmol/s]	-	0.15	0.04	0.25	0.47	0.47	0.55		1.02	0.00	0.00	0.26	0.00	0.26	-
Composition															
xCH4	-	-	-	-	6.07%	6.07%	0.52%	-	-	-	-	-	-	-	-
xC2H4	-	-	-	-	1.61%	1.61%	0.00%	-	-	-	-	-	-	-	-
xCO	-	-	-	-	14.47%	14.47%	17.90%	-	-	-	-	-	-	-	-
xCO2	-	-	-	-	12.48%	12.48%	12.84%	-	-	-	-	16.96%	-	16.97%	-
xH2	-	-	-	-	27.99%	27.99%	40.57%	-	-	-	-	-	-	-	-
xH2O	-	100 %	100 %	-	36.25%	36.25%	27.05%	-	-	-	-	4.03%	-	4.03%	-
xO2	-	-	-	20.70%	-	-	0.00%	-	-	-	-	3.00%	-	2.99%	-
xN2	-	-	-	77.30%	1.11%	1.11%	1.01%	-	-	-	-	75.06%	-	75.06%	-
xAr	-	-	-	0.97%	0.00%	0.00%	0.08%	-	-	-	-	0.94%	-	0.94%	-
zCaO	-	-	-	-	-	-	-	-	-	-	-	-	-	-	-
zCaCO3	-	-	-	-	-	-	-	-	-	-	-	-	-	-	-
zCchar	-	-	-	-	100 %	-	-	-	3.46%	-	-	-	-	-	-
zOlivFE	-	-	-	-	-	-	-	-	39.43%	40.84%	40.84%	40.84%	40.84%	40.84%	-
zOliveMG	-	-	-	-	-	-	-	-	57.11%	59.16%	59.16%	59.16%	59.16%	59.15%	-
yBio	100 %	-	-	-	-	-	-	100%	-	-	-	-	-	-	100
yash	-	-	-	-	100.00%	-	-	-	100%	-	100%	100%	100%	100%	-

B.4. INDIR_EL_53% Results

Table B-4: main operative points of 53% electrification hybrid mode

	Streams														
Variable	**Biomass feed (1)**	**Steam - in (2)**	**Steam sealing (3)**	**Burner air (15)**	**Gass-Out (4)**	**Syngas raw (6)**	**Syngas raw (13)**	**Burner biomass (19)**	**Solid recycle (5)**	**Olivine make up (20)**	**Burner recycle (22)**	**Burner out (21)**	**Solid recycle (22)**	**Flue gases (23)**	**biosaved (18)**
T [°C]	80.00	400.00	400.00	270.00	815.00	815.00	800.00	80.00	814.78	25.00	910.00	910.00	910.00	910.00	80.00
P [bar]	1.01	3.90	3.90	1.60	1.43	1.23	1.10	1.01	1.43	1.01	1.43	1.43	1.43	1.43	1.01
Gm [kg/s]	-	2.62	0.69	5.74	8.72	8.72	9.21	-	-	-	-	6.16	-	6.16	-
Gc [kg/s]	-	-	-	-	164.07	-	-	-	164.07	0.28	60.87	224.80	224.58	0.22	-
Gnc [kg/s]	5.71	-	-	-	4.11	-	-	0.00	4.10	-	1.51	5.61	5.55	0.06	0.93
Qm [kmol/s]	-	0.15	0.04	0.20	0.47	0.47	0.55		1.02	0.00	0.00	0.20	0.00	0.20	-
Composition															
xCH4	-	-	-	-	6.07%	6.07%	0.52%	-	-	-	-	-	-	-	-
xC2H4	-	-	-	-	1.61%	1.61%	0.00%	-	-	-	-	-	-	-	-
xCO	-	-	-	-	14.47%	14.47%	17.90%	-	-	-	-	-	-	-	-
xCO2	-	-	-	-	12.48%	12.48%	12.84%	-	-	-	-	17.74%	-	17.74%	-
xH2	-	-	-	-	27.99%	27.99%	40.57%	-	-	-	-	-	-	-	-
xH2O	-	100.00%	100.00%	-	36.25%	36.25%	27.05%	-	-	-	-	1.00%	-	1.00%	-
xO2	-	-	-	20.70%	-	-	0.00%	-	-	-	-	2.99%	-	2.99%	-
xN2	-	-	-	77.30%	1.11%	1.11%	1.01%	-	-	-	-	77.30%	-	77.30%	-
xAr	-	-	-	0.97%	0.00%	0.00%	0.08%	-	-	-	-	0.97%	-	0.97%	-
zCaO	-	-	-	-	-	-	-	-	-	-	-	-	-	-	-
zCaCO3	-	-	-	-	-	-	-	-	-	-	-	-	-	-	-
zCchar	-	-	-	-	100.00%	-	-	-	3.46%	-	-	-	-	-	-
zOlivFE	-	-	-	-	-	-	-	-	39.43%	40.84%	40.84%	40.84%	40.84%	40.84%	-
zOliveMG	-	-	-	-	-	-	-	-	57.11%	59.16%	59.16%	59.16%	59.16%	59.16%	-
yBio	100.00%	-	-	-	-	-	-	100.00%	-	-	-	-	-	-	100.00%
yash	-	-	-	-	100.00%	-	-	-	100.00%	-	100.00%	100.00%	100.00%	100.00%	-

B.5. INDIR_EL_77% Results

Table B-5: main operative points of 77% electrification hybrid mode

Variable	**feed (1)**	**in (2)**	**sealing (3)**	**air (15)**	**Gass-Out (4)**	**raw (6)**	**raw (13)**	**biomass (19)**	**recycle (5)**	**make up (20)**	**recycle (22)**	**Biochar (21)**	**recycle (22)**	**gases (23)**	**biosaved (18)**	**Biochar (-)**
T [°C]	80.00	400.00	400.00	270.00	815.00	815.00	800.00	80.00	814.78	25.00	910.00	910.00	910.00	910.00	80.00	814.80
P [bar]	1.01	3.90	3.90	1.60	1.43	1.23	1.10	1.01	1.43	1.01	1.43	1.43	1.43	1.43	1.01	1.43
Gm [kg/s]	-	2.62	0.69	3.15	8.72	8.72	9.21	-	-	-	-	3.39	-	3.39	-	-
Gc [kg/s]	-	-	-	-	164.08	-	-	-	163.89	0.28	60.87	224.81	224.58	0.22	-	0.19
Gnc [kg/s]	5.71	-	-	-	4.10	-	-	0.00	4.10	-	1.50	5.60	5.55	0.06	0.93	-
Qm [kmol/s]	-	0.15	0.04	0.11	0.47	0.47	0.55	-	1.00	0.00	0.00	0.11	0.00	0.11	-	-
Composition																
xCH4	-	-	-	-	6.07%	6.07%	0.52%	-	-	-	-	-	-	-	-	-
xC2H4	-	-	-	-	1.61%	1.61%	0.00%	-	-	-	-	-	-	-	-	-
xCO	-	-	-	-	14.47%	14.47%	17.90%	-	-	-	-	-	-	-	-	-
xCO2	-	-	-	-	12.48%	12.48%	12.84%	-	-	-	-	17.74%	-	17.74%	-	-
xH2	-	-	-	-	27.99%	27.99%	40.57%	-	-	-	-	-	-	-	-	-
xH2O	-	100.00%	100.00%	-	36.25%	36.25%	27.05%	-	-	-	-	1.00%	-	1.00%	-	-
xO2	-	-	-	20.70%	-	-	0.00%	-	-	-	-	2.99%	-	2.99%	-	-
xN2	-	-	-	77.30%	1.11%	1.11%	1.01%	-	-	-	-	77.30%	-	77.30%	-	-
xAr	-	-	-	0.97%	0.00%	0.00%	0.08%	-	-	-	-	0.97%	-	0.97%	-	-
zCaO	-	-	-	-	-	-	-	-	-	-	-	-	-	-	-	-
zCaCO3	-	-	-	-	-	-	-	-	-	-	-	-	-	-	-	-
zCchar	-	-	-	-	100.00%	-	-	-	1.93%	-	-	-	-	-	-	100.00%
zOlivFE	-	-	-	-	-	-	-	-	40.05%	40.84%	40.84%	40.84%	40.84%	40.84%	-	-
zOliveMG	-	-	-	-	-	-	-	-	58.01%	59.16%	59.16%	59.16%	59.16%	59.16%	-	-
yBio	100.00%	-	-	-	-	-	-	100.00%	-	-	-	-	-	-	100.00%	-
yash	-	-	-	-	100.00%	-	-	-	100.00%	-	100.00%	100.00%	100.00%	100.00%	-	-

List of Figures

List if Tables

List of symbols

Variable/Acronym	Description
AGR	Acid Gas removal
AR	as received
ASU	Air Separation Unit
ATR	Auto Thermal Reformer
BEP	Break-Even Prices
BFB	Bubbling Fluidized Bed
BtL	Biomass to liquid
BtMeOH	Biomass to methanol
BtX	Biomass to X
CAPEX	Capital Expenditure
CCS	Carbon Capture and Storage technology
CEC	Cation Exchange Capacity
CF	Capacity Factor
CFB	Circulating Fluidized Bed
CGE	Cold Gas Efficiency
CHP	Combined Heat and Power
DME	DiMethyl Ether
ECF	European Climate Foundation
ECN	Energieonderzoek Centrum Nederland
ECO	economizer
EV	Electric vehicle
EVA	evaporator
FT	Fischer-Tropsch
FTR	Fired tubular reformer
GHG	Green House Gases
GHSV	Gas Hourly Space Velocity
HRSC	Heat Recovery Steam Cycle

IAPWS	International Association for the Properties of Water and Steam
ICE	Internal Combustion Engine
IEA	International Energy Agency
IRENA	International Renewable Energy Agency
IRR	Internal Rate of Return
KPI	Key Performance Parameter
LCCP	Laboratory of Catalyst and Catalytic Processes
LHV	Lower Heating Value
M	syngas Module
MDEA	Methyl Diethanolamine
MEA	Monoethanolamine
MeOH	Methanol
MTBE	Methyl Tert Butyl Ether
NGE	Net Gasifier Efficiency
NPV	Net Present Value
NZE	Net Zero Emissions
OCFG	oxygen-containing surface functional group
OPEX	Operational Expenditure
P	Pressure
PEM	Proton Exchange Membrane
PV	Photovoltaics
RKS-BM	Redlich-Kwong-Soave Boston-Mathias
RON	Research Octane Number
RWGS	Reverse Water Gas Shift
RR	Recycle Ratio
S/C	Steam to Carbon ratio
SH	Superheater
SR	Steam Reforming
T	Temperature
TPES	Total primary energy supply
WGS	Water Gas Shift

Ringraziamenti

Ringraziamo il nostro relatore, il Professor Matteo Romano, per il supporto, gli spunti di riflessione, i Kinder Bueno scommessi ed i preziosi consigli che ci ha dedicato in questi mesi, sempre con grande passione.

Un sentito ringraziamento e probabilmente anche qualche birra, va al nostro co-relatore Andrea Nava per l'incredibile disponibilità e per averci sopportato anche ad orari impensabili.

Ringraziamo anche l'ingegner Alessandro Poluzzi per averci guidato nelle prime fasi di questo percorso.

Con la vostra costante presenza avete reso questo lavoro stimolante e ricco di sfide.

Matteo e Francesco

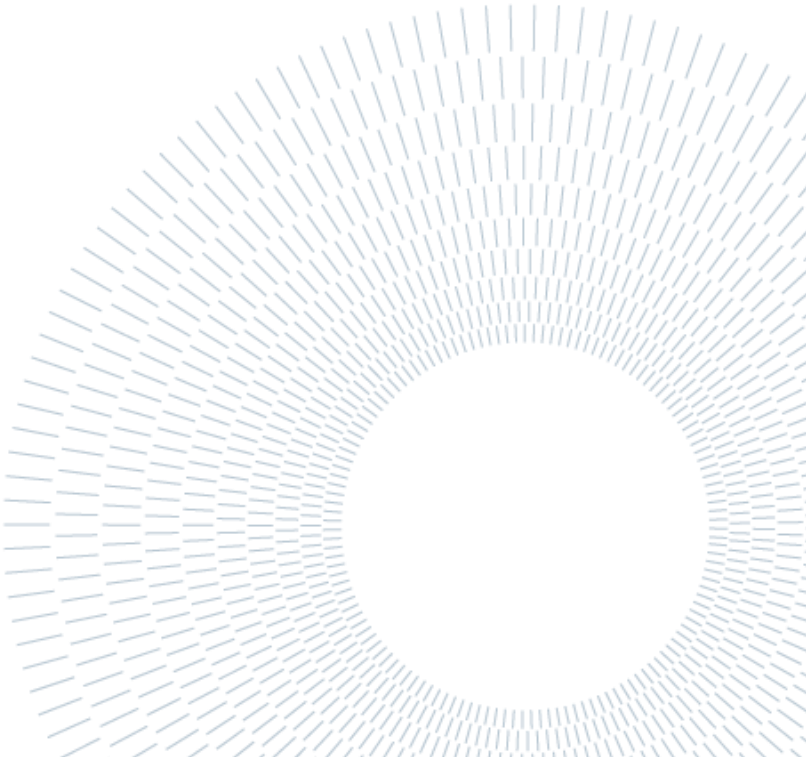

Matteo

A conclusione di questo elaborato, desidero menzionare tutte le persone, senza le quali questo lavoro di tesi non esisterebbe nemmeno.

Ringrazio di cuore la mia famiglia, papà Giorgio, mamma Annamaria e mia sorella Sara, per essersi districati egregiamente nel loro ruolo, per nulla banale, di guide nel percorso della vita e soprattutto per aver reso possibile tutto ciò. Letteralmente, senza di loro, non sarei quello che sono ora. Grazie per avermi sempre sostenuto e per non avermi mai fatto mancare il vostro affetto.

Ringrazio gli zii Eugenio, Marinella, Roberta, Carlo e i cugini Marco, Alessia e Umberto.

Un ringraziamento particolare va al mio collega e amico Francesco Enni per la pazienza di avermi avuto come co-autore di questo elaborato. Sono stati 9 mesi lunghi spero non di vederti mai più, con affetto.

Un grazie e sicuramente un drink a Leonardo My fondamentale consulente di vita e ventennale amico con cui ho da sempre condiviso i traguardi della mia esistenza e spero vivamente di continuare a farlo.

Ringrazio, inoltre, la SQUAD composta da Enrico Antonellini e Alberto Cantagalli per il bel tempo passato insieme nell'affrontare questi anni universitari.

E visto che dopotutto siamo ingegneri, prendo spunto da un'idea di Francesco. Di seguito un elenco delle persone a cui tengo e che comunque in un modo o nell'altro hanno contribuito o condiviso con me questo bellissimo percorso di 5 anni.

Agli amici Lorenzo Gamba, Marco Locatelli, Alice Bertoncelli, Nicola Morandi, Pietro Ceribelli, Alessandro Cellini, Syria Carminati, Marco Salvi, Giulia Bianzini, Mitia Ceriani, Mattia Mercanti, Francesco Marinucci, Niccolò Ghezzi, Chiara Nozza, Matteo Paganelli, Emanuele Peccio, Michele Minicuci, Chiara Riva, Kemal Senguler, Francesco Lardaioli, Andrea Lorini, Andrea Sironi, Alessandro Rota, Jacopo Bianco, Marco Genini, Riccardo Brambillasca, Giacomo Cantù, Filippo Braschi, Alberto Buttini, Chiara Bussolati, Giulia Filippi, Sara Finiguerra.

E per finire ci terrei a ringraziare, il sottoscritto, per la costanza e l'impegno dimostrati nel raggiungimento di questo fondamentale punto di partenza per la mia carriera accademica e lavorativa.

Francesco

Alla mia Famiglia,

a papà Franco e mamma Cecilia, a mia sorella Mariaelena, ai nonni Dino, Giovanna e Corinna.

Non so per quale specifico motivo, ma negli anni passati ho sempre pensato come conclusione del mio percorso di studi non tanto la laurea o la tesi in sé quanto l'atto stesso di scriverne i ringraziamenti. L'ho sempre visto come un punto di sintesi, di realizzazione, di riconciliazione con le persone a me care. Un venire a patti con quello che sono diventato grazie alle persone che mi hanno accompagnato.

Persone che, in pieno stile Brandon Sanderson, scrittore a cui sono particolarmente affezionato, voglio riportare con un lungo elenco.

A Bono, Fred, Robert e Bruno.

A Bruno, Chicca, Ele, Ire, Kyara, Maddi, Maffo, Mati, Max, Michele, Mitia (quanti con la M, wow), Vale e Tom di Tzatziki.

A Matte C, Matteo C, Matteo F, Matteo R (ho legato con tanti tanti Matteo) Manuel, Davide, Daniele, Simone Fabris.

Ad Anna, Eleonora, Fausto, Laura, Lorenzo, Lucif, de "Il culto di Mitia". Ad Alessia, Ester, Ginevra, L00c4, Paolo, Rachele, Sergio, Stefano, Teresa, di "Tanto Enni non c'è". A Claudia C, Daniela, Elia, Gloria, Lorenzo, Marta, Matteo, Sofia, Claudia A, Albino, Flavio, Walter di Teatro. Ai compagni di progetto e amici dell'università Matte, Enri, Albi, Fra Larda, Davide, Duccio, Ruben, Michela, Edo, Francesca, Beppe, Jacopo, Marta, Sara, Silvia, Kemal, Hamidreza, Chiara. Ad Anna, Camilla, Chiara, Marco, Silvia, Frappe della biblioteca di Alzano e del B:vacco. Ai pazzi asper Luigi, Sandro, Omar, Peter, Riccardo, Paolo, Fedele e agli amici di SludgeToEdge Sandro, Rebecca, Nidhin. E poi ad Ale, Luca, Ferr, Visca, Citte, Davide, Pav, Paolo, Enea, Laura, Michela, Cecilia, Nico, Pitti, Ale, Guarne, Pitte, Desa, Paga, Philippe.